**Comparative III-As-Bi Surface Morphologies and Microstructure
and Disciplinary Literacy in MSE**

by

Veronica L. Caro

A dissertation submitted in partial fulfillment
of the requirements for the degree of
Doctor of Philosophy
(Materials Science and Engineering)
in The University of Michigan
2023

Doctoral Committee:

Professor Joanna Millunchick, Chair
Assistant Professor Robert Hovden
Professor Zetian Mi
Professor Pierre Ferdinand P. Poudeu

Veronica L. Caro
vcaro@umich.edu
ORCID iD: 0000-0002-9827-0345

DEDICATION

This dissertation is dedicated to the hours of 1-3 AM,
when it feels like most of it was written,
and to my friends and family,
who kept me sane through all the other hours
Ora et Labora

ACKNOWLEDGEMENTS

Characterization, and would like to thank all the staff especially for the guidance I received in making my samples cooperate with the microscopes there.

TABLE OF CONTENTS

LIST OF TABLES

LIST OF FIGURES

ABSTRACT

The first section of the dissertation concerns the growth and characterization of III-V-Bi films. The class of III-V semiconductors contains materials that are well-suited for applications in computation, detection, and energy conversion. Most common among these are the III-As materials, such as GaAs and InAs. When alloyed with Bi in small amounts, the bandgap of these materials decreases, allowing their use in applications in the infrared range, particularly sensing and lasing. The challenge lies in the controlled growth of III-As-Bi materials, as Bi tends to segregate in films and is immiscible with Ga, leading to inhomogeneous growths and rough surface morphologies. Addressing this challenge, we carried out a series of molecular beam epitaxy growths of GaAsBi and InAsBi films at different growth conditions, paying special attention to the resulting surface morphologies, microstructures, and Bi-compositions, as well as the kinetics and thermodynamics of the systems. We found that GaAsBi and InAsBi both exhibit four surface morphologies, those being different combinations or absences of droplets. In GaAsBi, the presence of Bi droplets particularly is associated with highly inhomogeneous films. The effect is still present in InAsBi films but is less prevalent. Our GaAsBi films reached Bi-compositions of 18.3% with droplets and 13.6% without droplets. The InAsBi films had Bi-compositions of up to 3.9% with droplets and 1.6% without droplets. The GaAsBi films generally match previous growth modeling, allowing us to estimate its kinetic parameters for growth. The InAsBi films match the modeling in some ways, allowing us to estimate parameters, but show features indicating that there are other kinetic processes to account for.

The second section of the dissertation studies materials science and engineering (MSE) education. The process of disciplinary education involves introducing students to and enculturating students in the disciplinary culture, making students literate in the practices and values of the discipline. The theoretical framework of Disciplinary Literacy prompts researchers and instructors to ask, "What are the discipline-specific practices and values that are necessary to become a disciplinary practitioner, and how do we support students in becoming literate in those practices and values?" Though there are concepts and tactics that have been suggested for use in disciplinary-literacy-guided education, there remain the questions of how the concepts and tactics have been applied to education, and how they could be applied. To study the prevalence of disciplinary literacy concepts and tactics in contemporary MSE education, we conducted a literature review on published crystal structures and crystallography learning activities. Our findings suggest that certain concepts and tactics, such as the disciplinary cycle and the use of multiple types of representations, are implicitly understood and addressed in activities, while the tactic of learner role is not implicitly understood and certain aspects of it are neglected. To study the application of the disciplinary literacy concept of representational fluency in MSE education, we conducted studies comparing how students use paper-based and virtual-reality-based (VR) representations to complete activities about crystal structures, as well as how effective those different representations are. We found that students tend to use the two types of representations in different ways, and that while the VR-based representations helped students to complete difficult parts of the activity more correctly, they were less likely to remember what they learned.

Implications of our findings for both sections are further discussed.

CHAPTER 1

Introduction

This dissertation is split into two sections. The first section, Chapters 2.1-2.6, centers on III-As-Bi semiconductor materials, their growth challenges, and their characterization in terms of morphology, microstructure, kinetics, and thermodynamics. It is guided by the overarching research question of ***What surface morphologies, microstructures, and Bi-compositions arise in MBE-grown III-As-Bi films, and what can this tell us about their kinetics and thermodynamics?*** The second section, Chapters 3.1-3.4, centers on Materials Science and Engineering (MSE) Education, and specifically on the application of the framework of disciplinary literacy to MSE. The section is guided by the overarching research question of ***How are instructors using concepts of disciplinary literacy in MSE education?***

CHAPTER 2.1

Introduction

The mid-infrared (IR) range (2-30 μm or 0.04-0.62 eV [1]) of the electromagnetic spectrum is important for many applications, as it includes an atmospheric transmission window as well as characteristic frequencies for IR spectra of environmentally-, medically-, and industrially-important chemicals [1]. It has use particularly in gas sensing [2-3] and thermal imaging [4]. However, the mid-IR range is not well accessed by current technologies, with sources often being low in intensity or broadband (as in the case of Fourier transform infrared spectrometers, and leading to high power consumption and inefficient and low-coherence outputs) [1]. For many sensing applications, narrowband, coherent, and efficient optics sources are thus desired. The III-V semiconductors, including GaAs, GaSb, InAs, and InSb, have the capability to meet that desire, with bandgaps either higher than or in the general range of those needed for mid-IR applications (1.441 eV for GaAs, 0.70 eV for GaSb, 0.356 eV for InAs, and 0.180 eV for InSb [5]), and with tunability in the bandgaps through the addition of Bi. Bi lowers the bandgap by increasing the energy of the valence band, as Bi-induced localized defect states increase the energy of the heavy hole and light hole bands [6], and can also increase the spin-orbit splitting energy, which can in turn suppress Auger recombination in laser diodes [7].

The ultimate goal with these materials is to maintain full control over the microstructure of epitaxially-grown films while still achieving high, and tunable, Bi content. Full

microstructural control could allow for the growth of uniform bulk films or of regular substructures, such as superlattices. Achieving high and tunable Bi content would allow the electronic properties of the film, particularly the bandgap, to be tuned and to target wavelengths in the mid-IR range of 2-30 μm (0.62-0.04 eV) [1] for devices such as lasers and detectors. Inhibiting that goal, however, is the fact that Bi substitutes into the III-As compound in As sites and has low miscibility with III-As compounds such as GaAs and InAs [8-9]. These poor thermodynamic properties mean that III-As-Bi materials need to be grown by methods that can take advantage of kinetic factors to grow metastable films. In such methods, such as Molecular Beam Epitaxy (MBE) or Metalorganic Vapor Phase Epitaxy (MOVPE), precise fluxes of molecules under vacuum (MBE) or precursors gasses (MOVPE) are applied to temperature-controlled substrates, resulting in epitaxial growth on the substrate surface through either physical deposition (MBE) or chemical reaction (MOVPE) [10-11]. In both cases, fine control of the input fluxes, the growth rate, and the substrate temperature allow for growth of metastable alloys despite their unfavorable thermodynamics, and can also allow for alloy growth with particular structures, such as quantum wells [12], superlattices [13], or nanowires [14]. Even with such kinetically-limited growth, Bi has the tendency to self-segregate in III-As-Bi films [15-18], resulting in inhomogeneous Bi composition and the formation of droplets on the surface. There have been some studies in III-V-Bi materials systems [19-21] to examine how certain combinations of growth parameters result in different surface morphologies and film quality in the past, but such studies have either been conducted with III-Sb-Bi systems [19] or examine only subsections of the III-V-Bi system under study [20-21].

    In this work, we seek to establish the growth conditions for MBE-grown films of two III-As-Bi materials systems, GaAsBi and InAsBi, and characterize them in terms of morphology,

microstructure, and Bi content. In this way, we can both broadly sketch out what growth conditions lead to what types and qualities of films, granting an inductive understanding of the systems, and also use the data from the growths to estimate the inherent kinetic parameters of the systems, allowing them to be more-accurately modeled. Additionally, conducting these studies for two materials systems allows us to examine how the change in thermodynamics caused by the substitution of the group-III species affects the films grown and the kinetics.

We center our work here around one overarching question: ***What surface morphologies, microstructures, and Bi-compositions arise in MBE-grown III-As-Bi films, and what can this tell us about their kinetics and thermodynamics?*** To address this larger question, we focus on specific research questions to guide our inquiry, split between the two materials systems. For both systems, we focus on the following two questions: 1. *What surface morphologies, microstructures, and Bi-compositions arise in III-As-Bi materials, and how does this change across a range of conditions?* 2. *How do the kinetics and thermodynamics of this particular III-As-Bi system impact the observed morphologies, microstructures, and Bi-compositions?* For GaAsBi specifically, we also address this question: 3. *Does the observed GaAsBi system agree with previous computational predictions?* For InAsBi, we focus on this third question instead: 3. *How do different group III elements compare, and what can this tell us about the kinetics and thermodynamics of the systems?*

To address these questions, we first describe the background of these materials systems, their synthesis, and previous work and challenges found in growth of these materials (Chapter 2.2). Next, we explain our methods and the details of growth and characterization used for this study (Chapter 2.3). After the methods, we discuss our results for the GaAsBi materials system

(Chapter 2.4) and for the InAsBi materials system (Chapter 2.5). We then conclude with a

summary and address our overarching research question (Chapter 2.6).

References

[1]   D. Jung, S. Bank, M. L. Lee, and D. Wasserman, "Next-generation mid-infrared sources," *Journal of Optics*, vol. 19, p. 31, 2017.

[2]   P. Werle, F. Slemr, K. Maurer, R. Kormann, R. M. Ucke C, and B. J. Anker, "Near-and mid-infrared laser-optical sensors for gas analysis," 2002.

[3]   U. Willer, M. Saraji, A. Khorsandi, P. Geiser, and W. Schade, "Near- and mid-infrared laser monitoring of industrial processes, environment and security applications," *Opt Lasers Eng*, vol. 44, no. 7, pp. 699–710, Jul. 2006, doi: 10.1016/j.optlaseng.2005.04.015.

[4]   H. Kaplan, *Practical Applications of Infrared Thermal Sensing and Imaging Equipment*, 3rd edn. Bellingham, WA: SPIE Press, 2007.

[5]   L. I. Berger, "Properties of Semiconductors," in *CRC Handbook of Chemistry and Physics*, 94th ed., W. M. Haynes, D. R. Lide, and T. J. Bruno, Eds. Boca Raton: CRC Press, 2013, pp. 80–93.

[6]   Dip Prakash Samajdar, Tushar Dhabal Das, Sunanda Dhar, "Calculation of Valence Band Structure of GaSb1−xBix Using Valence Band Anticrossing Model in the Dilute Bi Regime," *Springer Proceedings in Physics*, vol. 178, pp. 243–248, 2017, doi: 10.1007/978-3-319-29096-6.

[7]   B. Fluegel, S. Francoeur, A. Mascarenhas, S. Tixier, E. C. Young, and T. Tiedje, "Giant spin-orbit bowing in GaAs1-xBix," *Phys Rev Lett*, vol. 97, no. 6, pp. 11–14, 2006, doi: 10.1103/PhysRevLett.97.067205.

[8]   N. Elayech, H. Fitouri, Y. Essouda, A. Rebey, and B. el Jani, "Thermodynamic study of the ternary system gallium-arsenic-bismuth," *Physica Status Solidi (C) Current Topics in Solid State Physics*, vol. 12, no. 1–2, pp. 138–141, 2015, doi: 10.1002/pssc.201400147.

[9]   K. Y. Ma, Z. M. Fang, R. M. Cohen, and G. B. Stringfellow, "Organometallic vapor-phase epitaxy growth and characterization of Bi-containing III/V alloys," *J Appl Phys*, vol. 68, no. 9, pp. 4586–4591, 1990, doi: 10.1063/1.346166.

[10]   A. Y. Cho and J. R. Arthur, "Molecular Beam Epitaxy," *Progress in Solid-State Chemistry*, vol. 10, no. 3, pp. 157–191, 1975, [Online]. Available: http://ac.els-cdn.com/0079678675900059/1-s2.0-0079678675900059-main.pdf?_tid=f84a880a-0e5b-11e2-a10a-

00000aab0f6b&acdnat=1349380074_03e479ca1b13cbe9e3560257b7dac73f%5Cnpapers2
://publication/uuid/1A993044-2D13-4D6B-92DC-71EEF845231D

[11]   C. A. Wang, "Early history of MOVPE reactor development," *J Cryst Growth*, vol. 506, pp. 190–200, Jan. 2019, doi: 10.1016/j.jcrysgro.2018.10.004.

[12]   Y. Zhang, L. Yue, X. Chen, J. Shao, X. Ou, and S. Wang, "Wavelength extension in GaSbBi quantum wells using delta-doping," *J Alloys Compd*, vol. 744, pp. 667–671, 2018, doi: 10.1016/j.jallcom.2018.02.027.

[13]   R. Rehm *et al.*, "InAs/GaSb superlattice infrared detectors," *Infrared Phys Technol*, vol. 70, pp. 87–92, Jul. 2015, doi: 10.1016/j.infrared.2014.09.034.

[14]   J. H. Paek, T. Nishiwaki, M. Yamaguchi, and N. Sawaki, "MBE-VLS growth of GaAs nanowires on (111)si substrate," *Physica Status Solidi (C) Current Topics in Solid State Physics*, vol. 5, no. 9, pp. 2740–2742, 2008, doi: 10.1002/pssc.200779248.

[15]   C. R. Tait, L. Yan, and J. M. Millunchick, "Spontaneous nanostructure formation in GaAsBi alloys," *J Cryst Growth*, vol. 493, pp. 20–24, 2018, doi: 10.1016/j.jcrysgro.2018.04.026.

[16]   C. R. Tait, L. Yan, and J. M. Millunchick, "Droplet induced compositional inhomogeneities in GaAsBi," *Appl Phys Lett*, vol. 111, no. 4, pp. 1–5, 2017, doi: 10.1063/1.4996537.

[17]   L. Dominguez *et al.*, "Formation of tetragonal InBi clusters in InAsBi/InAs(100) heterostructures grown by molecular beam epitaxy," *Applied Physics Express*, vol. 6, no. 11, Nov. 2013, doi: 10.7567/APEX.6.112601.

[18]   N. Baladés *et al.*, "Analysis of Bi Distribution in Epitaxial GaAsBi by Aberration-Corrected HAADF-STEM," *Nanoscale Res Lett*, vol. 13, no. 1, pp. 0–7, 2018, doi: 10.1186/s11671-018-2530-5.

[19]   J. Hilska, E. Koivusalo, J. Puustinen, S. Suomalainen, and M. Guina, "Epitaxial phases of high Bi content GaSbBi alloys," *J Cryst Growth*, vol. 516, no. March, pp. 67–71, 2019, doi: 10.1016/j.jcrysgro.2019.03.028.

[20]   Z. Batool *et al.*, "Bismuth-containing III-V semiconductors: Epitaxial growth and physical properties," *Molecular Beam Epitaxy*, pp. 139–158, 2013, doi: 10.1016/B978-0-12-387839-7.00007-5.

[21]   P. T. Webster *et al.*, "Molecular beam epitaxy using bismuth as a constituent in InAs and a surfactant in InAs/InAsSb superlattices," *Journal of Vacuum Science & Technology B, Nanotechnology and Microelectronics: Materials, Processing, Measurement, and Phenomena*, vol. 32, no. 2, p. 02C120, 2014, doi: 10.1116/1.4868111.

CHAPTER 2.2

Background

Bismuth in III-V Semiconductor Materials

The alloying of Bi to III-V semiconductor materials is of interest for several reasons. First, Bi is the heaviest stable group V element with an atomic weight of 208.98 Da, acts as a metal, and has a much lower toxicity than many other heavy metals [1], with applications ranging from being a medicinal component to replacing lead in solders and pipes [1]. The incorporation of Bi into III-V semiconductor materials affects the structure of the material's valence band [2], with the heavy hole and light hole E_+ bands increasing in energy with Bi content in the valence band due to Bi-induced localized defect states [2]. In contrast, nitrogen alloyed III-V materials, known as nitrides, tend to have changes in the conduction band [3], as interactions with N resonance slightly above the conduction band edge leads to the original conduction band minimum splitting into higher and lower energy bands, the latter essentially becoming the new conduction band minimum [3]. Particularly, one effect on the valence band in III-V-Bi materials that is seen upon the addition of Bi is an increase in the spin-orbit (SO) splitting energy [4]. The SO splitting energy is related to the interaction of electrons with the atomic nuclei, and thus the addition of Bi as a heavy element makes it significantly larger [4]. If the SO splitting energy increases to where it is larger than the bandgap of the material, however,

Auger recombination will be suppressed as it will take more energy for the Auger recombination

to proceed than it would to excite an electron into the conduction band. Thus, materials with

large and tunable SO splitting are attractive to applications such as diodes and lasers [5] which

have Auger recombination as a significant source of performance degradation [6]. Another

benefit of alloying III-V materials with Bi is changing the Bi content allows us to tune the

bandgap [7-11]. The exact dependence of the bandgap on the Bi content changes across material

systems, with GaAsBi having a dependence of around 88 meV/% Bi [8], as seen in Fig. 2.2.1A,

and InAsBi having a dependence of between 42-55 meV/% InBi [12, 13], as seen in Fig. 2.2.1B.
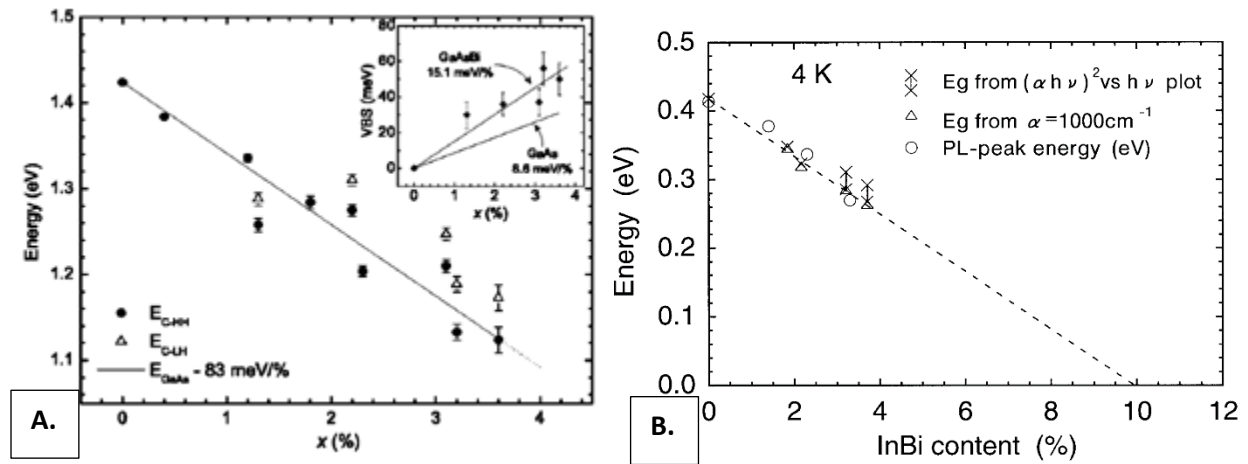
Figure 2.2.1: A. Band-gap energy of GaAsBi as a function of the Bi composition, x. The inset shows the heavy-holes and light-holes valence band splitting as a function of composition. [8] B. Band-gap energy dependence on InBi content for InAsBi determined from the $(h)^2$ vs. h plot and from energies at = 1000 cm^{-1}. The dependence of the PL-peak energies on InBi content is also plotted [12].

Figure 2.2.1 shows that large relative changes in the magnitude of the bandgap is seen for even

small amounts of Bi incorporation, allowing the bandgap of III-V-Bi alloys to access the mid-IR

frequencies for applications despite the alloys' low Bi content.

A variety of different III-V-Bi materials have come under study for these applications,

the most common being GaAsBi, InAsBi, GaSbBi, and InSbBi. Bismide semiconductors have

been made or attempted using different methods, the most prominent of which are

organometallic vapor phase epitaxy (OMVPE) [13-15], liquid phase epitaxy (LPE) [16-18], and molecular beam epitaxy (MBE) [7, 19-27]. Most growths of III-V-Bi materials have been done using MBE due to the wide range of controllable parameters, particularly substrate temperature and time-sensitive control of material fluxes. This time-sensitive control allows for the epitaxial growth of complex structures including quantum wells [28] and superlattices [29]. MBE-grown GaAsBi and InAsBi materials will be the primary concern of the remainder of this work.

Binary and ternary phase diagrams for the Ga-As-Bi and In-As-Bi systems have previously been computed using the Calphad method as seen in [30-32], and parts of these diagrams have been validated by experimental data including Differential Thermal Analysis (DTA) and electron dispersion spectroscopy (EDS). The relevant binary phase diagrams are seen in Fig. 2.2.2, and samples of ternary phase diagram isotherms can be seen in Fig. 2.2.3A (Ga-As-Bi) and Fig. 2.2.3B (In-As-Bi).
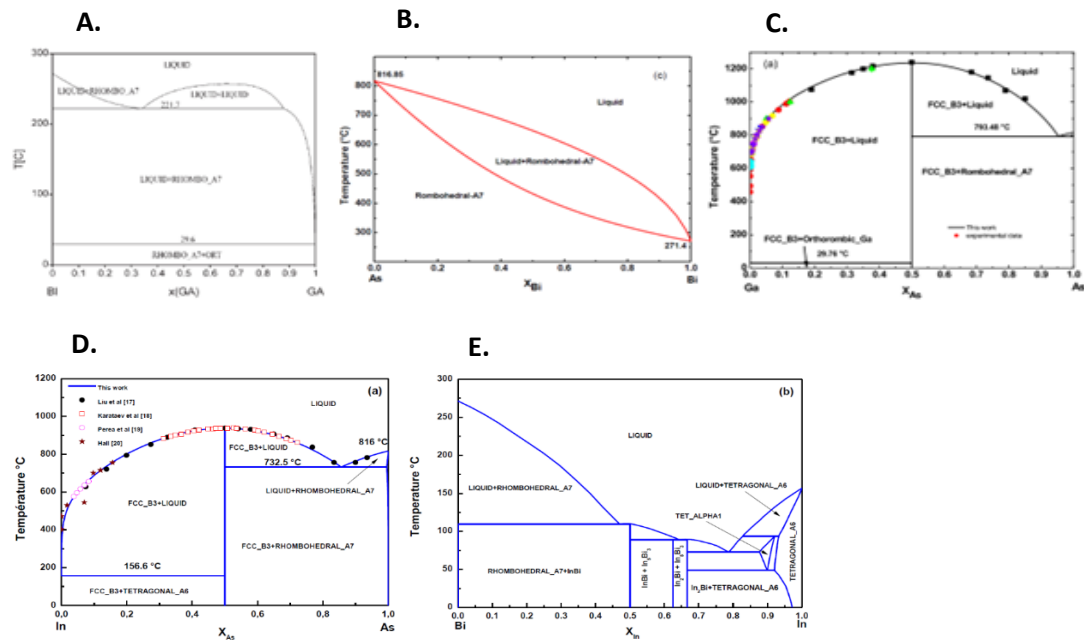
Figure 2.2.2: A. Calculated phase diagram of Bi-Ga binary system [30]. B. Calculated phase diagram of As-Bi binary system [31]. C. Calculated phase diagram of Ga-As binary system. (References to other works noted on the diagram can be found in [31]) [31]. D. Calculated phase diagram of In-As binary system [32]. E. Calculated phase diagram of In-Bi binary system [32].

9
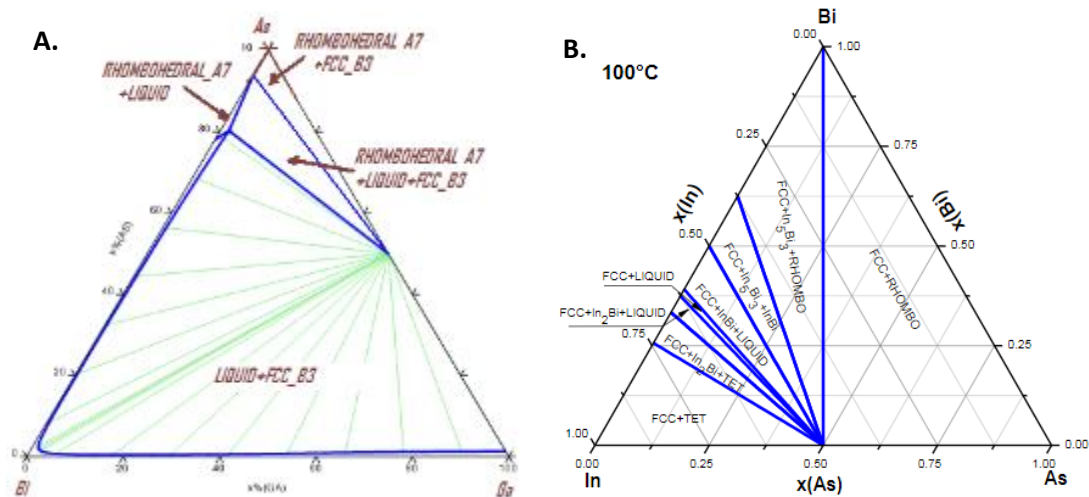
Figure 2.2.3: A. Calculated isothermal section of the Ga-As-Bi ternary system at 750 ºC [31]. B. Calculated isothermal section of the In-As-Bi ternary system at 100 ºC [32].

From Fig. 2.2.2A and 2.2.2B, we can see one major difference between the GaAsBi and InAsBi material systems, that being that Bi is immiscible in Ga but forms multiple compounds with In. For MBE growth of these compounds, that means that Bi tends to segregate or precipitate out of GaAsBi films at regular growth temperatures [33], while in InAsBi films there is the possibility for In and Bi to form InBi, In_2Bi, or In_5Bi_3 phases in the film instead of epitaxial growth. For Ga-V-Bi, the two solutions are to do low-temperature growths in an attempt to kinetically freeze the Bi in place and to use a group V overpressure during growth [19]. For InAsBi, films must be carefully characterized to determine if other phases are present.

Simulations of Bismide Growth

Experimental observation of materials systems are critical to understanding how a system behaves. When coupled with mathematical models and simulations, however, observation-informed models can be used to predict and guide further experiments. The growth in interest in III-V-Bi semiconductors has led to different proposed models for Bi incorporation into the III-V crystal.

10

Early Modeling

The first III-V-Bi model, proposed in 2008 by Lu, Beaton, Lewis, Tiedje, and Whitwick for the GaAsBi materials system [34], proposes that the Bi incorporation into the surface of the growing crystal is controlled by three processes, as follows. First, a Bi atom may incorporate into the film's surface from a surfactant layer through the simultaneous formation of an As-Ga bond and a Ga-Bi bond. Second, a Bi atom may incorporate into the film through the simultaneous formation of two Ga-Bi bonds, a process energetically excluded due to the formation of the unfavorable Bi-Ga-Bi bond. Third, a Bi atom may be displaced from a Ga-Bi bond through the insertion of an As atom. The first two processes, the Bi incorporation, are together described as proportional to the term $\theta_{Bi}F_{Ga}(1-x)$, where θ_{Bi} is the surface coverage of Bi in the surfactant layer, F_{Ga} is the flux of Ga, and x is the Bi incorporation. The final process, the displacement of Bi, is described as proportional to the term $F_{As}e^{-U1/kT}x$ where F_{As} is the flux of As, U_1 is an activation energy for the breaking of a Ga-Bi bond, k is the Boltzmann constant, and T is the temperature. Taking these processes together, the rate of change of Bi incorporation as a function of time can be described as the following, where b is a fitting parameter:

$$\frac{dx}{dt} \propto \theta_{Bi}F_{Ga}(1-x) - bF_{As}e^{-\frac{U_1}{kT}}x. \qquad \text{Eqn. 2.2.1}$$

This model is able to replicate some experimental observations but it does not examine what conditions lead to the formation of varying types of droplets or of compositional inhomogeneities nor does it examine the behavior of the Bi incorporation once droplets form.

A second model of growth for the GaAsBi system, proposed in 2012 by Lewis, Masnadi-Shirazi, and Tiedje, was designed to account for the As-flux-independent incorporation of Bi at

low As/Ga beam equivalent pressure ratios [35]. In this model, similar to the Lu model, the rate of Bi incorporation x into the surface of the crystal is given by

$$\frac{dx}{dt} \propto \theta_{Ga}\theta_{Bi} - a_1 x F_{Ga} - a_2 x e^{-\frac{U_1}{kT}},$$ Eqn. 2.2.2

where the symbols are defined the same as in the Lu model above, θ_{Ga} is the fraction of the surface that is Ga-terminated, and a_1 and a_2 are constants. The Bi surfactant layer exists on top of the crystal layer, and so its coverage is independent of the other coverages, which otherwise must add to 1. The first term on the right side of Eqn. 2.2.2 relates to the incorporation of the Bi atom, the second term describes the attachment of a free Ga atom to an incorporated Bi atom, and the third term is the thermal ejection of Bi, similarly to the Lu model. The Lewis model then adds a second relation for the surface coverage of As with respect to time in order to account for the saturation of Bi incorporation at the low As/Ga flux ratios used in many growths:

$$\frac{d\theta_A}{dt} = F_{As}(1 - \theta_{As} - x)\sum_{n=0}^{\infty}[(\theta_{As} + x)(1 - P_{As})]^n$$

$$-F_{Ga}\theta_{As}\sum_{n=0}^{\infty}[(1 - \theta_{As})(1 - P_{Ga})]^n$$ Eqn. 2.2.3

where θ_{As} is the surface coverage of As, P_{As} is the probability of As evaporation, and P_{Ga} is the probability of Ga lost to droplet formation. In this way, Eqn. 2.2.3 accounts for the presence of Bi incorporation as the surface coverage of As changes over time. This model is designed to take the possible presence of Ga droplets into account and agrees with experimental data for low As/Ga flux ratios, but does not consider Bi droplets or biphasic droplet formation.

Kinetic Monte Carlo Simulations

A different kind of model has also been used to simulate the growth of III-V-Bi semiconductors with varying flux ratios of the different components, that model being Kinetic Monte Carlo (KMC) simulations completed by Rodriguez et al [36]. The KMC model under discussion uses GaAsBi as a representative system and is made using an assumed zinc-blende lattice structure that does not include *a priori* assumptions about the stoichiometry of the resulting growth. The lack of stoichiometric assumption then allows for growths of simulated samples that result in droplets. At each simulation step, an atom could remain in place or do one of four actions: adsorb onto a vacant surface lattice site, switch positions with a neighboring atom, diffuse from its occupied site to an adjacent vacant site, or desorb from its occupied surface site. Except for transitions between atomic configurations involving adsorption, transition rates for all inter-atomic-configuration transitions are given by Arrhenius relations. Activation energies used for the Arrhenius relations are determined by nearest-neighbor and next-nearest-neighbor bond counting, where bond energies for that summation are specified using previous simulations and experimental data [37, 38]. The growth temperature for all simulated growths was 533 K, and the simulations, after initial trial growths to observe model behavior, were only allowed to run for up to 15 monolayers of growth before characterization of the results by the researchers. The initial trial growths were done to replicate the nucleation, growth, and diffusion of the different possible droplet types at the expected relative ratios of the III, V, and Bi fluxes, in order to demonstrate that this KMC model is reasonable and able to reproduce experimental observations. For the remainder of the growths, the V/III and Bi/V flux ratios were varied and the growths were characterized according to observed surface morphology

and the % Bi incorporation. The resulting map of the growths in this flux ratio space is seen in

Fig. 2.2.4.
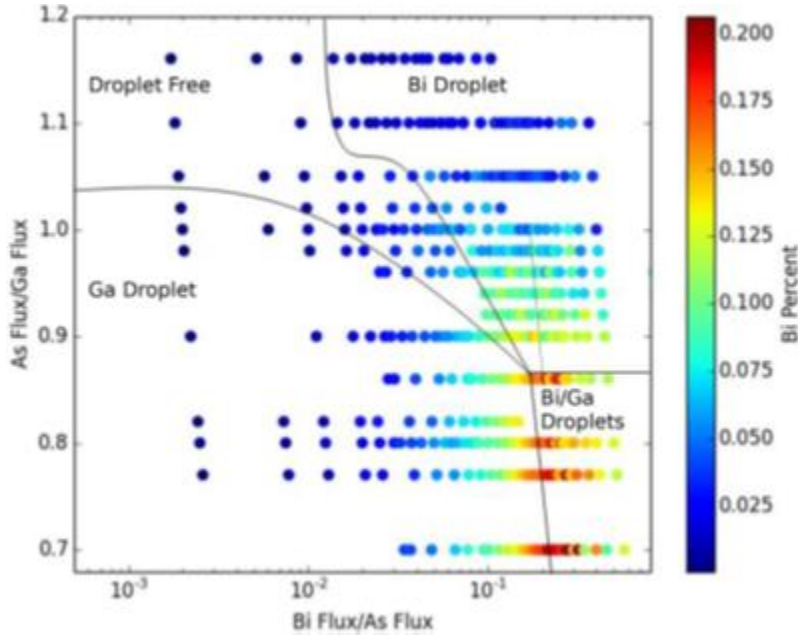
Figure 2.2.4: Droplet formation and Bi incorporation for GaAsBi film growths. F_{Ga} was held at 0.50 ML/s, while F_{As} and F_{Bi} were varied. The upper left area exhibited droplet free growth, while the upper right exhibited Bi droplet formation; the lower left exhibited Ga droplet formation, while the lower right area exhibited both Ga and Bi droplet formation during film growth. Bi incorporation is represented by the color of the marker, ranging from 0% (dark blue) to 21% (dark red). (The dotted line depicts the corollary experimental GaSbBi growth reported by Duzik [20]) [36].

From the mapping of simulated growths at a range of V/III and Bi/V flux ratios, the regions

corresponding to each observed surface morphology can be delimited. While each region

occupies the corner where it was expected and all four regions meet at a point, the center of the

surface morphology map exhibits unexpected bending of the morphology boundaries in the flux

ratio space, creating a channel of unexpectedly droplet-free conditions at specific ranges of V/III

and Bi/V flux ratios. The amount of simulated Bi incorporation increased towards the biphasic

Bi/Ga droplet region and was generally highest near to the Ga droplet to biphasic droplet

boundary. In contrast, most of the droplet-free region has low Bi incorporation, with the highest

incorporation being found in the channel area mentioned above.

Surface Kinetics Simulations

      To account for droplet formation and compositional inhomogeneities in the films, another model of growth of III-V-Bi materials was presented by Tait et al [39]. The deposition and incorporation of Bi into a III-V film in this model is controlled by four operating mechanisms, as shown in Fig. 2.2.5 and explained following.
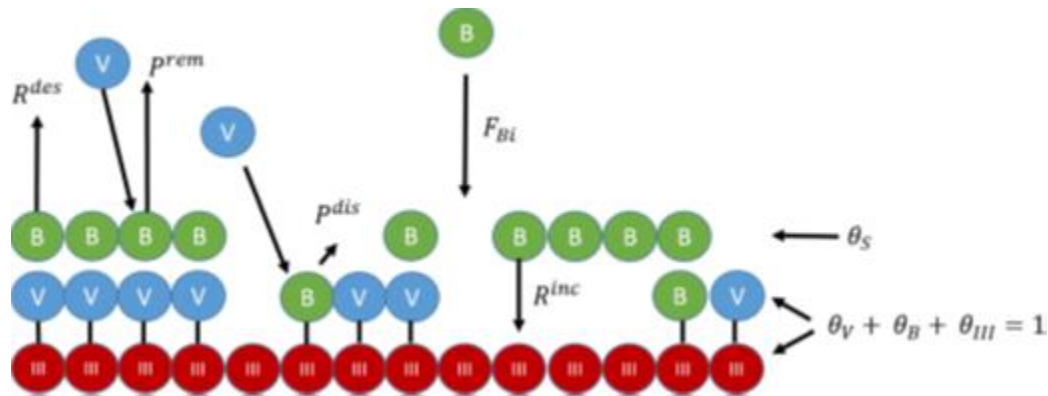
Figure 2.2.5: Illustration of possible operating mechanisms during the deposition of Bi in the growth of III-V-Bi. [39]

Covering the uppermost layer of the film is a loosely-bound surfactant layer made primarily of Bi, where the surfactant layer coverage is θ_S. The total coverage of the film in the epilayer is the sum of the coverages of III, V, and Bi atoms (θ_{III}, θ_V, and θ_B, respectively). The surfactant coverage is governed by the incoming flux of Bi (F_B), the rates of Bi incorporation from the surfactant layer (R^{inc}) and spontaneous desorption from the surfactant layer (R^{des}), and the probabilities of group-V-flux-mediated removal from the surfactant layer and displacement from the epilayer (P^{rem} and P^{dis}, respectively), where the group V flux is denoted as F_v. P^{dis} is equivalent to the third process in the Lu model [34], R^{inc} is equivalent to the first term of the Lewis model (Eqn. 2.2.2) [35], and R^{des} is equivalent to the third term of the Lewis model (Eqn. 2.2.2) [35], whereas P^{rem} is introduced in the Tait model here discussed. All four rates and probabilities are given by simple Arrhenius relationships, and probabilities differ from rates only

in their units, where rates have units of s^{-1} and probabilities are unitless. The flux of the III element affects the coverage of Bi and the group III species in the epilayer and is used in their calculation. Overall, the system is modeled with the following three equations:

$$\frac{d\theta_S}{dt} = F_B - \theta_S R^{des} - \frac{\theta_{III}\theta_S(R^{inc})^2}{F_V} + \theta_B F_V P^{dis} - F_V \theta_S P^{rem}, \qquad \text{Eqn. 2.2.4}$$

$$\frac{d\theta_{III}}{dt} = F_{III} - \frac{\theta_{III}\theta_S(R^{inc})^2}{F_V} - \theta_{III}F_V, \qquad \text{Eqn. 2.2.5}$$

$$\frac{d\theta_B}{dt} = \frac{\theta_{III}\theta_S(R^{inc})^2}{F_V} - \theta_B F_V P^{dis} - \theta_B F_{III}, \qquad \text{Eqn. 2.2.6}$$

where $\frac{d\theta_S}{dt}$, $\frac{d\theta_{III}}{dt}$, and $\frac{d\theta_B}{dt}$ are the rate of change with respect to time of θ_S, θ_{III}, and θ_B, respectively. From these equations, an expression for the Bi content in the film as a function of growth parameters is given as follows:

$$x = \frac{F_{III}R^{inc^2}F_{Bi}}{(F_{III}+F_V P^{dis})(F_V^3 P^{rem}+F_V^2 R^{des}+R^{inc^2}F_{Bi})}. \qquad \text{Eqn. 2.2.7}$$

While the trends indicated by the model are consistent with experimental data, the model cannot be used predictively as the exact values of the mechanism parameters R^{inc}, R^{des}, P^{dis}, and P^{rem} are unknown.

Similarly, a fourth model of the surface kinetics of III-V-Bi materials was introduced by Schaefer et al. [40] and was designed to both expand on the Tait model by more precisely describing the relevant fluxes and by explicitly extending the model to include quaternary alloys, particularly InAsSbBi. This model, similarly to the Tait model [39], denotes six processes occurring at the surface, seen in Fig. 2.2.6.
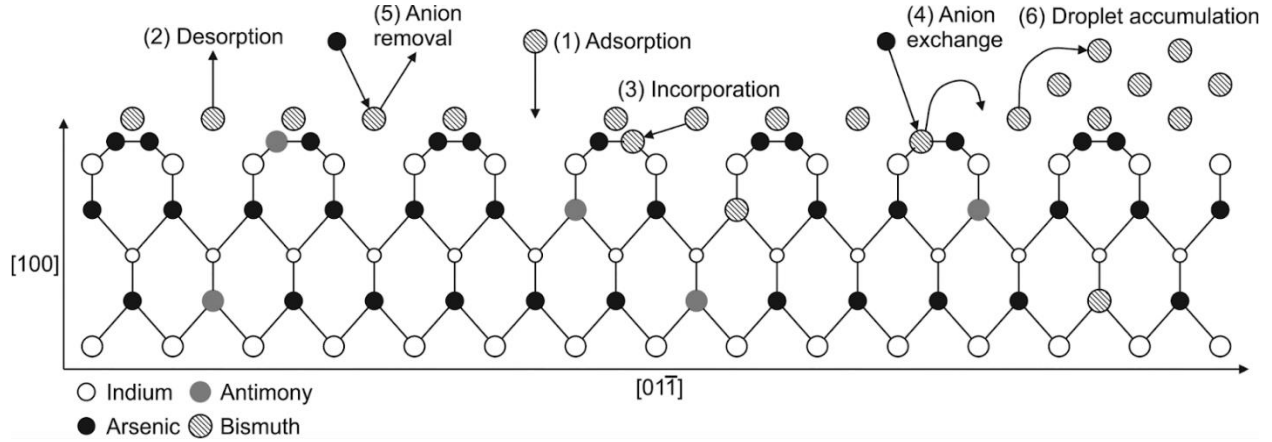
Figure 2.2.6: Schematic of (100) growth surface illustrating the six processes occurring during molecular beam epitaxy growth. (1) Adsorption of incident Bi flux into the surface layer. (2) Desorption of Bi from the surface layer. (3) Incorporation of Bi on a group-V lattice site. (4) Anion exchange wherein an incident As or Sb atom displaces a Bi atom from a group-V lattice site back into the adsorbed surface layer. (5) Anion-assisted removal wherein the desorption of As or Sb from the surface participates in the removal of Bi from the surface layer. (6) Accumulation of adsorbed Bi into Bi-rich surface droplets. From [40].

The processes as numbered in Fig. 2.2.6 are as follows: 1. The adsorption of incoming Bi flux onto the growth surface in a weakly-bound layer. 2. The spontaneous desorption of Bi from said weakly-bound surface layer (accounted for by R^{des} in the Tait model). 3. The incorporation of Bi into a group-V lattice site in the epilayer, marked by the formation of an In-Bi bond (accounted for by R^{inc} in the Tait model). 4. The displacement of Bi from a group-V lattice site back into the surface layer by an incident non-Bi group-V atom, replacing the In-Bi bond with an In-(As, Sb) bond (accounted for by P^{dis} in the Tait model). 5. The desorption of Bi from the weakly-bound surface layer by means of an incident group-V atom (accounted for by P^{rem} in the Tait model). 6. The coalescence of excess Bi from the surface layer into droplets. Notably, the fifth process is dependent on only the portion of the group-V flux that is not incorporated into the crystal, rather than the entire group-V flux as used in the Tait model [39, 40]. They then model these processes with the following two equations:

$$F_{Bi} + \hat{x}\big(F_{As}P_{exc,As} + F_{Sb}P_{exc,Sb}\big)$$

$$= \theta_{Bi}\big(R_{des} + R_{inc} + R_{dro} + \Delta F_{As}P_{rem,As} + \Delta F_{Sb}P_{rem,Sb}\big), \qquad \text{Eqn. 2.2.8}$$

and

17

$$\hat{x} F_{In} = \theta_{Bi} R_{inc} - \hat{x} \left(F_{As} P_{exc,As} + F_{Sb} P_{exc,Sb} \right), \qquad \text{Eqn. 2.2.9}$$

where on the left side of Eqn. 2.2.8, which includes terms increasing the surface coverage of Bi,

F_{Bi} is the incident Bi flux, $\hat{x}$ is the Bi mole fraction, F_{As} and F_{Sb} are respectively the incident As

and Sb fluxes, and $P_{exc, As}$ and $P_{exc, Sb}$ are the probabilities that a Bi atom is displaced back into

the surface layer by respectively an As atom or a Sb atom. On the right side of Eqn. 2.2.8,

including all terms that decrease the Bi surface coverage fraction θ_{Bi}, R_{des} is the rate of Bi self-

desorption, R_{inc} is the rate of Bi incorporation in the epilayer, R_{dro} is the rate of droplet

accumulation, ΔF_{As} and ΔF_{Sb} are respectively the excess As and Sb fluxes, and $P_{rem, As}$ and $P_{rem,}$

$_{Sb}$ are the probabilities of Bi removal from the epilayer by As or Sb atoms, respectively. In Eqn.

2.2.9, which sums up the rates of Bi incorporation into and removal from the growth epilayer, F_{In}

is the flux of In that is observed to fully incorporate into the epilayer. When Eqns. 2.2.8 and 2.2.9

are treated as a system, it is possible to solve for θ_{Bi} and $\hat{x}$, which yields one solution for θ_{Bi}:

$$\theta_{Bi} = \frac{F_{Bi}(F_{In} + F_{As} P_{exc,As} + F_{Sb} P_{exc,Sb})}{(F_{In} + F_{As} P_{exc,As} + F_{Sb} P_{exc,Sb})(R_{des} + R_{dro} + \Delta F_{As} P_{rem,As} + \Delta F_{Sb} P_{rem,Sb}) + F_{In} R_{inc}}, \qquad \text{Eqn. 2.2.10}$$

and two solutions for $\hat{x}$:

$$\hat{x} = \frac{\theta_{Bi} R_{inc}}{(F_{In} + F_{As} P_{exc,As} + F_{Sb} P_{exc,Sb})}, \qquad \text{Eqn. 2.2.11a}$$

$$\hat{x} = \frac{F_{Bi} R_{inc}}{(F_{In} + F_{As} P_{exc,As} + F_{Sb} P_{exc,Sb})(R_{des} + R_{dro} + \Delta F_{As} P_{rem,As} + \Delta F_{Sb} P_{rem,Sb}) + F_{In} R_{inc}}, \qquad \text{Eqn. 2.2.11b}$$

Using these equations, the authors are able to use measured growth parameters and

characteristics of a set of various InAsSbBi growths to fit the kinetic model parameters at various

substrate temperatures and for various species.

References

[1]   D. E. Polyak, "2016 Minerals Yearbook: Bismuth," *US Geological Survey*, no. September, p. 50.1, 2018, [Online]. Available: https://minerals.usgs.gov/minerals/pubs/commodity/mercury/myb1-2016-mercu.pdf

[2]   Dip Prakash Samajdar, Tushar Dhabal Das, Sunanda Dhar, "Calculation of Valence Band Structure of GaSb1−xBix Using Valence Band Anticrossing Model in the Dilute Bi Regime," *Springer Proceedings in Physics*, vol. 178, pp. 243–248, 2017, doi: 10.1007/978-3-319-29096-6.

[3]   D. Utsa, R. Thangavel, and S. Dhar, "First principles study of the structural, electronic and optical properties of epitaxial GaSb1-x-yNyBix, lattice matched to GaSb," *Mater Res Express*, vol. 5, no. 11, 2018, doi: 10.1088/2053-1591/aadbf1.

[4]   B. Fluegel, S. Francoeur, A. Mascarenhas, S. Tixier, E. C. Young, and T. Tiedje, "Giant spin-orbit bowing in GaAs1-xBix," *Phys Rev Lett*, vol. 97, no. 6, pp. 11–14, 2006, doi: 10.1103/PhysRevLett.97.067205.

[5]   O. Delorme *et al.*, "GaSbBi/GaSb quantum well laser diodes," *Appl Phys Lett*, vol. 110, no. 22, 2017, doi: 10.1063/1.4984799.

[6]   T. D. Eales, I. P. Marko, A. R. Adams, J. R. Meyer, I. Vurgaftman, and S. J. Sweeney, "Quantifying Auger recombination coefficients in type-I mid-infrared InGaAsSb quantum well lasers," *J Phys D Appl Phys*, vol. 54, no. 5, 2020, doi: 10.1088/1361-6463/abc042.

[7]   M. K. Rajpalke *et al.*, "Growth and properties of GaSbBi alloys," *Appl Phys Lett*, vol. 103, no. 14, 2013, doi: 10.1063/1.4824077.

[8]   S. Francoeur, M. J. Seong, A. Mascarenhas, S. Tixier, M. Adamcyk, and T. Tiedje, "Band gap of GaAs 1-x Bi x , 0<x< 3.6%," *Appl Phys Lett*, vol. 82, no. 22, pp. 3874–3876, 2003, doi: 10.1063/1.1581983.

[9]   J. Kopaczek *et al.*, "Temperature dependence of the band gap of GaSb1-xBix alloys with $0 < x \leq 0.042$ determined by photoreflectance," *Appl Phys Lett*, vol. 103, no. 26, pp. 0–4, 2013, doi: 10.1063/1.4858967.

[10]   L. Yue *et al.*, "Molecular beam epitaxy growth and optical properties of high bismuth content GaSb1-xBix thin films," *J Alloys Compd*, vol. 742, pp. 780–789, 2018, doi: 10.1016/j.jallcom.2018.01.329.

[11]   C. Z. Zhao, X. T. Li, X. D. Sun, S. S. Wang, and J. Wang, "Composition Dependence of the Band Gap Energy of the Sb-Rich GaBi x Sb 1−x Alloy ($0 \leq x \leq 0.26$) Described by the Modified Band Anticrossing Model," *J Electron Mater*, vol. 48, no. 3, pp. 1599–1603, 2019, doi: 10.1007/s11664-018-06895-9.

[12] H. Okamoto and K. Oe, "Structural and Energy-Gap Characterization of Metalorganic-Vapor-Phase-Epitaxy-Grown InAsBi," *Jpn J Appl Phys*, vol. 38, p. 1022, 1999.

[13] Z. M. Fang, K. Y. Ma, R. M. Cohen, and G. B. Stringfellow, "Photoluminescence of InAsBi and InAsSbBi grown by organometallic vapor phase epitaxy," *J Appl Phys*, vol. 68, no. 3, pp. 1187–1191, 1990, doi: 10.1063/1.346715.

[14] H. Okamoto and K. Oe, "Growth of Metastable Alloy InAsBi by Low- Pressure MOVPE," *Jpn J Appl Phys*, vol. 37, p. 1608, 1998.

[15] K. Y. Ma, Z. M. Fang, R. M. Cohen, and G. B. Stringfellow, "OMVPE growth and characterization of Bi-containing III-V alloys," *J Cryst Growth*, vol. 107, no. 1–4, pp. 416–421, 1991, doi: 10.1016/0022-0248(91)90496-R.

[16] D. P. Samajdar, M. K. Bhowal, T. D. Das, and S. Dhar, "Investigation of the below band gap infrared absorption properties of GaSbBi epitaxial layers grown on GaSb substrates," *Journal of Materials Science: Materials in Electronics*, vol. 27, no. 8, pp. 8641–8645, 2016, doi: 10.1007/s10854-016-4884-8.

[17] A. S. Sharma and S. Dhar, "Influence of Bi on the temperature dependent fundamental band gap parameters of GaSb 1-x Bi x," *Mater Res Express*, vol. 6, no. 4, 2019, doi: 10.1088/2053-1591/aafeee.

[18] T. D. Das, D. P. Samajdar, M. K. Bhowal, S. C. Das, and S. Dhar, "Photoluminescence studies of GaSbBi quantum dots grown on GaAs by liquid phase epitaxy," *Current Applied Physics*, vol. 16, no. 12, pp. 1615–1621, 2016, doi: 10.1016/j.cap.2016.09.012.

[19] J. Hilska, E. Koivusalo, J. Puustinen, S. Suomalainen, and M. Guina, "Epitaxial phases of high Bi content GaSbBi alloys," *J Cryst Growth*, vol. 516, no. March, pp. 67–71, 2019, doi: 10.1016/j.jcrysgro.2019.03.028.

[20] A. Duzik and J. M. Millunchick, "Surface morphology and Bi incorporation in GaSbBi(As)/GaSb films," *J Cryst Growth*, vol. 390, pp. 5–11, 2014, doi: 10.1016/j.jcrysgro.2013.12.001.

[21] S. Wang, I. Saha Roy, P. Shi, and A. Hallen, "Growth of GaSb 1−x Bi x by molecular beam epitaxy," *Journal of Vacuum Science & Technology B, Nanotechnology and Microelectronics: Materials, Processing, Measurement, and Phenomena*, vol. 30, no. 2, p. 02B114, 2012, doi: 10.1116/1.3672025.

[22] M. K. Rajpalke *et al.*, "High Bi content GaSbBi alloys," *J Appl Phys*, vol. 116, no. 4, 2014, doi: 10.1063/1.4891217.

[23] N. Segercrantz, J. Kujala, F. Tuomisto, J. Slotte, Y. Song, and S. Wang, "Defect studies in MBE grown GaSb1−xBix layers," vol. 174, no. February 2015, pp. 174–177, 2014, doi: 10.1063/1.4865629.

[24]   O. Delorme, L. Cerutti, E. Tournié, and J. B. Rodriguez, "Molecular beam epitaxy and characterization of high Bi content GaSbBi alloys," *J Cryst Growth*, vol. 477, pp. 144–148, 2017, doi: 10.1016/j.jcrysgro.2017.03.048.

[25]   M. K. Rajpalke, W. M. Linhart, K. M. Yu, T. S. Jones, M. J. Ashwin, and T. D. Veal, "Bi flux-dependent MBE growth of GaSbBi alloys," *J Cryst Growth*, vol. 425, pp. 241–244, 2015, doi: 10.1016/j.jcrysgro.2015.02.093.

[26]   A. J. Duzik, "Bismuth-induced surface structure and morphology in III-V semiconductors," *Nanosensors, Biosensors, and Info-Tech Sensors and Systems 2015*, vol. 9434, no. April 2015, p. 943413, 2015, doi: 10.1117/12.2085430.

[27]   E. Luna, O. Delorme, L. Cerutti, E. Tournié, J. B. Rodriguez, and A. Trampert, "Transmission electron microscopy of Ga(Sb, Bi)/GaSb quantum wells with varying Bi content and quantum well thickness," *Semicond Sci Technol*, vol. 33, no. 9, 2018, doi: 10.1088/1361-6641/aad5c4.

[28]   L. Yue *et al.*, "Structural and optical properties of GaSbBi/GaSb quantum wells [Invited]," *Opt Mater Express*, vol. 8, no. 4, p. 893, 2018, doi: 10.1364/ome.8.000893.

[29]   P. T. Webster *et al.*, "Optical properties of InAsBi and optimal designs of lattice-matched and strain-balanced III-V semiconductor superlattices," *J Appl Phys*, vol. 119, no. 22, 2016, doi: 10.1063/1.4953027.

[30]   D. Manasijević, D. Minić, D. Živković, I. Katayama, J. Vřešťál, and D. Petković, "Experimental investigation and thermodynamic calculation of the Bi-Ga-Sn phase equilibria," *Journal of Physics and Chemistry of Solids*, vol. 70, no. 9, pp. 1267–1273, 2009, doi: 10.1016/j.jpcs.2009.07.010.

[31]   N. Elayech, H. Fitouri, Y. Essouda, A. Rebey, and B. el Jani, "Thermodynamic study of the ternary system gallium-arsenic-bismuth," *Physica Status Solidi (C) Current Topics in Solid State Physics*, vol. 12, no. 1–2, pp. 138–141, 2015, doi: 10.1002/pssc.201400147.

[32]   N. Elayech, H. Fitouri, R. Boussaha, A. Rebey, and B. el Jani, "Calculation of In-As-Bi ternary phase diagram," *Vacuum*, vol. 131, pp. 147–155, 2016, doi: 10.1016/j.vacuum.2016.06.009.

[33]   C. R. Tait, L. Yan, and J. M. Millunchick, "Droplet induced compositional inhomogeneities in GaAsBi," *Appl Phys Lett*, vol. 111, no. 4, pp. 1–5, 2017, doi: 10.1063/1.4996537.

[34]   X. Lu, D. A. Beaton, R. B. Lewis, T. Tiedje, and M. B. Whitwick, "Effect of molecular beam epitaxy growth conditions on the Bi content of GaAs1-x Bix," *Appl Phys Lett*, vol. 92, no. 19, pp. 1–4, 2008, doi: 10.1063/1.2918844.

[35]   R. B. Lewis, M. Masnadi-Shirazi, and T. Tiedje, "Growth of high Bi concentration GaAs1-xBixby molecular beam epitaxy," *Appl Phys Lett*, vol. 101, no. 8, pp. 1–5, 2012, doi: 10.1063/1.4748172.

[36] G. V. Rodriguez and J. M. Millunchick, "Predictive modeling of low solubility semiconductor alloys," *J Appl Phys*, vol. 120, no. 12, pp. 0–6, 2016, doi: 10.1063/1.4962849.

[37] K. Reyes *et al.*, "Unified model of droplet epitaxy for compound semiconductor nanostructures: Experiments and theory," *Phys Rev B Condens Matter Mater Phys*, vol. 87, no. 16, Apr. 2013, doi: 10.1103/PhysRevB.87.165406.

[38] E. C. Young, S. Tixier, and T. Tiedje, "Bismuth surfactant growth of the dilute nitride GaNxAs 1-x," *J Cryst Growth*, vol. 279, no. 3–4, pp. 316–320, 2005, doi: 10.1016/j.jcrysgro.2005.02.045.

[39] C. R. Tait and J. M. Millunchick, "Kinetics of droplet formation and Bi incorporation in GaSbBi alloys," *J Appl Phys*, vol. 119, no. 21, p. 6, 2016, doi: 10.1063/1.4952988.

[40] S. T. Schaefer, M. S. Milosavljevic, R. R. Kosireddy, and S. R. Johnson, "Kinetic model for molecular beam epitaxy growth of InAsSbBi alloys," *J Appl Phys*, vol. 129, no. 3, Jan. 2021, doi: 10.1063/5.0035193.

CHAPTER 2.3

Methods

Growth and Calibration

In MBE growth, the fluxes used for particular samples are usually measured using Beam Flux Measurement (BFM). For the work described here, BFM was used each growth day to acquire Ga, In, Bi, and As_2 beam equivalent pressures (BEPs), reported in units of torr. Beam equivalent pressures (BEPs) were measured for Ga, In, Bi, and As_2 using a retractable ion gauge placed in front of the substrate manipulator. In each BFM session, the BFM was allowed to outgas before measurements were recorded for a minimum of 30 minutes after turning on the ion gauge. After those 30 minutes, the BFM was exposed to a flux of the group III element (Ga or In) until the pressure reading stabilized, in order to getter the ion gauge and reduce the baseline measurement. This process left the BFM more sensitive to smaller BEP variations. For a given BFM measurement of Ga, In, or Bi, the BFM was exposed to a flux of the element for a set period of time before the flux was removed and the BFM was allowed to return to baseline pressure. The stabilized baseline pressure was recorded 30 seconds after the removal of the element flux, and subtracted from the stabilized on-flux measurement to record the net BEP in units of torr. Measurements were repeated at least twice again, with an off-flux gap of 60 seconds after the baseline measurement, and once the net BEP measurements had been reproduced a total of three times, the average was taken as the overall net BEP measurement for

that element. For Ga and In, the flux period was 30 seconds. For Bi, the flux period was 90 seconds.

BEP measurements for As_2 were taken in a slightly different manner, due to the valved cracker. A flux of a group III element (Ga or In) was applied to the ion gauge to getter. When the flux was removed the baseline BEP was allowed to equilibrate with the As_2 valve closed and the shutter cutting off all flux. Once stability was reached, the shutter was opened and the BEP was allowed to stabilize again. Once a baseline was established, the valve position was serially increased, with each valve position allowed to sit for 30 seconds to equilibrate before a BEP measurement in torr was taken. Net BEPs were calculated based on the difference between the BEP at the valve position and the baseline BEP measured with a closed valve and open shutter. Initial valve positions to take measurements at were chosen based on previous measurements, but subsequent positions were chosen based on target BEPs. Once a range of valve positions were identified as possibilities, the measurements were repeated without the intervening valve positions to account for hysteresis until the net BEP values converged. The pattern of these repeated measurements were equilibration with a closed valve, 30 seconds of the valve opened to the desired position, and then the valve closed to the 0 position and the baseline measured again after the valve had been closed for 30 seconds. The net BEP measurement was taken from the difference between the BEP at the selected valve position and the previous baseline measurement.

Reflection high energy electron diffraction (RHEED) oscillations were used to measure the group III flux. A dedicated RHEED sample of the same substrate as the growth samples was heated to 600°C on the optical pyrometer and monitored on the RHEED camera to ensure a smooth RHEED pattern was obtained. The pattern was rotated until a 2x4 reconstruction was

found and centered just off the reconstruction in the pattern. The intensity of the brightest point was monitored while the sample was under As flux, and then the group III element shutter was opened to expose the sample to group III flux. The RHEED intensity would oscillate as the group III element would deposit on the surface and grow layers of [Ga, In]As film, with the highest intensity corresponding to full monolayers grown and the lowest intensity corresponding to patchy parts of a monolayer grown. After the system equilibrated and the intensity oscillations became too noisy, the group III shutter was closed to cut off the group III flux, and the average length of an oscillation was calculated, according to the following: $N_{periods}$ / ($T_{final} - T_{first}$), where $N_{periods}$ is the number of full non-noisy oscillations counted peak-to-peak or trough-to-trough between the shutter opening and the last non-noisy peak or trough, T_{final} is the time recorded at the final non-noisy peak or trough, and T_{first} is the time recorded at the first peak or trough after the shutter was opened. The process was repeated at least twice to ensure consistency.

Ga and In rates were measured using RHEED oscillations, and Bi and As_2 rates were estimated based on the Ga or In rate and the ratio of BEPs, as follows: $R_{As} = R_{III}$ * (BEP_{As} / BEP_{III}), $R_{Bi} = R_{III}$ * (BEP_{Bi} / BEP_{III}), where R_{As} is the rate of As growth, R_{III} is the rate of the group III growth, BEP_{As} is the BEP of As, BEP_{III} is the BEP of the group III element, R_{Bi} is the rate of Bi growth, and BEP_{Bi} is the BEP of Bi. RHEED was also used for in-situ monitoring of surface oxide desorption and general surface quality.

The substrate temperature was measured using a low temperature optical pyrometer with calibration to ensure accurate measurements in the low end of the effective detection range (250°C-1400°C). The temperature measured by the optical pyrometer was calibrated for the low temperature range (here referring to temperatures below 330°C according to the optical pyrometer) by doing a series of heating steps in the temperature setpoint. Starting at 0°C, the

substrate heater was set to a particular value and allowed to equilibrate for at least 5 minutes. After the equilibration, the temperature on the pyrometer was recorded and the substrate heater was set to a new temperature 10°C higher and the process was repeated until a substrate heater temperature of 500°C was reached. This process was repeated in the temperature range of 270-500°C both with and without an ambient As flux applied in order to measure consistency between common between-film-growth conditions. In this manner, the relationship in temperature between substrate heater and pyrometer could be modeled and used to confirm temperatures in growth temperature ranges between 295-325°C.

All samples were prepared on (001) oriented GaAs and InAs substrate wafers in a solid source EPI 930 MBE chamber using standard effusion cells for Ga (with two heating zones), In, and Bi and a valved cracking cell for As, with As cracked at 1000°C to obtain As_2. Samples were grown using the following process. A (001) oriented GaAs or InAs substrate wafer approximately 1 cm^2 in size was heated to about 650°C (for GaAs) or 510°C (for InAs) and monitored on RHEED until a smooth, uninterrupted pattern emerges, indicating the desorption of the oxide layer. The temperature was reduced to 600°C (for GaAs) or 465°C (for InAs) on the pyrometer, and a 1µm buffer layer matching the substrate was grown at As overpressure, generally at a valve position of 100, giving an As BEP of 1-2 x 10^{-6} torr, compared to the group III BEP usually being 3-6 x 10^{-7} torr. Finally, the temperature was set at 325°C ±5°C for GaAs or 300°C ±10°C for InAs and a ~500nm GaAsBi film or InAsBi film was grown. The substrate was not rotated during growth. Once the film was finished, the sample was annealed at the growth temperature for 5 min before it was quenched to 200°C.

The film growths we did were spread across the flux-ration-space, focusing on regions of interest, namely the morphology transitions and the central point of the droplet-free region

predicted in Fig. 2.2.4. A hypothetical set of growths illustrating the general pattern can be seen in Fig. 2.3.1.
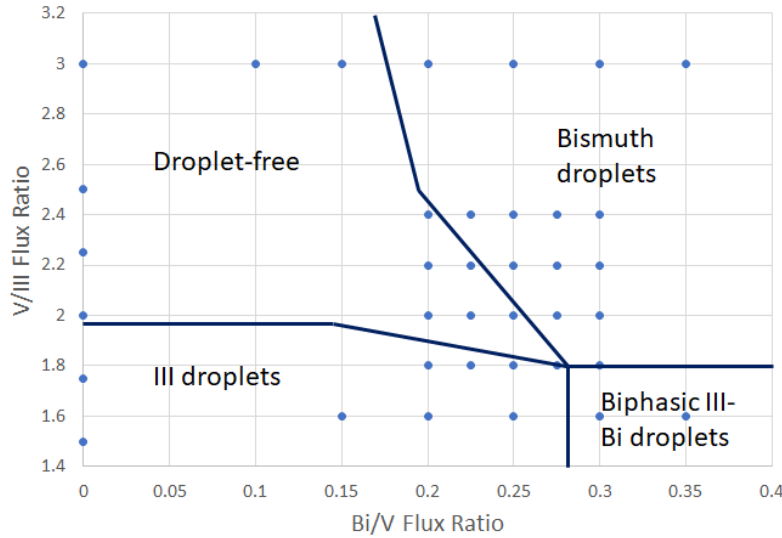
Figure 2.3.1: Hypothetical series of MBE growths to recreate the KMC morphology map [1]. The points in blue represent individual growth series. Exact target parameters would depend upon the specific system and previous growths' surface morphologies. The black lines are guides to the eye and only represent hypothetical placement of the surface morphology boundaries.

This method of recreating the morphology map was chosen to allow us to check if the trends seen in the KMC-predicted map [1] hold true and to put values on the flux ratios (or ranges of ratios) at which the morphology transitions occur.

Characterization

After growth, all samples were characterized by Scanning Electron Microscopy, Energy Dispersive Spectroscopy, and X-Ray Diffraction. Certain representative samples were studied with Scanning Transmission Electron Spectroscopy and Atomic Probe Tomography.

The surface of all samples were characterized using Scanning Electron Microscopy (SEM) using a JEOL JSM IT500-SR with a secondary electron detector. Characteristic x-rays for

Ga, In, As, and Bi using Energy Dispersive Spectroscopy (EDS) were used to ascertain the constitution of sample surfaces and morphological features. In cases where multiple morphologies were apparent on a sample (due to BEP gradients across the non-rotating sample based on the placement of effusion cells in the MBE chamber), the morphology seen at the center of the sample was taken as the true morphology.

Average film composition and microstructure was characterized using X-Ray Diffraction (XRD). For GaAsBi, ω-2θ rocking curves around the (0 0 4) substrate peak, found at $66.06°$, were done in order to determine the angle of the film peak and film quality. For InAsBi, ω-2θ rocking curves were done around the (0 0 4) substrate peak found at $61.1°$, instead. The peak shift between the film peak and the substrate peak was used to infer the percent of Bi in the film based on Vergard's law, using a theoretical lattice constant for GaBi of 6.33 Å [2], and extrapolating the lattice constant of InBi (zincblende) using powder diffraction database files for $InAs_{0.97}Bi_{0.03}$ [3]. Film quality was inferred based on the width of the film peaks. Due to the irregular peak shape and many inhomogeneities found in Bi-containing films, film quality was not judged by the Full-Width-Half-Maximum (FWHM) as is standard, but rather by the width of the peak one order of magnitude lower than its highest point (w_{OOM}). This value was calculated by finding the film peak maximum, calculating the intensity one order of magnitude below the peak, and determining the width of that intensity line. In cases where that line met the substrate peak, the intensity line was terminated at the substrate peak position and not at the high angle side of the substrate peak. The median value on this intensity line was taken as the median Bi composition for the sample for use in Vergard's law. In this way, the width of highly-inhomogeneous film peaks could be compared to others, even when there were relatively sharp film peaks within the larger inhomogeneities.

Focused Ion Beam (FIB) was used to prepare thin (<100 nm-thick) Transmission

Electron Microscope (TEM) liftouts of representative samples of each surface morphology. Most

samples were prepared in a Thermo Fisher Nova 200 Nanolab SEM/FIB, with additional

preparation being done in a Thermo Fisher Helios 650 Nanolab SEM/FIB. Each liftout was

prepared by depositing protective layers of carbon and platinum on the sample surface (~0.5 μm

layer of C deposited with both the SEM and FIB beams and ~1 μm of Pt deposited with the FIB

beam, depending on instrument conditions) and then milling grooves around the sample to allow

the in-progress liftout to be removed from the surface and fastened to a TEM grid. Once the

sample was welded to the TEM grid with more Pt, the sample was serially thinned towards the

center of the liftout using FIB milling with progressively smaller voltages and currents. The

starting conditions were 30 kV and 0.5 nA for thinning, and the final milling steps were

generally done at 2-5 kV and 0.072-0.12 nA, depending on which instrument was used. The

exact thickness of the completed liftouts was not measured but were thin enough to be imaged in

a TEM.

The completed liftouts were examined in various transmission electron microscopes,

including a JEOL 2100 Probe-Corrected Analytical Electron Microscope, a JEOL 3100R05, and

a Thermo Fisher Talos F200X G2 S/TEM. In the JEOL 3100R05, used for high-resolution

imaging, the beam accelerating voltage was 300 kV and both High Angle Annular Dark Field

(HAADF) and Bright Field (BF) detectors. In the Talos F200X, used for element mapping

through EDS, the beam accelerating voltage was 200 kV, and the EDS beam conditions were

200 kV accelerating voltage and ~259 pA of current. The obtained STEM micrographs were

analyzed using FIJI, an ImageJ-based image processing software (https://fiji.sc/#).

Atomic Probe Tomography (APT) was done for some representative samples in order to
see the dispersion of Bi in the film. APT samples were prepared using FIB in a similar method to
that used for the TEM liftouts, where the sample was placed on an APT array instead of a TEM
grid and was thinned to a point through milling of concentric circles. APT was done using a
Cameca LEAP 5000XR. The APT conditions were a temperature of 25 K in laser pulsing mode,
a pulse energy of 0.2 pJ, a pulse rate of 125 kHz, and a detection rate of 0.50%. The tomographic
data obtained was analyzed using Cameca Integrated Visualization and Analysis Software
(IVAS).

References

[1]   G. V. Rodriguez and J. M. Millunchick, "Predictive modeling of low solubility
        semiconductor alloys," *J Appl Phys*, vol. 120, no. 12, pp. 0–6, 2016, doi:
        10.1063/1.4962849.

[2]   J. M. Puustinen *et al.*, "Variation of lattice constant and cluster formation in GaAsBi," *J
        Appl Phys*, vol. 114, 2013.

[3]   K. Y. Ma, Z. M. Fang, R. M. Cohen, and G. B. Stringfellow, "Organometallic vapor-phase
        epitaxy growth and characterization of Bi-containing III/V alloys," *J Appl Phys*, vol. 68,
        no. 9, pp. 4586–4591, 1990, doi: 10.1063/1.346166.

CHAPTER 2.4

GaAsBi

Background

Gallium arsenide (GaAs) is a III-V semiconductor with a unit cell length of 5.65 Å and a bandgap of 1.424 eV [1]. The compound does not appear in nature and must be manufactured [2], generally by either the cooling of a stoichiometric melt (producing polycrystalline GaAs) [3] or the Czochralski crystal pulling method (producing monocrystalline GaAs) [2]. GaAs began coming under serious study in the mid-1950s [2], and has since been used for a variety of electronic applications, including transistors [4], solar cells [5], and laser diodes [6].

While GaAs is useful on its own, it has been targeted for alloying with Bi in order to alter its bandgap without large changes in lattice constant [7] and with significant increases in the spin-orbit splitting energy [8]. Although Bi incorporation in GaAs is thermodynamically unstable, metastable GaAsBi semiconductors have been made using molecular beam epitaxy (MBE) [9-11]. Most growths of GaAsBi have been done using MBE due to the wide range of controllable parameters, particularly substrate temperature and time-sensitive control of material fluxes. MBE-growth of GaAsBi was first achieved in 2003, grown at 380°C on a GaAs (100) substrate and with a Bi BEP of up to 10^7 torr, a growth rate of ~0.06 ML/s and with a buffer layer grown before the film, and resulted in samples with a Bi incorporation of up to 3.1% [12].

To date, the highest reported Bi incorporation was obtained in 2012 [9]. The film was 22% Bi, had a biphasic Ga-Bi-droplet-covered morphology, and was grown at 200 ℃ on a GaAs (100) substrate and with a Bi/Ga BEP ratio of 0.59, a As_2/Ga BEP ratio of less than 0.5, and a growth rate of 0.01 ML/s [9]. GaAsBi has been used for applications including lasers [13, 14], such as a GaAs/GaAsBi single quantum well microdisk laser with 5.8% Bi-composition and a lasing wavelength of 1276 and 1407 nm [14], and photovoltaic cells [15], such as a GaAs/GaAsBi *pin* solar cell with 1.7% Bi-composition and a bandgap of 1.3 eV in the active GaAsBi layer which resulted in a fill factor of 62% and an efficiency η of 4.18%.

The growth and use of Ga-V-Bi semiconductor materials is limited by the immiscibility of Ga and Bi [16], leading to various difficulties with the incorporation of Bi in the film. In general, both Bi desorption from the surface and displacement of Bi by other group-V species lead to low Bi incorporation due to the low bonding energy between Ga and Bi. For example, Rodriguez et al. used kinetic Monte Carlo simulations to model the pair-wise interactions and found the interaction energies were 0.13 eV for Ga-Bi as compared to 0.30 eV, 0.18 eV, and 0.50 eV for Ga-Ga, Bi-Bi, and Ga-As respectively [17]. To prevent the loss of Bi by these mechanisms, many studies use two strategies simultaneously: a low substrate temperature and an overall V/III flux ratio a bit larger than 1 [18]. Low substrate temperatures can lead to lower-quality film growth, and so the substrate temperature used for MBE growths must be carefully optimized [10]. Similarly, different surface morphologies can appear when the V/Ga and Bi/V flux ratios are varied with respect to each other. In the case of GaAsBi, these surface morphologies range from droplet-free surfaces when the As/Ga ratio is high and the Bi/As ratio is low, to Ga-droplet-covered surfaces when both ratios are low, to Bi-droplet-covered surfaces when both ratios are high, and finally to biphasic Ga-and-Bi-droplet-covered surfaces when the

As/Ga flux ratio is low and the Bi/As ratio is high [18, 19]. Figure 2.4.1 displays the four surface morphologies (as they appear in GaAsBi and GaSbBi).
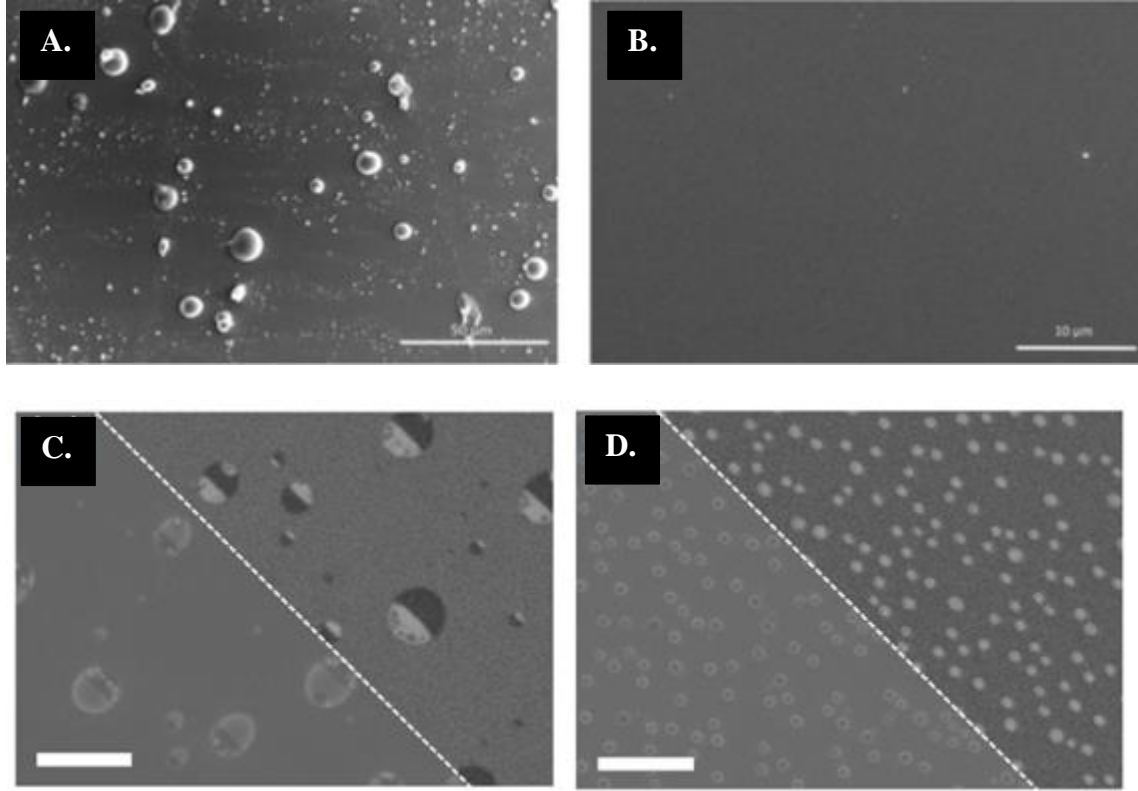
Figure 2.4.1: SEM of representative samples demonstrating four distinct surface morphologies attained throughout growth of GaAsBi, A. Ga droplet growth regime [18] B. Droplet-free growth regime [18], C. Biphasic Ga/Bi droplet growth regime [19], and D. Bi droplet growth regime [19]. The images in A. and B. were taken of GaAsBi samples, while the images in C. and D. were taken of GaSbBi samples. The horizontal scale bars in C. and D. correspond to 1 μm.

However, even in cases where Bi is able to be incorporated, the immiscibility of Ga and Bi leads to Bi segregation into high-Bi and low-Bi regions. Such Bi segregation leads to compositional inhomogeneities throughout the film [20], but compositional inhomogeneities are especially prevalent in the presence and vicinity of Ga droplets [19]. Understanding and controlling for the complex ways Bi interacts with the growing GaAsBi film is critical to being able to grow tuned high-Bi-content films.

In our work here, we will focus our efforts with GaAsBi on addressing the overall research question of ***What surface morphologies, microstructures, and Bi-compositions arise in MBE-grown GaAsBi films, and what can this tell us about their kinetics and thermodynamics?*** To guide our process, the question is split into three more-direct questions: 1. *What surface morphologies, microstructures, and Bi-compositions arise in Ga-As-Bi materials, and how does this change across a range of conditions?* 2. *How do the kinetics and thermodynamics of the GaAsBi system impact the observed morphologies, microstructures, and Bi-compositions?* 3. *Does the observed GaAsBi system agree with previous computational predictions?*

GaAsBi Growth Series

To study what surface morphologies and microstructures arise in III-As-Bi materials and how the kinetics and thermodynamics of the system impact the observed morphologies and microstructures, we grew 25 GaAsBi samples with various As/Ga and Bi/As BEP ratios, ranging from 1.62-3.46 for As/Ga BEP ratios and 0-0.37 for Bi/As BEP ratios. Each sample was grown according to the procedure outlined in Chapter 2.3, and after growth had its surface morphology categorized by SEM and EDS. Variable growth details for the 25 GaAsBi samples are shown in Table 2.4.1, while invariant parameters can be found in Chapter 2.3.

Table 2.4.1: Variable growth parameters for the 25 GaAsBi films

Sample number	Ga Rate (ML/s)	As$_2$ BEP	As$_2$/Ga BEP ratio	Bi/As$_2$ BEP ratio	% (at) Bi	w$_{OOM}$	Morphology
1	0.89	1.19E-06	2.41	0.088	5.00	0.26	Droplet-free
2	0.89	1.19E-06	2.41	0.185	10.36	0.38	Droplet-free
3	0.89	1.19E-06	2.41	0.253	10.53	1.78	Bi droplets
4	0.94	9.58E-07	1.91	0.300	18.26	0.80	Bi droplets
5	0.94	9.58E-07	1.91	0.196	10.89	0.39	Droplet-free
6	0.94	9.58E-07	1.91	0.094	5.26	0.22	Droplet-free

34

7	0.9	1.24E-06	2.49	0.121	8.37	0.38	Droplet-free
8	0.9	1.24E-06	2.49	0.193	10.38	1.75	Bi droplets
9	0.88	7.93E-07	1.62	0	0	0	Ga droplets
10	0.88	9.63E-07	1.97	0	0	0	Ga droplets
11	0.88	1.14E-06	2.33	0	0	0	Droplet-free
12	0.87	1.10E-06	2.25	0.134	9.75	0.38	Droplet-free
13	0.87	1.10E-06	2.25	0.211	14.31	0.67	Bi droplets
14	0.87	1.10E-06	2.25	0.255	13.97	0.59	Bi droplets
15	0.82	7.63E-07	1.62	0.374	8.72	1.55	Biphasic GaBi droplets
16	0.82	7.63E-07	1.62	0.241	4.33	0.77	Biphasic GaBi droplets
17	0.82	7.63E-07	1.62	0.135	6.48	1.16	Biphasic GaBi droplets
18	0.94	1.02E-06	1.93	0.175	11.17	0.58	Droplet-free
19	0.95	1.41E-06	2.76	0.329	6.53	1.08	Bi droplets
20	0.95	1.41E-06	2.76	0.224	10.00	1.69	Bi droplets
21	0.95	1.41E-06	2.76	0.127	8.27	0.37	Droplet-free
22	0.94	8.95E-07	1.78	0.049	2.77	0.51	Ga droplets
23	0.94	8.95E-07	1.78	0.097	7.17	1.28	Ga droplets
24	0.93	9.60E-07	1.95	0.246	13.63	0.40	Droplet-free
25	0.93	1.07E-06	2.17	0.173	11.21	0.37	Droplet-free

Film quality and Bi incorporation was assessed through XRD. Selected samples were characterized using TEM and APT. To see trends, the results for each sample were placed on a morphology map where the axes are the As/Ga and Bi/As BEP ratios, and the transitions between different morphologies were estimated according to boundaries between samples of different morphologies.

Surface Morphology

In this GaAsBi growth campaign, the expected four surface morphologies were observed, those being droplet-free, Bi-droplet-covered surfaces, Ga-droplet-covered surfaces, and biphasic Ga-Bi-droplet-covered surfaces. Examples of the four observed morphologies in our grown samples can be seen in Fig. 2.4.2.
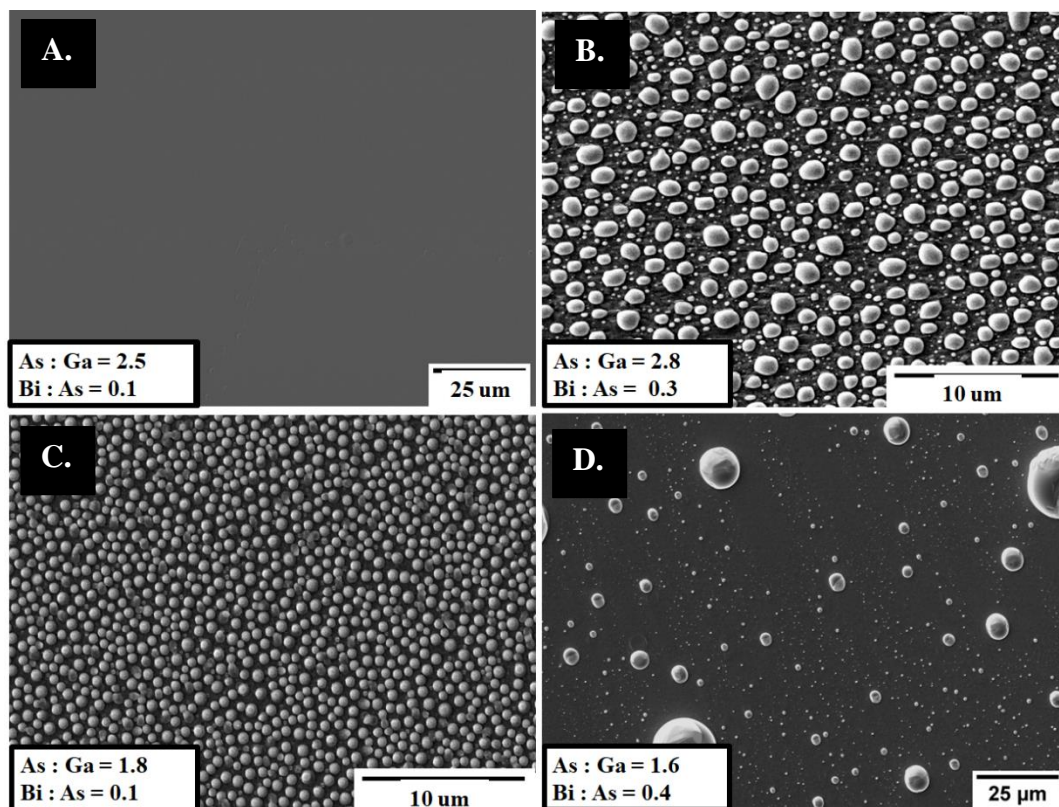
Figure 2.4.2: SEM micrographs of representative samples of each surface morphology regime. In order they are the (a) droplet-free surface regime, (b) Bi-droplet-covered regime, (c) Ga-droplet-covered regime, and (d) biphasic Ga-Bi-droplet-covered regime.

Figure 2.4.2.A shows a typical droplet-free surface. It is largely featureless, though the surface is not entirely smooth, and can be seen to have slight imperfections. In Fig. 2.4.2.B, a Bi-droplet-covered surface can be seen. The droplets are irregularly shaped and have a bi-modal size distribution, with there being both small droplets with diameters of around 100-500 nm and larger droplets with diameters of around 1-2.75 μm. The pattern of droplet placement suggests that the droplets move during growth, with larger droplets sweeping up and engulfing smaller droplets and leaving small areas devoid of droplets in their wake. The surface beneath the Bi droplets is visually uneven. A Ga-droplet-covered surface can be seen in Fig. 2.4.2.C, where the droplets are densely-scattered, round in shape and more homogeneous in diameter at around 400-600 nm. The surface beneath the droplets can be seen to have some roughness, with raised areas

36

surrounding a small pit left by a droplet moving to a different location or being ejected off by the SEM beam. The final surface morphology, biphasic Ga-Bi droplet-covered surfaces, can be seen in Fig. 2.4.2.D. The droplets are much sparser on the surface than either the Bi- or Ga-droplet-covered morphologies, and can be larger in size, ranging between 100 nm and 20 μm in diameter. The presence of droplet-void areas extending behind the larger droplets in roughly parallel directions indicates that the droplets sweep across the surface of the sample and engulf the smaller droplets. The droplets display two separate phases, those being the rounder Ga phase (darker in the SEM micrograph) and the faceted Bi phase (light-colored in the SEM micrograph).

Every sample had its surface morphology characterized by SEM and EDS and was placed onto a surface morphology map, seen in Fig. 2.4.3.

Figure 2.4.3: Morphological map of the 25 GaAsBi samples grown at 325°C and annealed for 5 min. The dashed lines represent the qualitative boundaries between the different regimes. The shape of the marker represents the surface morphology observed for the sample, with circles for droplet-free surfaces, squares for Bi-droplet-covered surfaces, triangles for Ga-droplet-covered surfaces, and diamonds for biphasic Ga-Bi-droplet-covered surfaces.

Split on the axes of Bi/As BEP ratio and As/Ga BEP ratio, the four surface morphologies are partitioned roughly into the four quadrants of the morphology map. When the As/Ga BEP ratio is more than approximately 1.8 and the Bi/As BEP ratio is less than 0.2, the droplet-free morphology arises, as the incoming As, Ga, and Bi fluxes are incorporated into the growing film. When the As/Ga BEP ratio is greater than 1.8 and the Bi/As BEP ratio is greater than about 0.2, the surface instead displays the Bi-droplet-covered morphology, as the amount of Bi flux reaches a critical point and allows Bi droplets to grow beyond nucleation. When the As/Ga and Bi/As BEP ratios are less than 1.8 and 0.12, respectively, the Ga-droplet-covered surface morphology can be found, as there is no longer enough Group V flux to bond with the incoming Ga and Ga droplets nucleate and grow. When the As/Ga BEP ratio is below approximately 1.8 and the Bi/As BEP ratio is above approximately 0.12, biphasic Ga-Bi droplets form, as the smaller proportion of As leads to Ga accumulation on the surface and the proportion of Bi becomes large enough that Bi on the surface can coalesce into droplets. The values for the BEP ratio boundaries are approximate, and not universal. There is a tendency as the Bi BEP increases and the Ga BEP decreases for droplet-free morphologies to remain, taking up the space in the center of the morphology map, but other morphologies emerge as the As/Ga and Bi/As ratios continue to increase and decrease, respectively.

Microstructure

When characterized by XRD, the film quality of samples found in the different morphology regimes also follow trends, which can be seen in Fig. 2.4.4.
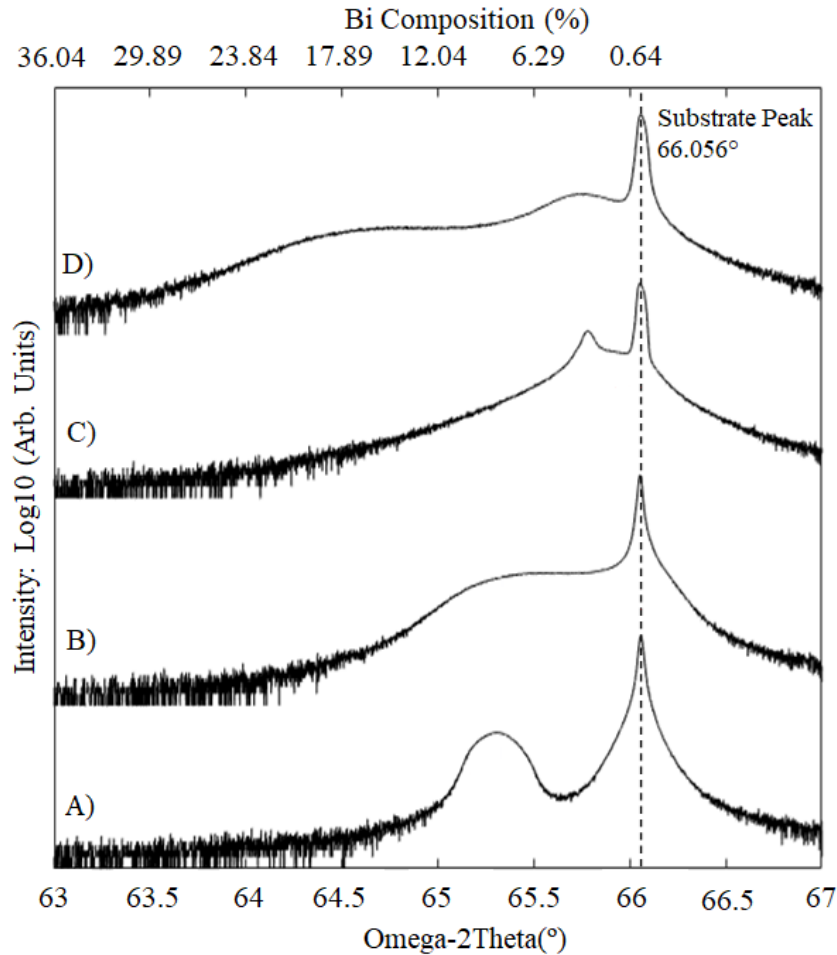
Figure 2.4.4: Representative ω-2θ XRD scan profiles associated with the four GaAsBi morphologies. The upper x-axis represents the atomic percentage of Bi calculated using Vergard's law.

Figure 2.4.4.A shows the representative ω-2θ XRD scan for the droplet-free-surface regime. The film peak is well-separated from the substrate peak and is broad in comparison, indicating that there minor but common inhomogeneities in the film, as there are a range of Bi-compositions grouped around the average composition marked by the film peak maximum. In Fig. 2.4.4.B, we see instead the representative ω-2θ XRD scan for the Bi-droplet-covered regime. Here, instead of a defined film peak, there is a wide film shoulder going from the substrate peak to Bi-composition above 10%, indicating widespread inhomogeneities throughout the film that are not centered around some sort of modal average composition. The representative ω-2θ XRD scan for

the Ga-droplet-covered regime is shown in Fig. 2.4.4.C. In this case, there is sharp film peak that

is not well-separated from the substrate peak, as well as a long trail of increased intensity over

the baseline that indicates small amounts of high-Bi-composition regions in the film. Overall, the

sharp film peak indicates a preferred Bi-composition in the film, but there are still significant

amounts of inhomogeneities in the Bi-composition, extending from near-zero Bi % to near 10%

Bi. Finally, Fig. 2.4.4.D shows the representative ω-2θ XRD scan for the biphasic Ga-Bi-droplet-

covered regime. For this regime, the scan resembles a superimposition of the Bi-droplet-covered

and Ga-droplet-covered regime scans, with a wide peak shoulder extending to high Bi-

composition and a broad local maximum film peak at low Bi-composition, indicating some

amount of preferred Bi-composition but widespread inhomogeneities throughout the film.

As can be seen in Fig. 2.4.4, most of the regimes result in ω-2θ XRD scans with broad

film peaks or shoulders, making it inappropriate to compare film quality between different

samples and between different regimes using the standard measurement of the full-width half-

maximum (FWHM, the width of the film peak at half of the maximum intensity value). For

instance, for a Ga-droplet-covered regime sample, the FWHM would capture only the small film

peak and not the long tail of high-Bi-composition. To judge film quality in our samples, we

instead use the measure of the width of the sample one order of magnitude below the film peak

maximum (w_{OOM}).

The amount of Bi-content in the films, as well as the w_{OOM} values for the different

GaAsBi samples are displayed in Fig. 2.4.5 in an XRD-focused version of the GaAsBi
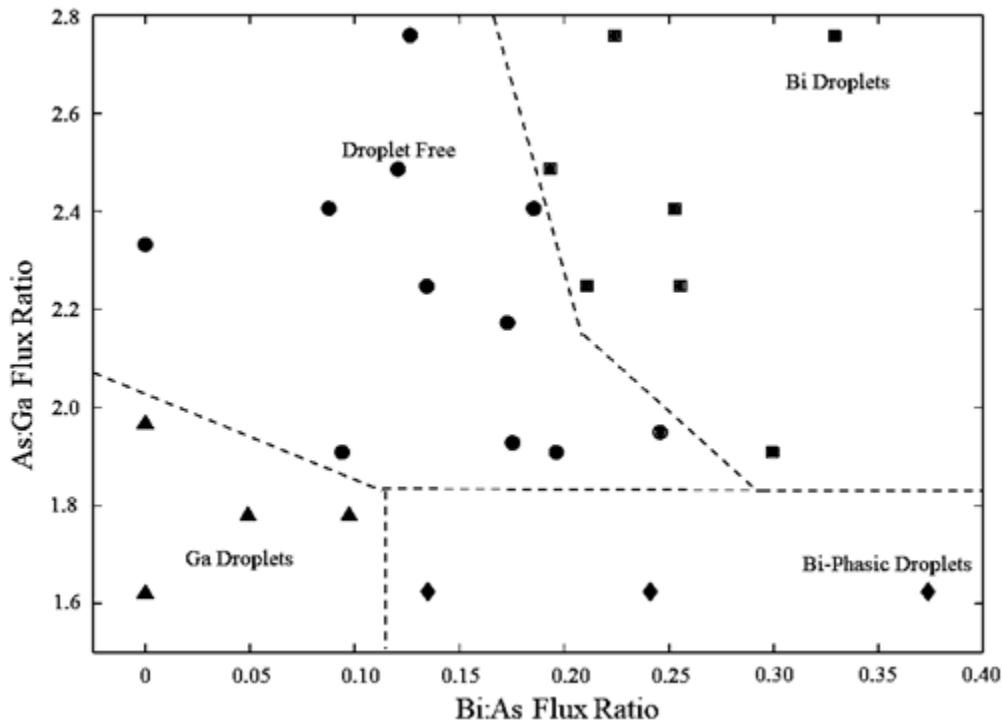
morphology map.
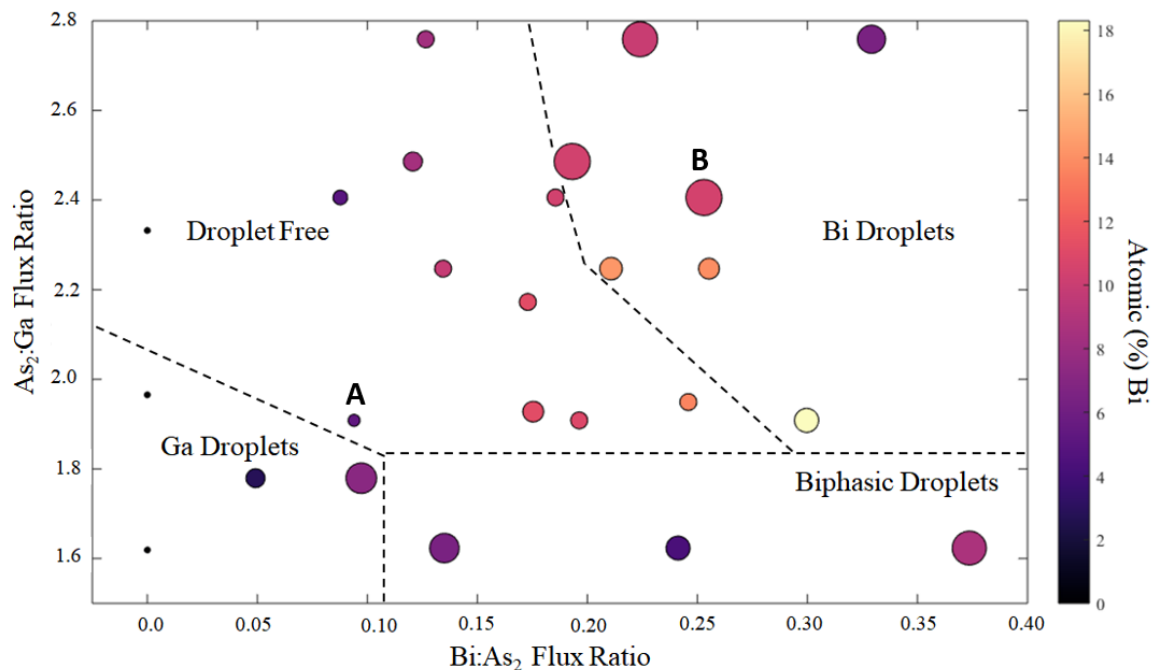
Figure 2.4.5: Morphological and XRD map of the 25 GaAsBi samples grown at 325°C and annealed for 5 min. The dashed lines represent the qualitative boundaries between the different regimes, while the color of the marker represents the atomic percentage of Bi in the sample determined by XRD. The size of the marker represents the w_{OOM} value of each sample except for the three samples with a Bi/As BEP ratio of zero, where the lack of film peak means no w_{OOM} could be calculated. For scale, the marked samples A and B have w_{OOM} of 0.21° and 1.78°, respectively.

Trends in Bi-composition of the samples, measured as the median Bi-composition, can be seen across the morphology map (Fig. 2.4.5). In general, the atomic percentage of Bi in the film increased as the Bi/As BEP ratio increased and the As/Ga BEP ratio decreased, reaching a maximum at 18.3% Bi for a sample grown at a As/Ga BEP ratio of about 1.9 and a Bi/As BEP ratio of 0.30. The exception to this trend was for samples in the biphasic Ga-Bi droplet regime, which tended to have relatively low and consistent atomic percentages of Bi, having an average composition of 3.1% Bi and a range of 2.1-3.6% Bi among the three samples in that regime.

In general, the w_{OOM} values seen in Fig. 2.4.5 indicate that the presence of droplets is detrimental to the film quality, but the impact of droplets within droplet-covered regimes is not monotonic, with different regimes exhibiting different trends. In the droplet-free-surfaces regime, the w_{OOM} values are relatively constant and the Bi-composition increases with the Bi/As

41

BEP ratio, reaching a maximum at the low As/Ga BEP ratio, high Bi/As BEP ratio edge. For the Bi-droplet-covered regime, higher As/Ga BEP ratios are associated with larger w_{OOM}, whereas the w_{OOM} is largely constant across different Bi/As BEP values. Likewise, the Bi-composition increases as the As/Ga BEP ratio lowers and is not affected by the Bi/As BEP ratio. For the Ga-droplet-covered regime, both Bi-composition and w_{OOM} increased with increasing Bi/As BEP ratio. Finally, for the biphasic Ga-Bi-droplet-covered regime, w_{OOM} varied but was largely constant as the Bi/As BEP ratio increased, with the Bi-composition increasing slightly as the Bi/As BEP ratio increased. In general, the occasional samples that had comparatively low w_{OOM} values compared to that expected by the noted trends in a regime also tended to have smaller amounts of Bi-composition.

While the ω-2θ XRD scans are useful for examining average Bi-composition and film quality, the widespread presence of inhomogeneities necessitates the close study of the microstructure by TEM instead. TEM of representative samples in the droplet-free-surface and Ga-droplet-covered regimes was previously done by [20] and [19], respectively, but is briefly discussed here for comparison with the novel TEM done of the Bi-droplet-covered and biphasic Ga-Bi-droplet-covered regimes in this work.
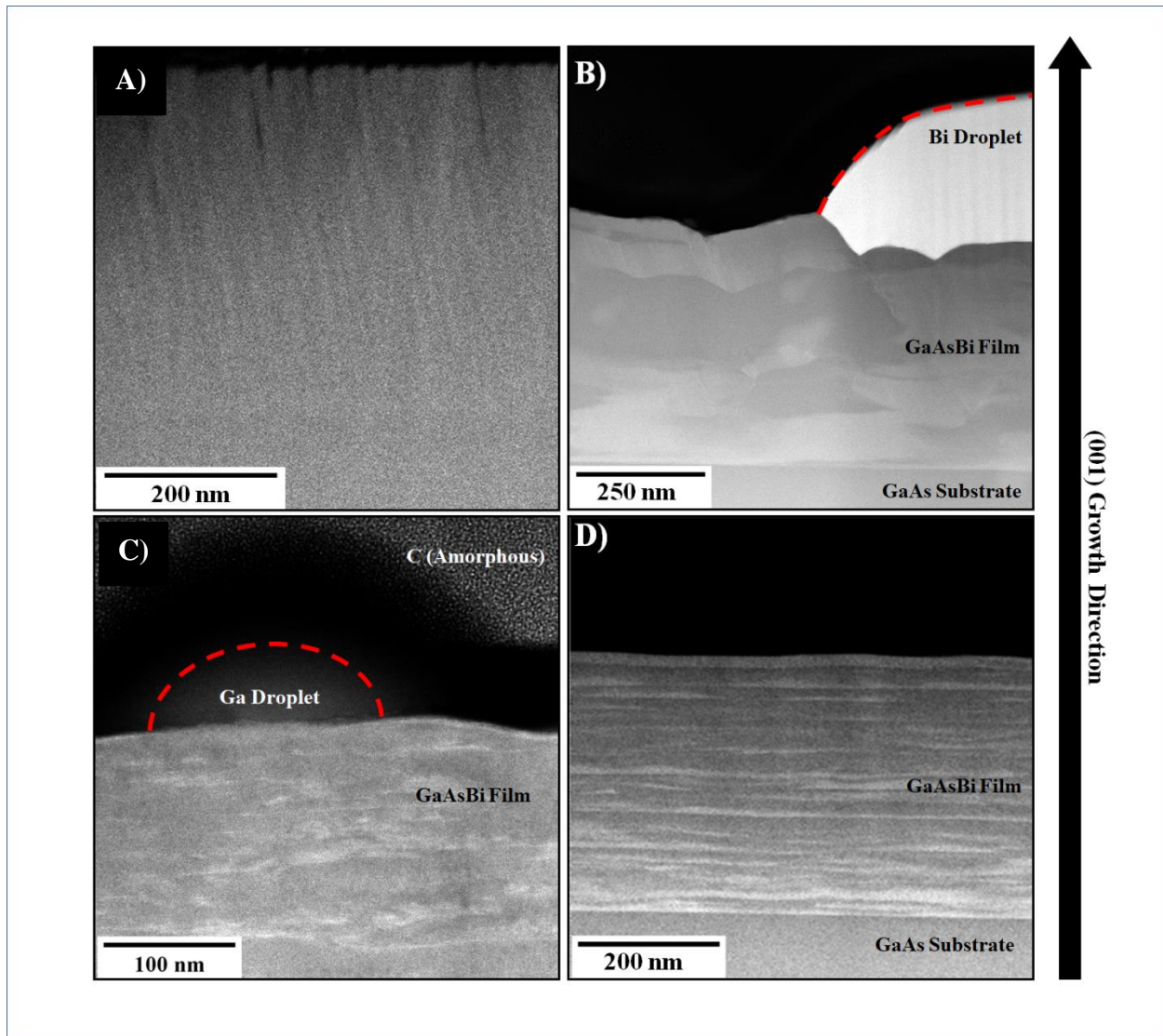
Figure 2.4.6: Cross-Sectional HAADF STEM of representative samples from each surface morphology regime. In order, they are the (a) droplet-free-surface regime [20], (b) Bi-droplet-covered regime, (c) Ga-droplet-covered regime [19], and (d) biphasic Ga-Bi-droplet-covered regime.

Figure 2.4.6 shows representative cross-sectional HAADF STEM taken of the four morphology regimes. In Fig. 2.4.6.A, a cross-section of a representative sample of the droplet-free-surface regime can be seen. The film is relatively homogenous, with some lateral Bi-composition inhomogeneities visible across the breadth of the cross-section. There are also small pin-hole-like voids in the sample extending to the surface. Further discussion of features of this film can be found in [20]. Figure 2.4.6.B shows a cross-section of a representative sample of the Bi-

droplet-covered regime. Areas with more Bi-composition can be identified by their relative lightness compared to other parts of the film and to the substrate visible below. There are large regions of varying Bi-composition, with differences in both the lateral and film growth directions, with some sharp boundaries between regions and some more-gradual differences in composition. A large Bi droplet can be seen on and embedded in the surface, and the area directly beneath it in the film can be seen to have less Bi-composition than much of the rest of the film. In Fig. 2.4.6.C, a cross-section of a representative sample of the Ga-droplet-covered regime is shown. Many film-growth-direction inhomogeneities in Bi-composition can be seen, and the variations are relatively diffuse compared to the sharp boundaries seen in Fig. 2.4.6.B. A Ga-droplet can be seen faintly on the surface, and is outlined in red dashes. On the surface of the film directly next to the droplet, there are regions of enhanced Bi-composition, while underneath the droplet there is no markedly-different Bi-composition. This trend is indicative of Ga's tendency to wick across a surface, meaning in the region directly next to the droplet there is more Ga present on the surface present to bind Bi, whereas the bulk of the droplet itself prevents Bi from easily reaching the area below the droplet to incorporate into the film. Finally, Fig. 2.4.6.D shows a cross-section of a representative sample of the biphasic Ga-Bi-droplet-covered regime. The film has many sharp growth-direction variations in Bi-composition, often looking like irregularly-spaced stripes. The high-Bi-composition inhomogeneities are thin in the growth direction in height but can extend laterally for the entire field of view. In form, the cross-section seen in Fig. 2.4.6.D is like the combination of those seen in Figs. 2.4.6.B and 2.4.6.C, having the sharply defined inhomogeneities of the Bi-droplet-covered regime sample and the growth-direction layered structure of the Ga-droplet-covered regime sample.

The behavior of the microstructure in the presence of Ga, Bi, and biphasic Ga-Bi droplets can be explained by considering the bonding energies of the different elements and assuming that all droplets move across the surface like the biphasic Ga-Bi droplets do. In the case of Ga droplets, the lower bonding energy of Ga-Ga bonds compared to Ga-As bonds [17] is expressed in Ga being known to wick across the surface of the film [22], which increases the availability of Ga on the film near the Ga droplet and makes it possible for Bi to incorporate into the film more readily. As the droplets move across the surface, this pattern of incorporation would result in regions of high-Bi-composition as remnants of where the wicking occurred, and otherwise the Bi-composition would be approximately the average composition in the sample. In the case of Bi droplets, the lower bonding energy of Ga-Bi and higher bonding energy of Bi-Bi [17] means that a Bi droplet would tend to pull Bi out of the film beneath it [21], resulting in low-Bi-composition areas tracing out the droplet path as the droplet moved around on the surface. For biphasic Ga-Bi droplets then, the process is the summation of both of the other mechanisms. At growth temperature, the biphasic droplets are composed of a liquid mixture of Ga and Bi [16], and the mixture does not separate out until cooling. As a result, the droplet acts like both a Ga droplet and a Bi droplet at the same time. A diagram of the biphasic Ga-Bi droplet behavior can be seen in Fig. 2.4.7.

a)

b)
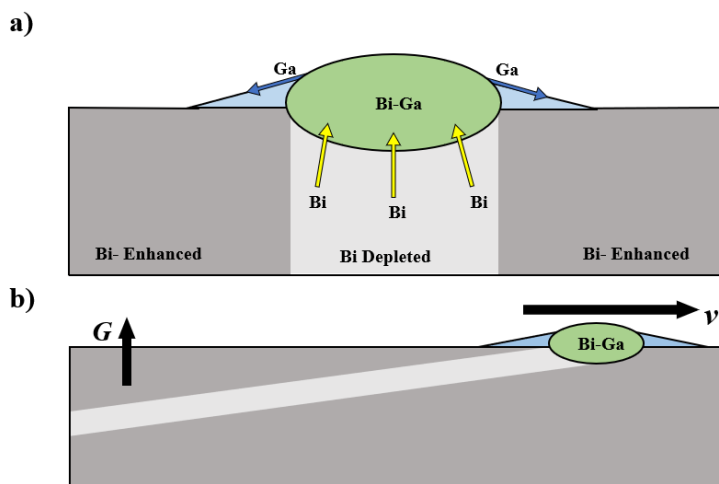
Figure 2.4.7: Bi-incorporation patterns and movement of biphasic Ga-Bi droplets. The diagram depicts the a) Bi distribution around a biphasic Ga-Bi droplet during growth and the b) growth patterns as the droplet moves across the surface. G is the velocity of growth in the growth direction, and v is the droplet velocity.

In Fig. 2.4.7.A, the distribution of Bi around a biphasic Ga-Bi droplet is shown. The Ga in the droplet wicks out along the surface, allowing for enhanced Bi-incorporation in a ring around the droplet on the surface of the film, while the Bi in the droplet pulls Bi out of the film below it, leaving a Bi-depleted region. As the droplet moves across the surface, as seen in Fig. 2.4.7.B, the Bi-depleted region extends into a wire embedded in the film, a lower-Bi-composition region surrounded by higher-Bi-composition regions. The velocity at which the droplet moves, v, and the velocity at which the film grows, G, impacts the angle of the embedded wire. If the droplet did not move, the wire would be vertical and perpendicular to the surface of the film. If v and G had similar magnitudes, the wire would be at an angle and look much like the one shown in the diagram in Fig. 2.4.7.B. However, if v >> G, as would happen with slow growths and quick droplet movement, the wire would look approximately horizontal and parallel to the surface of the film. This layered structure is what is seen in the STEM micrograph of biphasic Ga-Bi droplets seen in Fig. 2.4.6.D.

Atomic Probe Tomography (APT) of samples in this materials system have previously been reported in [20] and [19] for samples with droplet-free-surfaces and Ga-droplet-covered-surfaces, respectively. As seen in those articles, samples in the droplet-free-surface regime have largely-homogeneous Bi-compositions with occasional, ordered high-Bi-composition inclusions, whereas samples in the Ga-droplet-covered regime had larger-in-magnitude compositional inhomogeneities that were largely aligned perpendicular to the growth direction, as was seen in the STEM micrograph in Fig. 2.4.6.C. The APT for the Bi-droplet-covered regime, completed as part of this study, can be seen in Fig. 2.4.8.
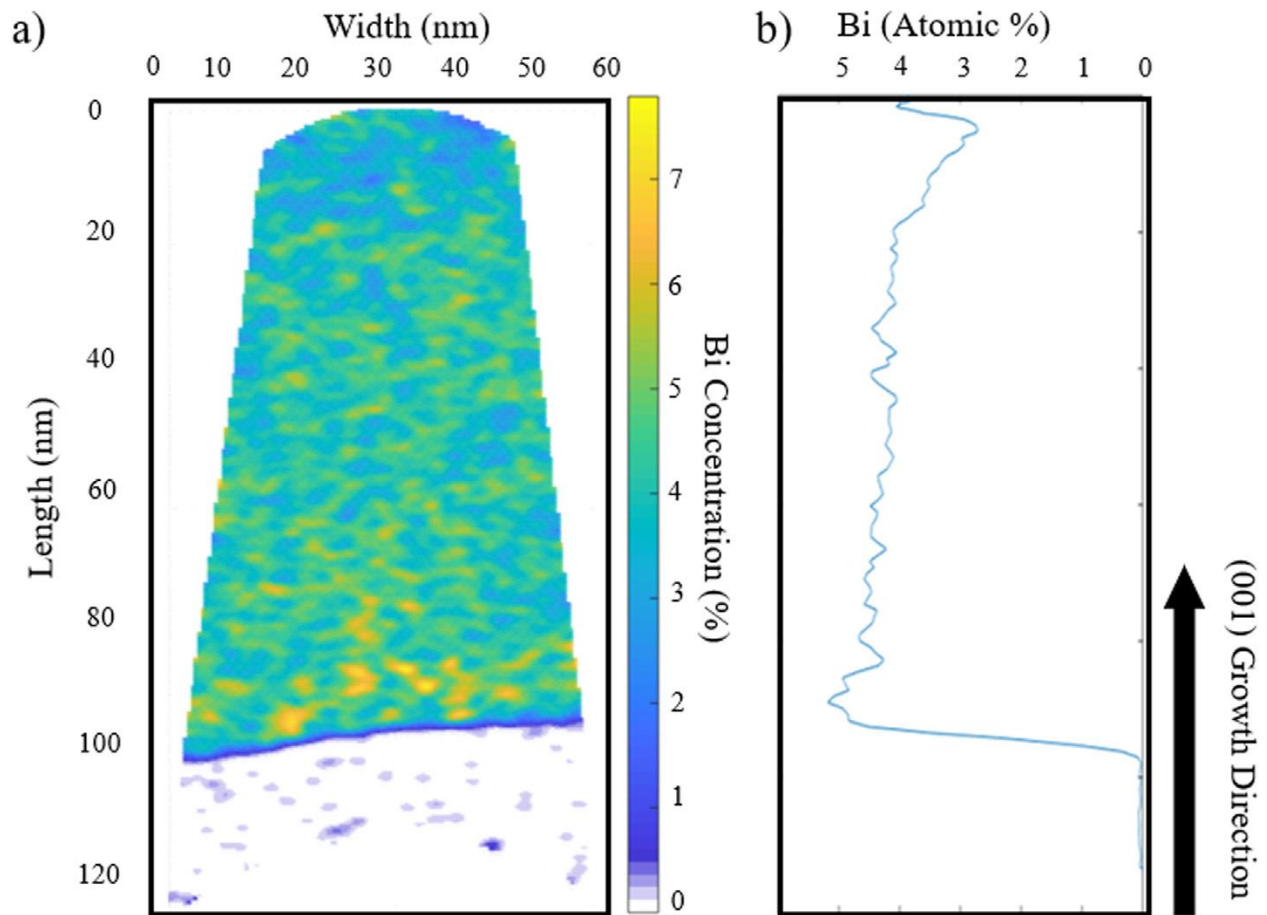
Figure 2.4.8: APT of a Bi-droplet-covered regime sample. A) A Bi-composition cross-section of the Bi-droplet-covered sample. It is unclear if the APT is taken from the film substrate interface or between bands of high and low Bi incorporation. B) Average Bi concentration throughout the length of the atom probe tip.

In the APT tomograph, a section of relatively-constant near-5%-Bi-composition can be seen, though there are apparent inhomogeneities evidenced by the bright yellow spots of greater than 6% Bi. At the bottom of the slide, the Bi-composition drops to essentially 0%, but it is unclear if this Bi-free area was part of the GaAs substrate (the APT probe then being taken from the interface between the film and the substrate) or from one of the regions seen in Fig. 2.4.6.B with low Bi-composition (the APT probe then being taken from the interface between a high-Bi-composition film region and a low-Bi-composition film region). While there do appear to be clusters of very small amounts of Bi in the low-Bi-composition area in the APT slide in Fig. 2.4.8.A, the Bi content in this region was within the noise of the APT acquisition.

Computational Predictions

This campaign or GaAsBi growths, summarized in Fig. 2.4.5 above, bears significant similarities to the computationally-determined morphology map [17], (see Fig. 2.2.4) described in Chapter 2.2, but there are also significant differences. In terms of similarities, the experimental map has the same layout of morphologies in the same relative positions. There is an encroachment of the droplet-free-surface regime towards higher Bi/As ratios as one approaches the droplet-free-surfaces to Ga-droplet-covered transition. The highest incorporation of Bi into the film is found near the intersection of the droplet-free-surface, Bi-droplet-covered, and biphasic Ga-Bi-droplet-covered regimes.

The differences between the experimental and computed morphology maps occur in three aspects: scale, boundaries, and Bi-composition. For example, in terms of scale, the experimental morphology map has the droplet-free-surfaces to Ga-droplet-covered regime transition occur at approximately an As/Ga BEP ratio of 2.1 when the Bi/As BEP ratio was 0 before decreasing to a

relatively steady 1.8 by its endpoint, whereas the computed morphology map covers the equivalent flux ratio space with the transition occurring between 1.05 and 0.85 As/Ga flux ratio. While the difference in independent variables could explain some of the differences seen (as BEP does not map exactly onto flux across different species), the droplet-free-surface to Bi-droplet-covered regime transition in the experimental map occurs at roughly the same Bi/As ratio as it is predicted to in the computed map. This inconsistency suggests that the difference in independent variables alone does not explain the differences in scale between the two maps.

The second type of difference, the boundaries, refers to how the shape of the boundaries between the morphology regimes varies between the two maps. In the computed map, the boundaries around the biphasic Ga-Bi-droplet-covered regime are linear, while the boundaries around the droplet-free-surface regime are curved and mark out approximately two different zones visually in that regime, a rectangle in the high As/Ga and low Bi/As flux ratios corner, and a point extending from that rectangle into lower As/Ga and higher Bi/As flux ratios to meet up with the boundaries surrounding the biphasic Ga-Bi-droplet-covered regime. Most crucially, all four boundaries, and thus all four regimes, meet at a single point. In contrast, in the experimental map, instead of there being one place where all four boundaries meet, there are instead two places where three boundaries, and thus three regimes, meet. This pattern traces to the fact that the two no-Bi-droplets to has-Bi-droplets transitions do not meet each other, with the Ga-droplet-covered to biphasic Ga-Bi-droplet-covered transition occurring at lower Bi/As BEP ratio than the droplet-free-surface to Bi-droplet-covered transition does. The discontinuity of the boundaries here suggests that the presence of Ga droplets may prevent Bi from incorporating into the film, and instead Bi builds up on the surface and in the liquid Ga-Bi droplets at lower Bi/As BEP ratios than those that are conducive to Bi droplets nucleating on an otherwise clean surface.

The third type of difference, the Bi-composition, is actually mostly similar between the two maps, both in placement and magnitude, with the exception of the biphasic Ga-Bi-droplet regime. That regime in the computed map has samples with the highest Bi-composition and tends to continue to increase in composition as the As/Ga flux ratio decreases and to increase and then decrease in composition as the Bi/As flux ratio increases. In contrast, in the experimental map, the Bi-composition in that region is much lower and does not follow the same trends as the As/Ga and Bi/As BEP ratios change.

Some of the differences seen between the computed and experimental morphology maps could be caused by limitations in how the computed morphology map was made. In each sample point, the classification of surface morphology happened after at most 15 monolayers of growth simulation, which is equivalent to approximately 15 seconds of growth for the samples grown in this campaign. The computed map thus cannot take into account factors such as the impact of droplets on growth, particularly the embedded nanowires proposed to occur in the presence of biphasic Ga-Bi droplets. Another limitation in similarities extends from the difference in growth temperatures. In the simulations making up the computed map, the growth temperature was set at 260°C, whereas the growths in this campaign were done at a substrate temperature of 325°C. It is expected that Bi is more likely to adhere to the surface and incorporate into the film at lower growth temperatures, and so the Bi-compositions in the computed morphology map can be assumed to be systematically higher.

Kinetic Modeling

The kinetic models described in Chapter 2.2 can inform our experimental design and let us both validate the models and elucidate possible values for the various kinetic terms included therein. From the Tait model [23] discussed in Chapter 2.2, we can derive expressions for the

steady-state behavior at the surface morphology boundaries. With these expressions and experimental values for the flux ratio values, we can then isolate and estimate the different rate parameters. First, we derive an expression for the droplet-free to Bi-droplet-covered boundary. At this boundary, R^{inc} and θ_B both tend to 0, as Bi incorporation generally drops off in the presence of Bi droplets. R^{des} can also be assumed to be approximately 0 at the low temperatures used for growths of Bi-containing materials [24], and so Eqn. 2.2.4 can be simplified, and the Bi/V flux ratio becomes:

$$\frac{F_B}{F_V} = P^{rem}.$$ Eqn. 2.4.1

Next, at the no-Bi-flux extreme of the droplet-free to group-III droplet boundary, the lack of Bi flux means that R^{inc} can be neglected. Then, Eqn. 2.2.5 can be simplified, and the V/III ratio can be calculated as

$$\frac{F_V}{F_{III}} = \frac{1}{\theta_{III}}.$$ Eqn. 2.4.2

Often the V/III flux ratio at this transition is assumed to be 1 [18], leading to a likewise-assumed θ_{III} value of 1, but that is not necessarily the case. Next, for the group-III droplet to biphasic droplet transition, R^{des} again is essentially 0 due to low substrate temperatures, and no assumptions are made about θ_S. Thus, Eqn. 2.2.4 can be simplified and the Bi/V flux ratio can be written as:

$$\frac{F_B}{F_V} = \theta_S P^{rem} + \frac{\theta_S \theta_{III}(R^{inc})^2}{F_V^2} - \theta_B P^{dis}.$$ Eqn. 2.4.3

Finally, for transition between the Bi droplet region and the biphasic region, R^{inc} can no longer be neglected, as opposed to the droplet-free to Ga-droplet-covered transition, and so Eqn. 2.2.5 can be simplified and the V/III ratio then becomes

$$\frac{F_V}{F_{III}} = \frac{F_V^2}{\theta_{III}(\theta_S(R^{inc})^2 + F_V^2)}.$$ Eqn. 2.4.4

A graphical representation of the different morphology transition relations can be seen in Fig. 2.4.9.
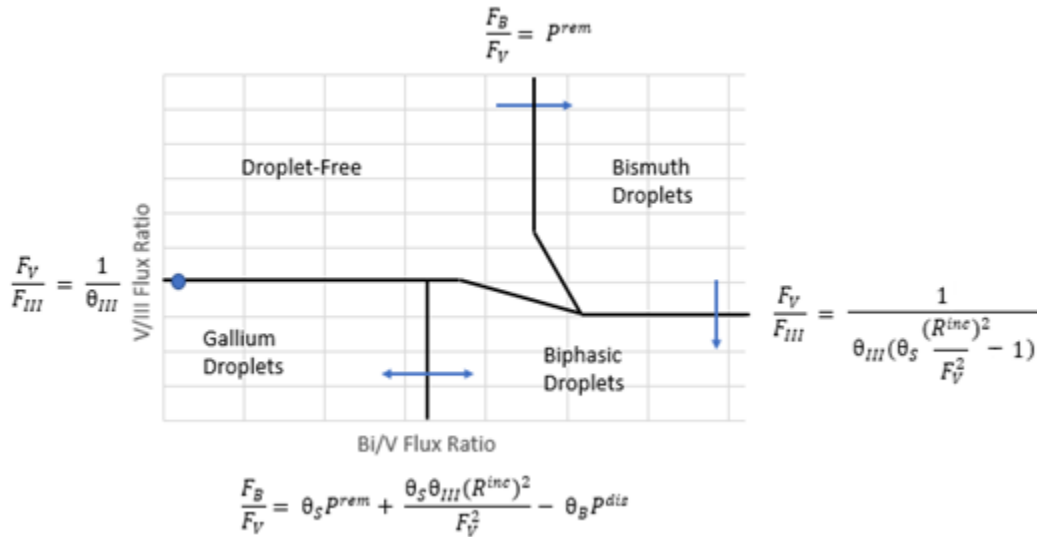
Figure 2.4.9: Expected directions of transition shift between surface phases as a function of increasing growth temperature. The arrows depict which direction the boundary should shift as growth temperature would increase. The Ga-droplet-to-biphasic-droplet boundary has a double-headed arrow due to the unclear nature of the rates impacting the boundary. The droplet-free-surface-to-Ga-droplet boundary has a dot instead of an arrow since it is expected to remain constant with respect to growth temperature.

With the experimentally-determined values for the flux-ratios at the transitions, P^{rem} and θ_{Ga} at particular growth temperatures can be pulled easily from the relations in Eqns. 2.4.1 and 2.4.2, respectively. The parameter R^{inc} can be estimated from Eqn. 2.4.4 if the θ_s coverage is assumed as 1 and the θ_{Ga} coverage is assumed to be the same as at the droplet-free to Ga-droplet-covered transition. With those assumptions, we get an estimate for R^{inc} (proportional to the F_{Ga})

as R^{inc}/F_{Ga} ~0.6. The parameter P^{dis} could be estimated from Eqn. 2.4.3, but would require different assumptions about the θ_S, θ_{Ga}, and θ_{Bi} coverages and is thus not a straightforward calculation. Instead, that kinetic parameter, as well as the others just mentioned, can be determined by taking the approach in [25] and using experimental parameters and results from multiple growths to build a dataset that can be used to solve the original Eqn. 2.2.7, discussed below. R^{des} will not be determined from these experiments, due to the consistent low growth temperatures involved. R^{des} has been previously determined in literature to be ~0 s^{-1} at growth temperatures commonly used for III-As-Bi MBE growths (~300-325 °C for the research described in this work) [24].

The number of samples grown in this campaign produces a data set of growth conditions and Bi-composition that can be used to model approximate values for the kinetic parameters of the system discussed in Chapter 2.2, and [23, 25]. To do this, the composition equation (Eqn. 2.2.7) is first converted into the following form by inserting our species for the flux ratios and dividing the numerator and the denominator by $1/F_{Ga}$, resulting in:

$$x = \frac{\frac{1}{F_{Ga}^2} R^{inc2} B}{\left(1 + A P^{dis}\right)\left(A^3 P^{rem} + \frac{A^2}{F_{Ga}} R^{des} + R^{inc2} \frac{B}{F_{Ga}^2}\right)} \qquad \text{Eqn. 2.4.5}$$

where x is the Bi composition, F_{Ga} is the Ga rate, R^{inc} is the rate of Bi incorporation into the film from the surfactant layer, B is the ratio $\frac{F_{As2}}{F_{Ga}}$, F_{As2} is the As$_2$ rate, A is the ratio $\frac{F_{Bi}}{F_{Ga}}$, F_{Bi} is the Bi rate, P^{dis} is the probability of Bi displacement to the surfactant layer from the film by an As atom, P^{rem} is the probability of Bi removal from the surfactant layer by an As atom, and R^{des} is the rate of spontaneous Bi desorption from the surfactant layer. In this version of the equation, the three experimental variables are the Bi-composition, known from XRD, and two rate ratios during growth, which we approximate with our measured BEP ratios, and the remaining 4 unknowns are

the kinetic parameters to be modeled. Rather than modeling R^{inc} exactly, the parameter is instead

treated as $\frac{R^{inc}}{F_{Ga}}$, making it proportional to the Ga rate. The equation does not account for growth in

the presence of droplets, and so only droplet-free-surfaces samples were included in the

modeling dataset.

The parameters were modeled using Wolfram Mathematica's NonlinearModelFit

function, which fits a dataset to an equation form with user-defined variables and parameters,

with defined convergence and iterations. Function options include the ability to place constraints

on the final values of parameters and to give initial guessed values for the parameters instead of

the initial default value of 1. In the modeling of Eqn. 2.4.5, P^{dis} was constrained to be greater

than 0 and less than 1, given that they are probabilities, and R^{inc} was constrained to be greater

than 0. Based on the Bi/As BEP ratio location of the droplet-free-surfaces to Bi-droplet-covered

transition in Fig. 2.4.5, (which from Eqn. 2.4.1 can be taken as equivalent to P^{rem}), P^{rem} was

constrained to be in the range 0.1-0.3, and we varied the initial guesses for P^{rem} to test for

consistency. Based on experimental work on the surface coverage of Bi at different temperatures

[26], the rate of desorption of Bi (R^{des}) at the growth temperature of 325°C was taken to be 0. All

other function options (particularly data weights and confidence levels) were left at their default

values listed in Wolfram Documentation [27]. Modeling inputs and parameter results can be seen

in Table 2.4.2.

Table 2.4.2: NonlinearModelFit inputs and resulting kinetic parameters

Model	Initial P^{rem}	R^{inc}/F_{Ga}	P^{dis}	P^{rem}
1	0	1.59	0.99	0.20
2	0.1	1.59	0.99	0.20
3	0.2	1.58	0.99	0.20
4	0.3	1.58	0.99	0.20

5	0.4	1.58	0.99	0.20
6	0.5	1.58	0.99	0.20
7	0.6	1.58	0.99	0.20
8	0.7	1.58	0.99	0.20
9	0.8	1.58	0.99	0.20

The nine models described in Table 2.4.2 are consistent with each other regardless of the initial guesses for P^{rem} and give average values for the parameters of $R^{inc}/F_{Ga} = 1.58 \pm 0.002$, $P^{dis} = 0.99$, and $P^{rem} = 0.20 \pm 0.001$. The P^{dis} values, written as 0.99, would round to 1 in most contexts but were written in that way to emphasize that they were close-to-but-not-quite unity. Given the kinetic processes described by these parameters, this combination of parameter values seems reasonable. The P^{dis} value of 0.99 suggests that Bi atoms in the film surface are displaced by As atoms almost all the time, which offsets the rate of incorporation, R^{inc}, being ~1.6 times larger than the rate of Ga arrival at the sample. Put another way, Bi atoms incorporate into the growing film at high rates, but are almost always displaced from the film by As atoms, resulting in an overall small amount of permanent Bi incorporation into the film as it grows. This scenario fits with the thermodynamic properties of the system. Ga and Bi are immiscible, and GaBi does not exist at standard temperature and pressure, whereas GaAs is a stable compound. The bonding energy for Ga-Bi bonds is much lower than that for Ga-As bonds (0.13 eV versus 0.50 eV) [17], and so Ga-Bi bonds would tend to be broken in favor of Ga-As bonds. The 0.20 value for P^{rem}, meanwhile, would suggest that Bi atoms are ejected from the surfactant layer by As atoms approximately 20% of the time, and is squarely in the range predicted from Fig. 2.4.5.

Using the parameters obtained from the nonlinear model fitting, we can insert them into our composition model (Eqn. 2.2.7) and plot the average incorporation of Bi into films grown

with various As_2/Ga and Bi/As_2 BEP ratios. A contour plot of the modeled Bi content across

roughly the droplet-free-surface morphology range is seen in Fig. 2.4.10.
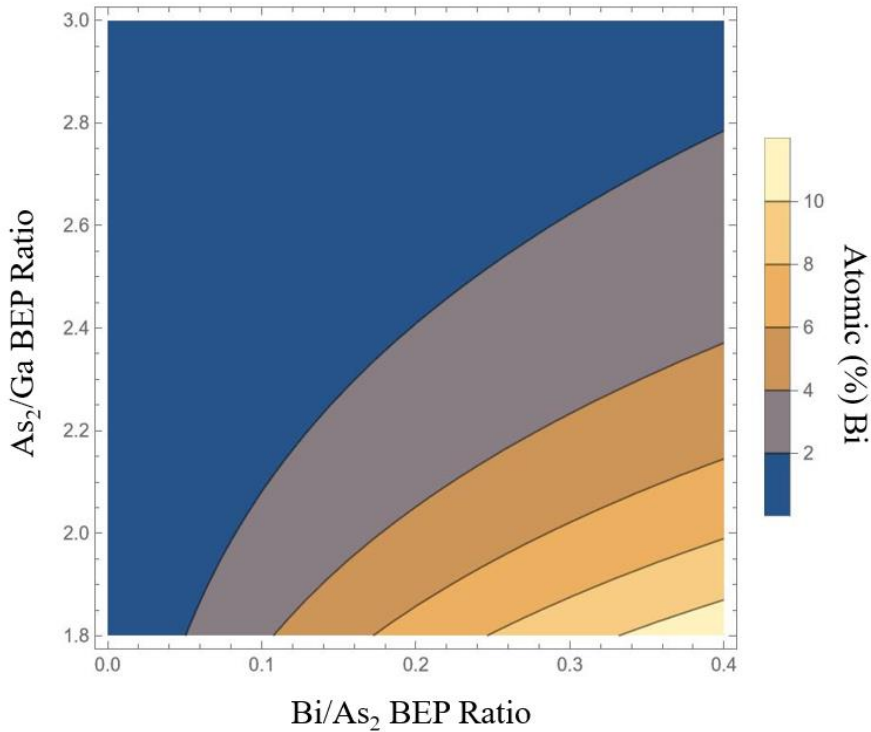
Figure 2.4.10: Contour plot of the average Bi-composition of films modeled using the incorporation model found in Eqn. 2.2.7 and the parameters estimated above. The range of the axes was chosen to roughly align with where the droplet-free-surface morphology was known to exist.

In Fig. 2.4.10, the amount of Bi incorporation increases as the Bi/As_2 BEP ratio increases and the

As_2/Ga BEP ratio decreases. The maximum amount of Bi incorporation is approximately 10%

Bi, found at the high-Bi/As_2, low-As_2/Ga extreme. The pattern of Bi content modeled in Fig.

2.4.10 largely matches the experimental Bi content seen in Fig. 2.4.5, though the average Bi

content seen in the morphology map tends to be a bit higher than that predicted here. However,

the difference in Bi content is small, and overall, the model can be seen as accurately predicting

the placement of the areas of highest Bi, even if it is a slight underestimate.

Conclusion

The campaign of GaAsBi growths shown here, as well as the characterization and modeling of the sample grown, allows us to address some of our overarching research questions. *What surface morphologies, microstructures, and Bi-compositions arise in III-As-Bi materials, and how does this change across a range of conditions?* In the case of GaAsBi, there are four surface morphologies, (droplet-free-surfaces, Bi-droplet-covered, Ga-droplet-covered, and biphasic Ga-Bi-droplet-covered), and those morphologies have been seen across a range of growth temperatures [28, 29] and the changes in morphology as the BEP ratios change at a constant temperature are seen in Figs. 2.4.3 and 2.4.5. The different morphologies have different patterns of microstructures, and the presence of droplets influences the microstructure in ways relating to the properties of the droplet itself. In the case of biphasic Ga-Bi droplets, this influence can result in embedded low-Bi nanowires in the film [21]. In the absence of droplets, films can still have defects in the microstructure including pitting [20]. The GaAsBi films have a range of average Bi-compositions from 2-14% Bi, with the Bi-content generally increasing as the Bi/As BEP ratio increases.

How do the kinetics and thermodynamics of the GaAsBi system impact the observed morphologies, microstructures, and Bi-compositions? While the kinetics of the system has some effect in terms of the normal growth and incorporation of Bi into the film, the larger impact on morphologies and especially microstructure comes from the thermodynamics of the system, mainly due to the immiscibility of Ga and Bi in the solid state and the properties of the liquid droplets. The Ga droplets tend to wick Ga across the surface, leading to areas near it with enhanced Ga availability and subsequently increased Bi incorporation [22, 19]. The Bi droplets tend to pull Bi out of the film due to the preferential Bi-Bi bonding over Ga-Bi bonding [17]. At

57

growth temperatures, Ga and Bi are both liquid and are miscible in each other, allowing for the presence of Ga-Bi liquid solution droplets that have both the Ga-wicking and Bi-leaching properties, leading to the growth of low-Bi-content embedded nanowires [21]. As the sample cools, the Ga-Bi liquid solution phase-separates into the biphasic Ga-Bi droplets that are seen in SEM.

Does the observed GaAsBi system agree with previous computational predictions? The observed GaAsBi system does not perfectly agree with the two kinds of computational predictions, but it generally agrees and the disparities can be attributed to the different sources of information. For the computed [17] and experimental [21] morphology maps, the results are qualitatively similar, and discrepancies can be attributed to the procedure used for computing the map in the case of Bi-composition or difference in axis or temperature in terms of the exact position of the morphology boundaries. The largest discrepancy, the shift in the Ga-droplet-covered to biphasic Ga-Bi-droplet-covered transition to lower Bi/As BEP ratios than expected, remains unattributed, however. For the kinetic modeling of the growth surface [23], there is no direct way to compare the results with the computational predictions, but when those kinetic models are applied to the experimental data, realistic values are obtained for the various kinetic parameters. The modeled rate of Bi incorporation and the probability of Bi displacement balance each other in a way that mirrors the results seen in the characterization of the samples. The modeled probability of Bi removal matches the version which is pulled more directly from the experimental morphology map. When the modeled kinetic parameters are used to make a map of Bi incorporation in the droplet-free-surface morphology, it matches the experimental map well in both scale and placement.

Not all of our research questions can be answered through the analysis of a single materials system. Both to support the answers found here to our questions by the contrast of another system and to answer the question of *How do different group III elements compare, and what can this tell us about the kinetics and thermodynamics of the systems*, a similar campaign must be done for another III-AsBi system, namely InAsBi.

References

[1]   J. S. Blakemore, "Semiconducting and other major properties of gallium arsenide," *Journal of Applied Physics*, vol. 53, no. 10, 1982, doi: 10.1063/1.331665.

[2]   H. J. Welker, "Discovery and Development of III-V Compounds," *IEEE Transactions on Electron Devices*, vol. 23, no. 7, pp. 664–673, 1976, doi: 10.1109/T-ED.1976.18471.

[3]   R. Barrie, F. A. Cunnell, Edmond J T, and Ross I M, "SOME PROPERTIES OF GALLIUM ARSENIDE," *Physica*, no. 11, 1954.

[4]   J. Naber, "Digital GaAs Integrated Circuits," in *Gallium-Arsenide IC Applications Handbook*, 1995, pp. 57–78.

[5]   H. Matsubara A'*, T. Tanabe, A. Moto, Y. Mine, and S. Takagishi, "Over 27% efficiency GaAs/InGaAs mechanically stacked solar cell," 1998.

[6]   R. N. Hall, G. E. Fenner, J. D. Kingsley, T. J. Soltys, and R. O. Carlson, "PHYSICAL REVIEW LETTERS COHERENT LIGHT EMISSION FROM GaAs JUNCTIONS," 1962.

[7]   S. Francoeur, M. J. Seong, A. Mascarenhas, S. Tixier, M. Adamcyk, and T. Tiedje, "Band gap of GaAs $_{1-x}$ Bi $_x$, 0<x< 3.6%," *Applied Physics Letters*, vol. 82, no. 22, pp. 3874–3876, 2003, doi: 10.1063/1.1581983.

[8]   B. Fluegel, S. Francoeur, A. Mascarenhas, S. Tixier, E. C. Young, and T. Tiedje, "Giant spin-orbit bowing in GaAs1-xBix," *Phys Rev Lett*, vol. 97, no. 6, pp. 11–14, 2006, doi: 10.1103/PhysRevLett.97.067205.

[9]   R. B. Lewis, M. Masnadi-Shirazi, and T. Tiedje, "Growth of high Bi concentration GaAs1-xBixby molecular beam epitaxy," *Applied Physics Letters*, vol. 101, no. 8, pp. 1–5, 2012, doi: 10.1063/1.4748172.

[10]   M. Yoshimoto, S. Murata, A. Chayahara, Y. Horino, J. Saraie, and K. Oe, "Metastable GaAsBi Alloy Grown by Molecular Beam Epitaxy," *Japanese Journal of Applied Physics*, vol. 42, no. 111, pp. 4–7, 2003, doi: 10.1143/JJAP.42.L1235.

[11] J. Puustinen, J. Hilska, and M. Guina, "Analysis of GaAsBi growth regimes in high resolution with respect to As/Ga ratio using stationary MBE growth," *Journal of Crystal Growth*, vol. 511, no. August 2018, pp. 33–41, 2019, doi: 10.1016/j.jcrysgro.2019.01.010.

[12] S. Tixier *et al.*, "Molecular beam epitaxy growth of GaAs1-xBix," *Applied Physics Letters*, vol. 82, no. 14, pp. 2245–2247, 2003, doi: 10.1063/1.1565499.

[13] J. Glemža *et al.*, "Low-frequency noise investigation of 1.09 μm GaAsBi laser diodes," *Materials*, vol. 12, no. 4, pp. 1–13, 2019, doi: 10.3390/ma12040673.

[14] X. Liu *et al.*, "Continuous wave operation of GaAsBi microdisk lasers at room temperature with large wavelengths ranging from 127 to 141 μm," *Photonics Research*, vol. 7, no. 5, p. 508, 2019, doi: 10.1364/prj.7.000508.

[15] A. Muhammetgulyyev, O. G. Erbas, B. Kinaci, O. Donmez, Y. G. Celebi, and A. Erol, " Characterization of a GaAs/GaAsBi pin solar cell ," *Semiconductor Science and Technology*, vol. 34, no. 8, p. 085001, 2019, doi: 10.1088/1361-6641/ab23ab.

[16] J. Đ. & D. P. D Minić, D Manasijević, D Živković, J Stajić-Trošić and To, "Experimental investigation and thermodynamic calculation of Bi–Ga–Sb phase diagram," *Materials Science and Technology*, vol. 27, no. 5, pp. 884–889, 2011, doi: 10.1179/174328409X430537.

[17] G. V. Rodriguez and J. M. Millunchick, "Predictive modeling of low solubility semiconductor alloys," *Journal of Applied Physics*, vol. 120, no. 12, 2016, doi: 10.1063/1.4962849.

[18] J. Hilska, E. Koivusalo, J. Puustinen, S. Suomalainen, and M. Guina, "Epitaxial phases of high Bi content GaSbBi alloys," *Journal of Crystal Growth*, vol. 516, no. March, pp. 67–71, 2019, doi: 10.1016/j.jcrysgro.2019.03.028.

[19] C. R. Tait, L. Yan, and J. M. Millunchick, "Droplet induced compositional inhomogeneities in GaAsBi," *Applied Physics Letters*, vol. 111, no. 4, pp. 1–5, 2017, doi: 10.1063/1.4996537.

[20] C. R. Tait, L. Yan, and J. M. Millunchick, "Spontaneous nanostructure formation in GaAsBi alloys," *Journal of Crystal Growth*, vol. 493, pp. 20–24, 2018, doi: 10.1016/j.jcrysgro.2018.04.026.

[21] B. A. Carter, V. Caro, L. Yue, C. R. Tait, and J. M. Millunchick, "The effect of III:V ratio on compositional and microstructural properties of GaAs1-xBix (0 0 1)," *Journal of Crystal Growth*, vol. 548, no. July, 2020, doi: 10.1016/j.jcrysgro.2020.125815.

[22] T. Suzuki and T. Nishinaga, "First real time observation of reconstruction transition associated with Ga droplet formation and annihilation during molecular beam epitaxy of GaAs," 1994.

[23] C. R. Tait and J. M. Millunchick, "Kinetics of droplet formation and Bi incorporation in GaSbBi alloys," *Journal of Applied Physics*, vol. 119, no. 21, p. 6, 2016, doi: 10.1063/1.4952988.

[24] T. Tiedje, E. C. Young, and A. Mascarenhas, "Growth and properties of the dilute bismide semiconductor GaAs 1-xBix a complementary alloy to the dilute nitrides," Int J Nanotechnol, vol. 5, no. 9–12, pp. 963–983, 2008, doi: 10.1504/IJNT.2008.019828.

[25] S. T. Schaefer, M. S. Milosavljevic, R. R. Kosireddy, and S. R. Johnson, "Kinetic model for molecular beam epitaxy growth of InAsSbBi alloys," *Journal of Applied Physics*, vol. 129, no. 3, Jan. 2021, doi: 10.1063/5.0035193.

[26] T. Tiedje, E. C. Young, and A. Mascarenhas, "Growth and properties of the dilute bismide semiconductor GaAs 1-xBix a complementary alloy to the dilute nitrides," *International Journal of Nanotechnology*, vol. 5, no. 9–12, pp. 963–983, 2008, doi: 10.1504/IJNT.2008.019828.

[27] Wolfram Research, "NonlinearModelFit," Wolfram Language function, 2008, https://reference.wolfram.com/language/ref/NonlinearModelFit.html.

[28] A. J. Ptak *et al.*, "Kinetically limited growth of GaAsBi by molecular-beam epitaxy," *Journal of Crystal Growth*, vol. 338, no. 1, pp. 107–110, 2012, doi: 10.1016/j.jcrysgro.2011.10.040.

[29] A. W. Wood, K. Collar, J. Li, A. S. Brown, and S. E. Babcock, "Droplet-mediated formation of embedded GaAs nanowires in MBE GaAs1-xBixfilms," *Nanotechnology*, vol. 27, no. 11, 2016, doi: 10.1088/0957-4484/27/11/115704.

CHAPTER 2.5

InAsBi

Background

Indium arsenide (InAs) is a III-V semiconductor with a unit cell length of 6.058 Å [1] and a bandgap of 0.356 eV [1]. Like other III-V semiconductor materials, the compound does not appear in nature and must be manufactured [2], originally generally by either the cooling of a stoichiometric melt producing polycrystalline InAs [3] or the Czochralski crystal pulling method producing monocrystalline InAs [2]. In the late-1950s InAs began coming under serious study [2], and it has since been used for a variety of electronic applications, including laser diodes [4], transistors [5], Hall sensors [6], infrared detectors [7], and solar cells [8].

Like GaAs, InAs has been targeted for alloying with Bi in order to alter the bandgap and target the mid-IR range. InAsBi was first synthesized in 1989 by OMVPE [9], and has a bandgap dependence of between 42-55 meV/% Bi [9-10]. The highest Bi-composition obtained in this material was 6.45% Bi, in a sample grown by MBE [11], but InAsBi is also commonly grown using MOVPE [12-14]. InAsBi has been used for a photodiode demonstrated to operate in the mid-IR region [15], and has been studied for use in lasers [16]. While Bi is expected to have an effect on the spin-orbit splitting energy, the bandgap of pure InAs is small enough that recent

calculations suggest that the alloying of Bi with InAs may not suppress Auger recombination, as the SO splitting energy is already greater than or about the same as the bandgap [17].

In contrast to Ga, In and Bi are miscible in each other, and can form a variety of fixed-composition compounds, namely InBi, In_2Bi, and In_5Bi_3, as seen in their binary phase diagram in Fig. 2.2.2.E. This variety of In-Bi compounds makes it challenging to control the incorporation of Bi into InAsBi, with the different In-Bi phases separated by only minute changes in overall composition, as seen in the InAsBi ternary phase diagram in Fig. 2.5.1.
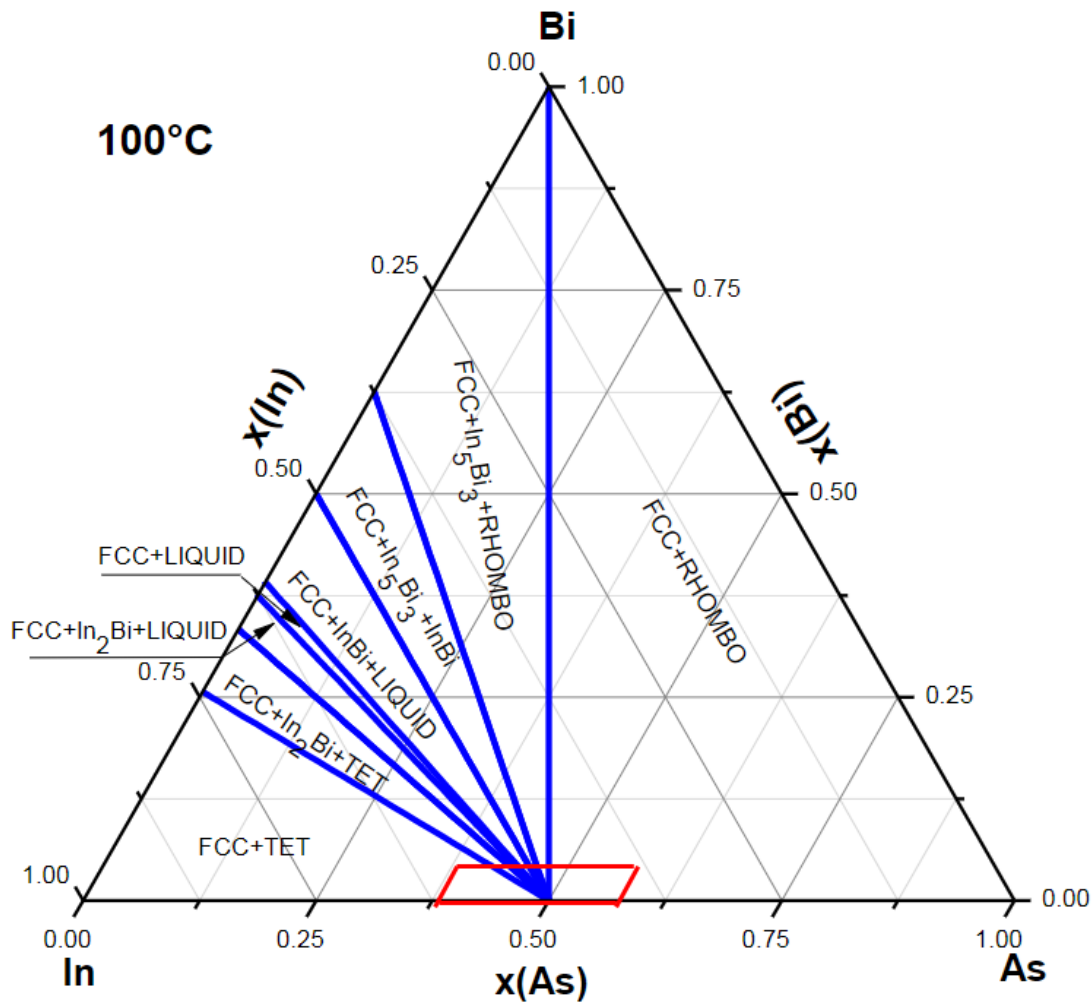
Figure 2.5.1: The ternary phase diagram for InAsBi at 100°C [18]. The red box indicates the range of compositions used for growths in this work.

As the thermodynamics of the In-As-Bi system allow for the presence of different In-Bi phases, the alloying of Bi substitutionally into InAs is done using low growth temperatures. As with GaAsBi, the low growth temperatures serve to kinetically freeze the Bi in place in the InAs lattice. Typical growth temperatures range from 260°C [19] to 370°C [20], with the highest incorporation samples grown at 270-280°C [11]. There is one example in the literature of an MBE sample grown containing InBi inclusions, where roughly-spherical InBi clusters were found embedded in a InAsBi film matrix with a tetragonal PbO structure [21]. Previous MBE growths of InAsBi have found two surface morphologies, droplet-free surfaces [11, 20], and droplet-covered surfaces [19, 22]. The droplets are identified as Bi droplets, but SEM or EDS of the surface is not provided. Previous growths tend to be done with capping layers, possibly affecting the observed morphologies. In MOVPE growths, the observed morphologies are droplet-free (usually cross-hatched) [23-24], droplet-covered, and whisker (likely droplet trails) [24]. Our studies focus on MBE-grown InAsBi without capping layers, and so different morphologies can be observed.

We will focus our efforts with InAsBi on addressing the overall research question of *What surface morphologies, microstructures, and Bi-compositions arise in MBE-grown InAsBi films, and what can this tell us about their kinetics and thermodynamics?* To guide our process, the question is split into three more-direct questions: 1. *What surface morphologies, microstructures, and Bi-compositions arise in In-As-Bi materials, and how does this change across a range of conditions? 2. How do the kinetics and thermodynamics of the InAsBi system impact the observed morphologies, microstructures, and Bi-compositions? 3. How do different group III elements compare, and what can this tell us about the kinetics and thermodynamics of the systems?*

InAsBi Growth Series

To address and attempt to answer our research questions above, namely to study what surface morphologies and microstructures arise in MBE-grown III-As-Bi materials and how the kinetics and thermodynamics of the system impact the observed morphologies and microstructures, we grew 23 InAsBi samples with various As/In and Bi/As BEP ratios, ranging from 0.47-3.05 for As/In BEP ratios and 0-0.14 for Bi/As BEP ratios. Variable growth parameters for the InAsBi samples are given in Table 2.5.1, while constant growth parameters can be found in Chapter 2.3.

Table 2.5.1: Variable growth parameters for the 23 InAsBi films

Sample number	In Rate (ML/s)	As_2 BEP	As_2/In BEP ratio	Bi/As_2 BEP ratio	% (at) Bi	w_{OOM}	Morphology
1	0.5	1.35E-06	3.05	0.056	0.00	NA	Bi droplets
2	0.51	9.49E-07	2.05	0.082	0.00	NA	Bi droplets
3	0.48	9.76E-07	2.10	0.049	0.00	NA	Bi droplets
4	0.5	9.78E-07	2.05	0.038	0.00	NA	Droplet-free
5	0.55	5.75E-07	1.08	0.054	3.18	0.14	Bi droplets
6	0.55	5.75E-07	1.08	0.049	1.64	0.35	Bi droplets
7	0.53	4.24E-07	0.83	0.104	1.20	0.34	Bi droplets
8	0.51	3.49E-07	0.74	0.097	3.44	0.16	Bi droplets
9	0.51	7.13E-07	1.56	0.073	0.00	NA	Bi droplets
10	0.51	7.13E-07	1.56	0.059	0.00	NA	Bi droplets
11	0.51	6.55E-07	1.50	0.047	0.00	NA	Bi droplets
12	0.51	6.55E-07	1.50	0.038	0.00	NA	Droplet-free
13	0.51	6.09E-07	1.51	0.029	0.00	NA	Droplet-free
14	0.5	5.35E-07	1.26	0.000	0.00	NA	Droplet-free
15	0.5	4.07E-07	0.96	0.000	0.00	NA	In droplets
16	0.49	2.37E-07	0.58	0.000	0.00	NA	In droplets
17	0.49	2.28E-07	0.54	0.139	3.92	0.22	Bi droplets
18	0.49	1.96E-07	0.47	0.085	0.03	0.05	Mixed In-Bi droplets
19	0.48	2.24E-07	0.56	0.057	0.11	0.08	Mixed InBi droplets
20	0.48	2.44E-07	0.77	0.035	1.32	0.07	Droplet-free
21	0.51	2.19E-07	0.51	0.047	0.21	0.09	Mixed InBi droplets

| 22 | 0.51 | 1.17E-06 | 2.73 | 0.013 | 0.00 | NA | Droplet-free |
| 23 | 0.5 | 4.21E-07 | 1.00 | 0.037 | 1.63 | 0.08 | Droplet-free |

The procedure outlined in Chapter 2.3 was used for each sample growth, and SEM and EDS were subsequently used to categorize each sample's morphology, while XRD was used to assess film quality and Bi incorporation. Representative samples of each morphology were characterized using TEM. To see trends, the morphology and composition results for each sample were placed on a morphology map like that created for GaAsBi in Chapter 2.4, where the axes are the As/In and Bi/As BEP ratios. The transitions between different morphologies on the map were estimated according to boundaries between samples of different morphologies.

Surface Morphology

In the samples grown for this campaign, the four expected InAsBi surface morphologies were observed, those being droplet-free, Bi-droplet-covered surfaces, In-droplet-covered surfaces, and mixed In-Bi-droplet-covered surfaces. Examples of these four morphologies observed in our samples can be seen in Fig. 2.5.2.
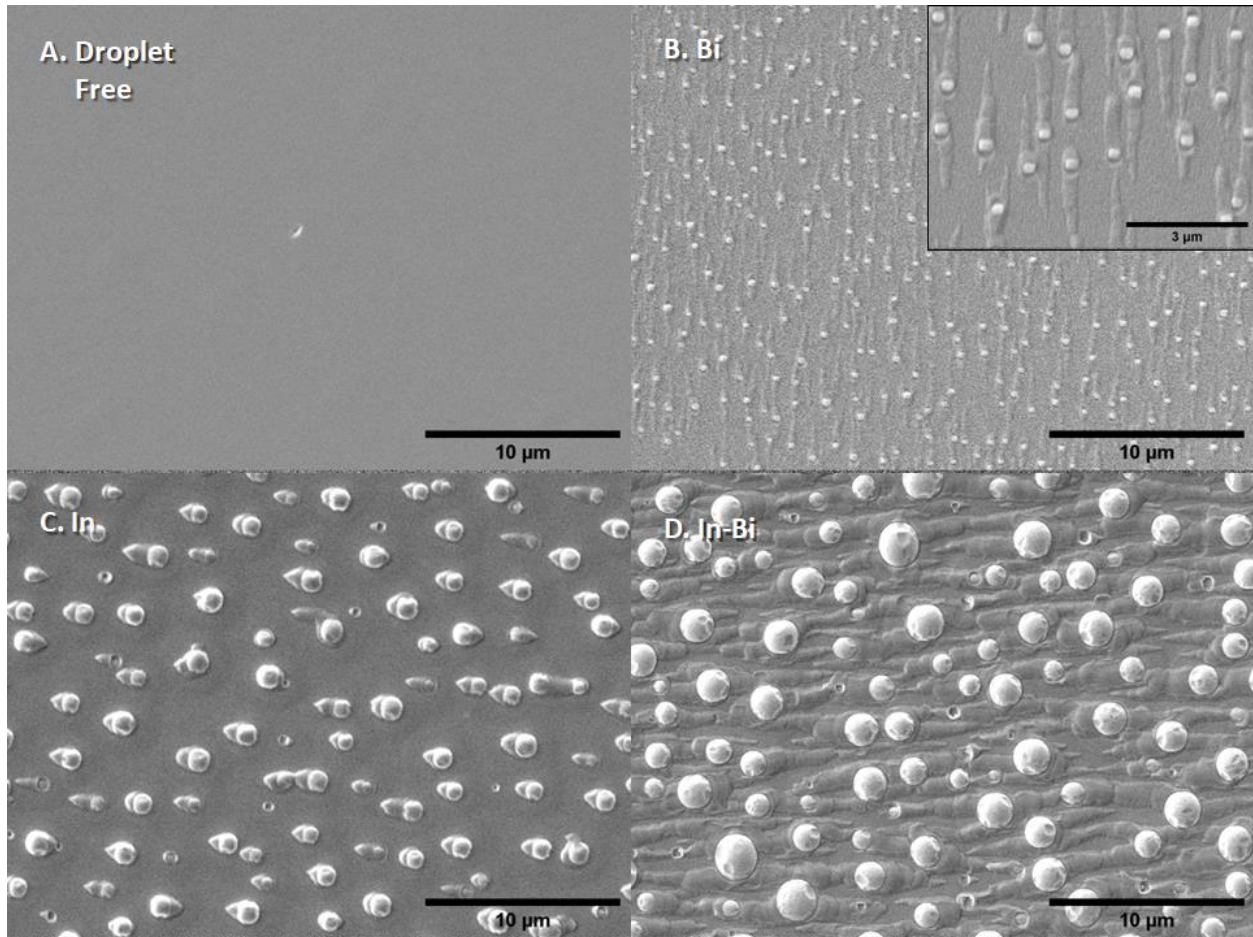
Figure 2.5.2: SEM micrographs of representative samples of each surface morphology regime. In order they are the (A) droplet-free surface regime, (B) Bi-droplet-covered regime with an inset to show details of the droplets, (C) In-droplet-covered regime, and (D) mixed In-Bi-droplet-covered regime.

In Fig. 2.5.2.A, a typical droplet-free surface is seen. It is largely featureless, though a small pit or imperfection can be seen. Figure 2.5.2.B shows a Bi-droplet-covered surface. The droplets are approximately uniform in shape, generally being slightly rectangular with an aspect ratio of around 5:4, and in size, ranging from 250-350 nm on the long side. There are visible droplet trails behind each Bi droplet that indicate the droplets move during growth, with visible lengths generally longer than 2 μm but not more than 2.5 μm. The droplet trails are oriented along the [1-10] or [-110] directions, and the longer side of each droplet is perpendicular to the droplet trail. The surface between the droplet trails exhibits some roughness, with anisotropic ripples running parallel to the droplet trails, with approximately 100 nm between peaks.

67

An In-droplet-covered surface can be seen in Fig. 2.5.2.C, where the In droplets are more lens-shaped than the Bi droplets seen in Fig. 2.5.2.B and are much larger, being around 0.6-1.1 μm in diameter. The In droplets also have droplet trails oriented parallel or antiparallel to each other, but they are usually short (less than 1 μm in length) and come to a sharp point, leaving an overall triangular shape. The larger droplets especially can be seen to have circular rings around them on the surface, suggesting they sit on a shallow cone extending approximately 1 μm from the edge of the droplet. Several square pits can also be seen on the surface and some have very short droplet trails extending from them, indicating that the pits were left behind after small In droplets desorbed from the surface. The final surface morphology, mixed In-Bi droplet-covered surfaces, can be seen in Fig. 2.5.2.D. The droplets have about the same density across the surface as the In droplets seen in Fig. 2.5.2.C, but can be larger and vary more in size, ranging from 0.5-2.4 μm in diameter. The mixed In-Bi droplets themselves are generally circular but exhibit some faceting on the surface. The droplets leave extensive droplet trails behind themselves, which are generally aligned parallel or antiparallel to each other and overlap to the extent that an average length cannot be ascertained. The droplet trails themselves are raised from the surface and are smooth or slightly rounded on top but slope more sharply to the sample surface at their edges over the course of around 200 nm. Very little of the surface can be seen between the droplet trails, but what is visible of it appears to have some roughness. There are some pits left behind at the ends of short droplet trails indicating some smaller droplets were desorbed off the surface. Unlike the equivalent morphology found in the GaAsBi system (biphasic Ga-Bi droplets), the In-Bi droplets display a single homogeneous phase in SEM and EDS, with the In and the Bi evenly mixed.

Microstructure

The microstructure of the InAsBi films of different morphology regimes, as characterized

by XRD, follows certain trends, which can be seen in Fig. 2.5.3.
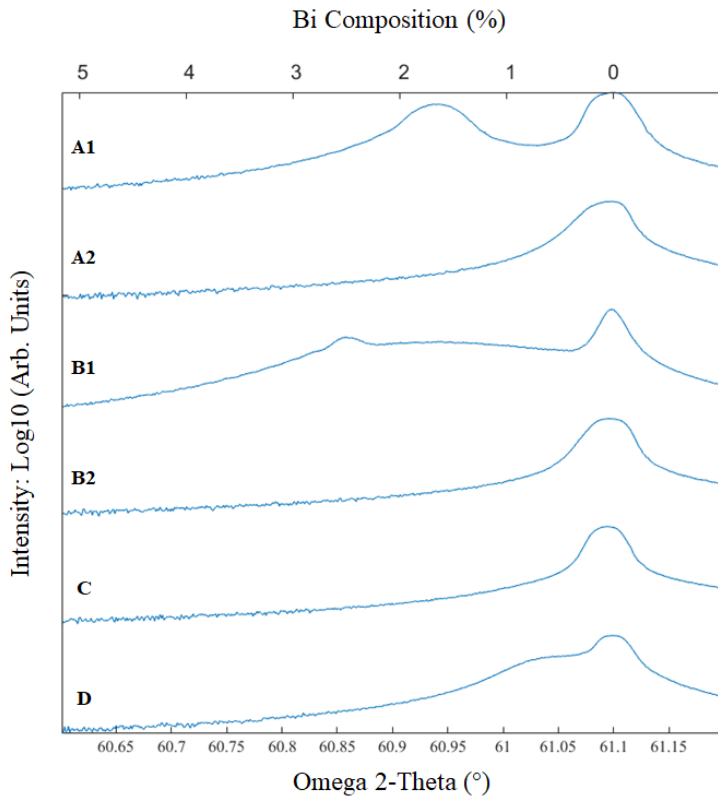
Figure 2.5.3: Representative ω-2θ XRD scan profiles associated with the four InAsBi morphologies. A) Droplet-free sample, B) Bi-droplet-covered sample, C) In-droplet-covered sample, D) Mixed In-Bi-droplet-covered sample. There are two profiles each for the droplet-free and Bi-droplet-covered morphologies to illustrate the lack of film peak in some samples. The upper x-axis represents the atomic percentage of Bi calculated using Vergard's law.

Figure 2.5.3.A1 shows the representative ω-2θ XRD scan for the droplet-free-surface regime.

The film peak at 60.94° (1.63% Bi) is well-separated from the substrate peak and is slightly

broader, indicating that there are minor and uncommon inhomogeneities in the film, as there are

a range of Bi compositions closely grouped around the average composition marked by the film

peak maximum. However, in Fig. 2.5.3.A2, we see another example of microstructure found

with the droplet-free-surface morphology, where there is no film peak at all. The samples from

which the two ω-2θ XRD scans were taken varied mainly in their As/In BEP ratios, where the sample with a film peak had an As/In BEP ratio of ~1 and the sample with no film peak had an As/In BEP ratio of ~1.5. None of the samples with the droplet-free morphology grown with As/In BEP ratios above 1.1 had film peaks. In Fig. 2.5.3.B1, we see instead the representative ω-2θ XRD scan for the Bi-droplet-covered regime. Here there is also a defined film peak at 60.86°, but it is overlaid on a broad and high-intensity film shoulder giving the sample a w$_{OOM}$ (width of the sample one order of magnitude below the film peak maximum) of 0.354 and a median peak of 60.94°, indicating that there is a somewhat-preferred Bi composition in the film but there are also widespread compositional inhomogeneities in the film. On the other hand, in Fig. 2.5.3.B2, there is another example of an absent film peak, this time in a sample with Bi droplets. Again, in this case, the main variation between the samples' growth conditions was the As/In BEP ratio, with values of ~1.1 and 1.5 for the present-film-peak and absent-film-peak, respectively. None of the samples with the Bi-droplet-covered morphology grown with As/In BEP ratios above 1.1 had film peaks.

The representative ω-2θ XRD scan for the In-droplet-covered regime is shown in Fig. 2.5.3.C. In this case, there is an absent film peak for the reason that the only samples that were found to have In, rather than mixed In-Bi, droplets were samples in which no Bi BEP was applied. The ω-2θ XRD scan profile is shown here for comparison only. Finally, Fig. 2.5.3.D shows the representative ω-2θ XRD scan for the mixed In-Bi-droplet-covered regime. For this regime, instead of a film peak there is a small film shoulder, indicating that some Bi incorporated into the film, but not very much and with inhomogeneous incorporation. The maximum incorporation is approximately 1.5% Bi and the midpoint of the w$_{OOM}$ width is 61.08°.

As can be seen in Fig. 2.5.3, overall only three of the morphology regimes were found with Bi incorporation, and all incorporation happened when the As/In BEP ratio was less than 1.1. When there is incorporation, some cases have defined film peaks while others are more likely to result in film shoulders. In all incorporation examples, there is some degree of inhomogeneity in composition present. Due to the presence of frequent film shoulders (much like as was seen in GaAsBi in Chapter 2.4), we once again use the w_{OOOM} measure to compare film quality between different samples and between different regimes.

Morphology Map

Every sample had its surface morphology characterized by SEM and EDS and its microstructure characterized by XRD and was placed onto an InAsBi surface morphology map, seen in Fig. 2.5.4.
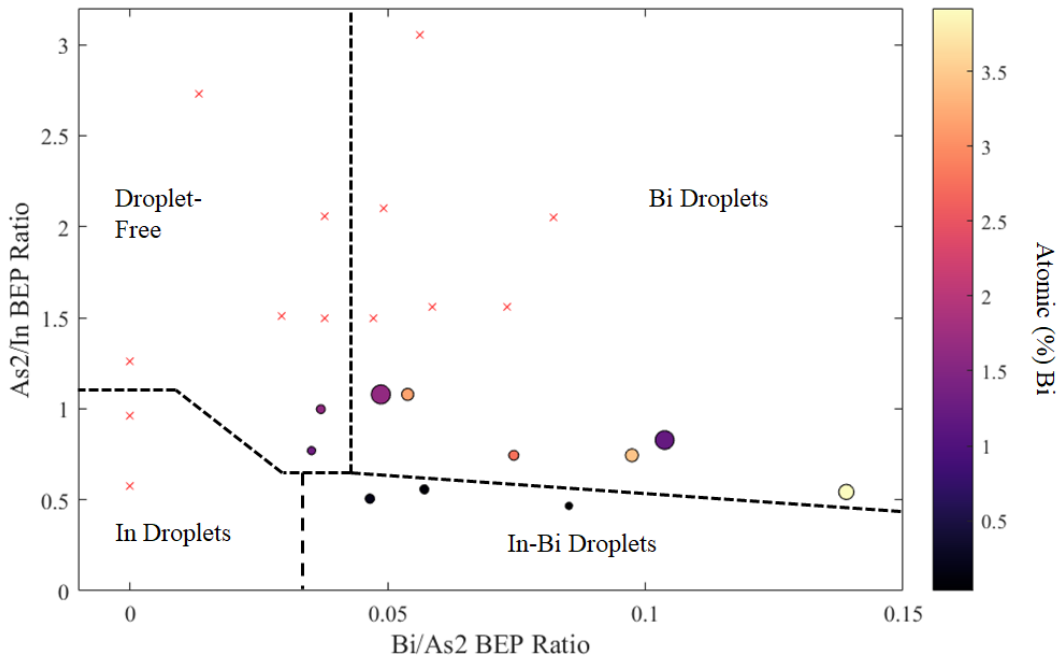
Figure 2.5.4: Morphological map of the 23 InAsBi samples grown at 300°C and annealed for 5 min. The small-dashed lines represent the qualitative boundaries between the different regimes, while the line with longer dashes is a hypothetical boundary and does not represent real data. The color of the marker represents the atomic percentage of Bi in the sample determined by XRD, and the size of the marker represents the w_{OOM} value of each sample except for the 13 samples that either had a Bi/As BEP ratio of zero or no film peak, where the lack of film peak means no w_{OOM} could be calculated. These samples are instead marked with an ×. For scale, the marked samples A and B have w_{OOM} of 0.08° and 0.35°, respectively.

The w$_{OOM}$ values for the different samples are used for the size of the point, with an × displayed for samples with no film peak. The four surface morphologies are partitioned roughly into the four quadrants of the morphology map made with the axes of Bi/As BEP ratio and As/In BEP ratio. When the As/In BEP ratio is more than approximately 0.6-1.1 and the Bi/As BEP ratio is less than 0.042, the droplet-free morphology can be seen. While XRD shows Bi incorporation in some of the samples, indicating that the incoming As, In, and Bi fluxes are being incorporated into the growing film, not all samples show incorporation. Thus, this morphology can only be said to be marked by the lack of In or Bi buildup on the surface of the sample. When the As/In BEP ratio is greater than 0.5 and the Bi/As BEP ratio is greater than about 0.042, the surface instead displays the Bi-droplet-covered morphology, where the Bi flux is high enough in comparison to the other fluxes to reach a critical point and allows Bi droplets to grow beyond nucleation. When the As/In and Bi/As BEP ratios are less than 1.1 and near-zero, respectively, the In-droplet-covered surface morphology can be found, as there is neither enough As flux to bond with the incoming In and incorporate into the film, nor is there enough Bi flux to lead to the nucleation and growth of mixed In-Bi droplets. When the As/In BEP ratio is below approximately 0.5 and the Bi/As BEP ratio is above approximately 0.4, mixed In-Bi droplets form, as the smaller proportion of As leads to In accumulation on the surface and the proportion of Bi becomes large enough that Bi on the surface can coalesce into droplets. The values for the BEP ratio boundaries are approximate, and not universal. Especially, the boundary marked between the In-droplet-covered and mixed In-Bi-droplet-covered is placed arbitrarily on the map merely to note that the boundary occurs somewhere. The exact location of said boundary could not be determined in this study due to the inability to grow samples in that range of BEP ratios. There is a tendency as the Bi BEP increases and the In BEP decreases for droplet-free

72

morphologies to remain, taking up the space in the center-left of the morphology map, being where the droplet-free samples with film peaks were located, but other morphologies emerge as the As/In and Bi/As ratios continue to increase and decrease, respectively.

Trends in Bi composition of the samples, measured as the median Bi composition, can also be seen across the morphology map in Fig. 2.5.4. In general for the droplet-free and Bi-droplet-covered morphologies, the atomic percentage of Bi in the film increased as the Bi/As BEP ratio increased and the As/In BEP ratio decreased, reaching a maximum at 3.92% Bi for a sample grown at a As/In BEP ratio of about 0.54 and a Bi/As BEP ratio of 0.14. There was one exception in the Bi-droplet-covered regime, but that sample did have a broad film shoulder, indicating there were parts of it that had higher Bi incorporation than that seen on the morphology map. On the other hand, in the mixed In-Bi droplet regime, samples tended to have relatively low and consistent atomic percentages of Bi, having inhomogeneous film Bi compositions between 0% Bi and 1.5% Bi among the three samples in that regime, due to the small film shoulders seen in the XRD data here. In general, the w$_{OOM}$ values seen in Fig. 2.5.4 indicate that the presence of droplets in conjunction with Bi incorporation is detrimental to the film quality, but the impact of droplets within droplet-covered regimes does not form a clear trend.

Phase Determination

While the ω-2θ XRD scans around the (0 0 4) substrate peak at 61.1° are able to elucidate what proportions of Bi are in the InAsBi films, they cannot tell us whether there are other phases present. Instead, to determine if there is only epitaxial InAsBi growth or if the In and Bi present have precipitated into the other thermodynamically-stable phases possible, ω-2θ XRD scans from 0-70° were done for a subset of the samples. These wide scans identified some low-

intensity but anomalous peaks at 22.5°, 42.1°, 45.9°, and 48.8°. Examples of the anomalous peaks can be seen in Fig. 2.5.5.
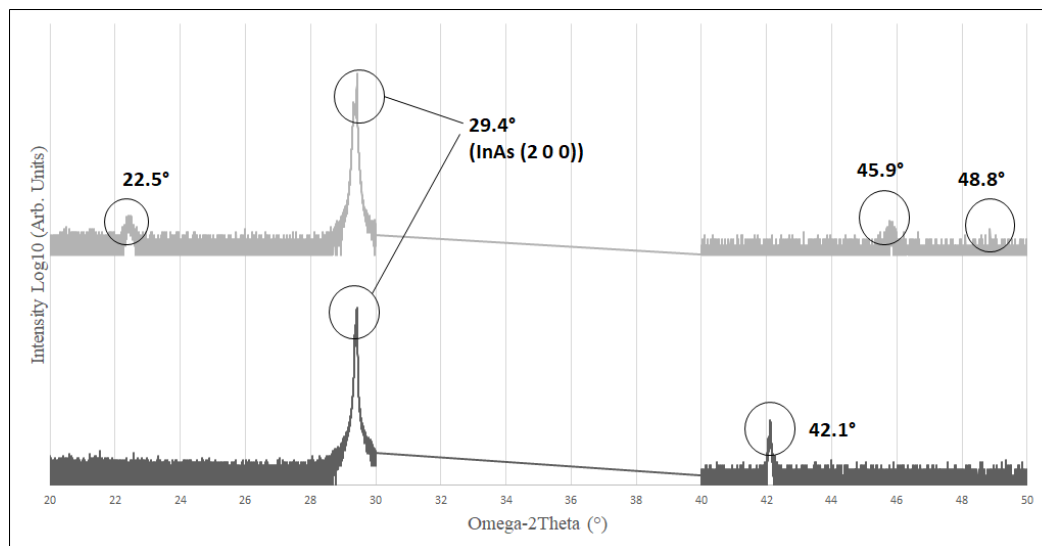
Figure 2.5.5: Representative ω-2θ XRD scan profiles of the 20-30° and 40-50° ranges displaying the anomalous peaks.

Subsequently, more, narrower high-resolution ω-2θ XRD scans were done for every sample near those locations to determine the prevalence of these peaks. A version of the morphology map showing the prevalence of the different anomalous peaks across the BEP ratio space can be seen in Fig. 2.5.6.
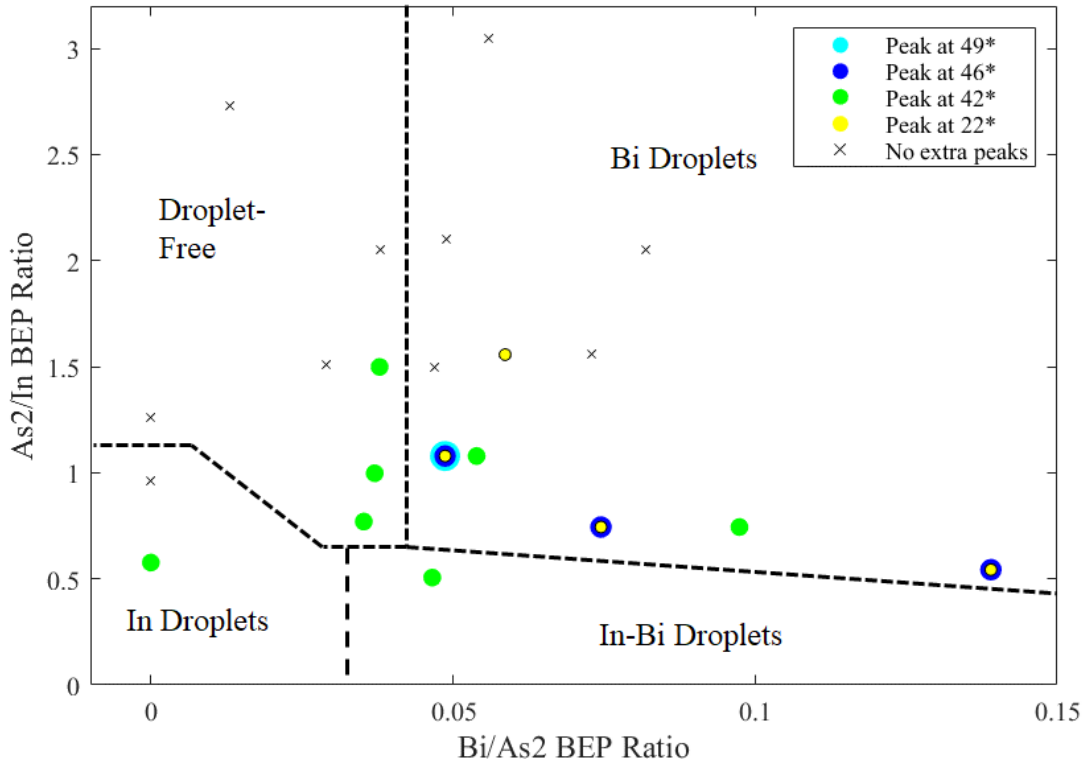
Figure 2.5.6: Map of non-InAsBi peaks seen in the various InAsBi samples. Samples marked with × had no anomalous peaks found, while all other samples are marked with colors indicating which peak was found in that sample. As given in the legend, yellow dots are for peaks at 22.5°, green dots for 42.1°, blue dots for 45.9°, and red dots for 48.8°.

In Fig. 2.5.6, the samples with the anomalous peaks are spread throughout the BEP ratio space, though they are generally found in samples with lower As/In BEP ratios. There are samples with low As/In BEP ratios that have no anomalous peaks, and there are some samples seen with the peaks that are above the 1.1 As/In BEP ratio associated with a lack of InAsBi film peaks. Based on the elements used in growth, there are a few possibilities for the identity of the anomalous peaks, as shown in Table 2.5.2.

Table 2.5.2: Possible peak matches for the anomalous peaks in our InAsBi samples. Bolded entries indicate the most likely identity.

Peak (°)	Matched Peak(s) (°)	Possible Phase	Matched Peak Identity	Reference
22.5	20.78	In$_5$Bi$_3$	200	[25]
	22.47	**Bi**	**003**	**[26]**
	24.31	In$_5$Bi$_3$	211	[25]
	25.25	As	003	[27]
	25.35	InBi	110	[28]
	25.44	InAs	111	[29]
42.1	42.12	InBi	102	[28]
	42.15	**InAs**	**220**	**[29]**
	42.28	In$_5$Bi$_3$	400	[25]
45.9	**45.86**	**Bi**	**006**	**[26]**
	46.08	InBi	112	[28]
	46.75	In$_2$Bi	002	[30]
48.8	48.26	As	110	[27]
	48.91	In$_5$Bi$_3$	413	[25]
	49.89	InAs	311	[29]

The possible peak matches listed in Table 2.5.2 do show a few trends. The 22.5° and 45.8° peaks are matched by the Bi (0 0 3) and (0 0 6) peaks, respectively. Given that these peaks only appeared in the presence of Bi droplets, it is likely that these small peaks are from the well-aligned Bi droplets on the surface. Second, although there are a few different possibilities for the identity of the 42.1° peak, the best match is likely InAs (2 2 0). This match is due to the presence of the 42.1° peak in one of the In-droplet-covered samples, which contained no Bi, leading us to reject the Bi-containing matches. The presence of an InAs (2 2 0) peak would suggest that there are some small, misaligned areas of InAs that have grown. The 48.8° peak has a few different possibilities, but as it only occurs in one sample it is difficult to rule out possible phases. Despite

the presence of the extra peaks, their intensity is low, with even the largest peak (a 42.1° peak in

one of the droplet-free samples) being three orders of magnitude smaller than the sample's film

peak. The low intensity suggests that any other phases would only be present in small amounts.

STEM

While the ω-2θ XRD scans are useful for examining average Bi-composition and film

quality, the widespread presence of inhomogeneities necessitates the close study of the

microstructure by STEM instead. STEM of representative samples in each of the three Bi-

containing regimes is presented here, and can be seen in Fig. 2.5.7.
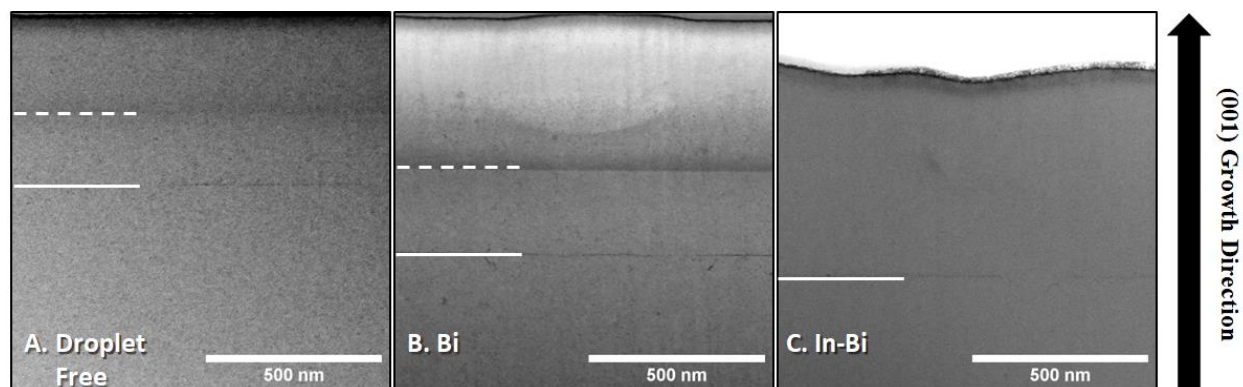
Figure 2.5.7: Cross-Sectional BF STEM of representative samples from the three Bi-containing surface morphology regimes. In order, they are the A) droplet-free-surface regime, B) Bi-droplet-covered regime, and C) mixed In-Bi-droplet-covered regime. The solid lines indicate the interface between the substrate and the buffer layer, while the dashed line indicates the interface between the buffer layer and the film. C) does not have a dashed line because the location of the buffer-film interface is unclear.

In Fig. 2.5.7.A, a representative STEM micrograph of a droplet-free-surface morphology sample

can be seen. The transition between the substrate and the buffer layers are marked by a thin line

of precipitates, whereas the transition between the buffer layer and the film is marked by a

diffuse drop in intensity, where darker areas in the micrograph indicate the presence of Bi. There

are speckles visible throughout the micrograph, which we found to be consistent across BF

micrographs. The speckles are seen in both the grown films and the substrate, suggesting that

they are not related to composition, and are not differentiated from the film when EDS is run.

The film shows uniform contrast in the lateral direction, which suggests laterally-uniform Bi content. Line profiles of the micrograph (not shown) indicate a consistent drop in intensity from left to right in all three sections of the sample, indicating that the lateral intensity drop is not related to composition. The intensity rises slightly again in the growth direction, suggesting the highest concentration of Bi is found in the initial growth of the film and then lowers somewhat as growth continues. The top of the micrograph shows part of the transition from the film to the protective C layer deposited during sample preparation in the FIB; in all micrographs shown here, there is still a substantial layer of FIB damage despite the protective layers due to the softness of InAs (InAs has a hardness of 3300 N/mm^2 compared to 7500 N/mm^2 for GaAs [1]). This layer of damage consists of a thin layer of In precipitates beneath the C layer, followed by a ~40 nm layer of amorphous damage, and so prevents observation of the surface of these samples.

Figure 2.5.7.B shows a representative STEM micrograph of a Bi-droplet-covered morphology sample, with the cross-section oriented perpendicular to the droplet trails seen on the surface of the sample. The substrate to buffer transition again is marked by a thin line of precipitates, and the buffer to film transition shows a stronger version of the trend seen in Fig. 2.5.7.A, where the lowest intensity, suggesting the highest concentration of Bi, is found near the transition and then drops off as the growth continues. In this case, the contrast difference is larger between the buffer and the first region of film growth, indicating higher Bi content, but after approximately 200 nm of growth there is almost no Bi present. Also visible in Fig. 2.5.7.B is a lens-shaped cross-section of a droplet trail in the film, containing essentially no Bi. While the rise in intensity after 200 nm of growth (suggestive of a lack of Bi in the film after that point) is likely related to the presence of droplets, it does not seem to indicate exclusive vapor-liquid-solid

(VLS) growth, due to the gradual nature of the transition. The distinctive underside of the droplet trail is only seen in some parts of the film and the trails do not overlap each other significantly, which they would need to do if all growth after 200 nm was in the presence of droplets. There are lateral fluctuations in intensity visible that are due to curtaining from FIB sample preparation, as they extend past the film layer into the buffer layer and the substrate.

Finally, in Fig. 2.5.7.C, a representative STEM micrograph of a mixed InBi-droplet-covered morphology sample can be seen. The cross-section was taken perpendicular to the direction of the droplet trails visible on the sample surface. The film has uniform intensity except for the section just below the surface damage, and no buffer-film interface is visible, though the sample according to XRD has very small amounts of Bi with an average Bi-content of 0.03% Bi. No explicit droplet trails are seen in this sample in the film, perhaps due to the small amount of Bi present in general leading to a lack of contrast, though the surface has roughness indicating droplet cross-sections that nonetheless are identical to the rest of the film in composition. There are still slight curtaining artifacts extending into the substrate layer and surface damage artifacts from the FIB sample preparation, though there are fewer of the speckles associated with BF micrographs here.

While all the Bi-containing morphologies show the same trend of laterally-homogeneous and growth-direction-variant Bi content, with much less inhomogeneity seen compared to GaAsBi films, there is still the question of what the cause of the missing-film-peaks are in samples grown with As/In BEP ratios above 1.1. To examine this, Fig. 2.5.8 shows a comparison of two Bi-droplet-covered morphology samples.
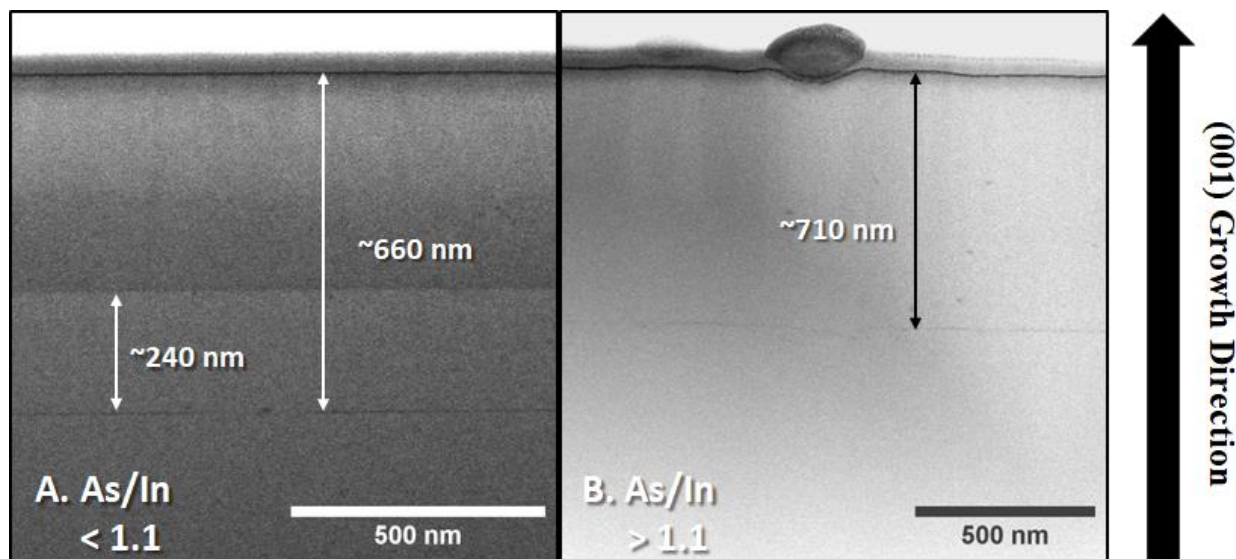
Figure 2.5.8: Cross-Sectional BF STEM of two Bi-droplet-covered morphology samples grown at different As/In BEP ratios. (A) shows a cross-section from a sample grown below a 1.1 As/In BEP ratio, while (B) shows a sample grown above a 1.1 As/In BEP ratio. The arrows show measurements of the different film thicknesses. Background subtraction was done on (B) due to irregular thickness of the sample.

In Fig. 2.5.8.A, a cross-section of a sample grown with a As/In BEP ratio of 0.54 and a Bi/As BEP ratio of 0.14 is shown. Both the substrate-to-buffer and buffer-to-film transitions are clearly visible, and the contrast between the film and buffer layer indicates the presence of Bi. The buffer layer is approximately 240 nm thick, whereas the entirety of the epitaxial growth on the substrate is about 660 nm thick before reaching the FIB-damaged surface. On the other hand, in Fig. 2.5.8.B, a cross-section of a sample grown with a As/In BEP ratio of 1.56 and a Bi/As BEP ratio of 0.06 is shown. In this sample, only one transition is visible, that of the substrate to buffer. The thickness of the epitaxially-grown film is approximately 710 nm before the FIB-damaged surface, meaning it includes both the buffer layer (nominally 250 nm) and the film (nominally 500 nm), despite the lack of a visible interface. There is no indication of Bi present in the film, though a Bi droplet is visible on the surface. The apparent lack of Bi in the film is puzzling, and suggests that some kinetic mechanism is preventing its incorporation into the film, but previous literature on MBE growths [11, 19-20] tends to hold to a As/In BEP ratio of ~1, with similar or

higher substrate temperatures and growth rates, meaning this high-As/In BEP-ratio area of growths has no previous growths to be compared to to find answers.

Comparison between InAsBi and GaAsBi

As touched on briefly above, there are similarities and differences between the behavior of the GaAsBi and InAsBi materials systems seen here. The major differences are in the identity and appearance of the surface morphologies, the placement of morphologies across flux ratio space, the kinetic parameters apparent in the different systems, and the thermodynamics involved in the two systems. To begin, while three of the four morphologies seen in each system are either the same or have direct equivalents in the other system, the biphasic Ga-Bi-droplet-covered and mixed In-Bi-droplet-covered morphologies are not equivalent. The biphasic Ga-Bi droplets exist due to the immiscibility of Ga and Bi, and films grown when the droplets are present have characteristics of essentially both Ga and Bi droplets being individually present. In the InAsBi system, in contrast, In and Bi are miscible in each other, and the microstructure of the films and trend of Bi composition as seen in the XRD are unique compared to the other morphologies. In the mixed InBi-droplet-covered regime, the XRD shows small film shoulders without a preferred composition, unlike the other morphologies, with very small amounts of Bi incorporation. Also as a result of the miscibility of In and Bi, the In-droplet-covered morphology does not exist in the presence of Bi flux, as Bi can readily bond to In in droplets during growth, then remain mixed in those droplets as the film is quenched. This trend is unlike the Ga-droplet-covered morphology in the GaAsBi system, which exists in the presence of Bi/As BEP ratios of up to 0.12, indicating that Bi will not aggregate in Ga droplets until a threshold Bi/As BEP ratio is reached.

Another difference can be seen in the appearance of the morphologies themselves in SEM (comparing Fig. 2.4.2 and Fig. 2.5.2). In GaAsBi, the Ga-droplet-covered and Bi-droplet-

81

covered morphologies have densely-packed droplets, and the droplets themselves are more or less round. Also, there is evidence that the Bi droplets move across the surface and sweep away smaller droplets in their wake (see Fig. 2.4.2.D, for example), and though the surface is visibly rough, the droplets do not leave raised droplet trails on it. Likewise, in the Ga-Bi-droplet-covered morphology, the biphasic Ga-Bi droplets can both be much larger than the other droplet-types (up to 20 μm) and have a wider range of droplet sizes (100 nm to 20 μm). The droplets are seen to move across the surface as evidenced by areas denuded of smaller droplets, as opposed to raised droplet trails grown in the surface. In contrast to all of these trends in GaAsBi, the droplet morphologies in InAsBi display a few key differences. The droplet density of In and Bi droplets is lower, and the Bi and mixed In-Bi droplets are smaller than their counterparts in GaAsBi, while the In droplets are slightly larger. The Bi droplets in InAsBi, besides being smaller than the ones in GaAsBi, are more uniform in shape and size, having a rounded rectangular shape with a 5:4 aspect ratio and size ranging from 250-350 nm on the long side. All three droplet types move across the surface and leave raised droplet trails grown on the surface of the film, and the lengths of these visible trails vary across morphologies.

A third area of difference can be seen from comparing the two surface morphology maps made for these material systems. The GaAsBi morphology map (Fig. 2.4.5) has the range of As/Ga BEP ratios shown between 1.5 and 2.8, with most transitions happening between 1.7 and 2.1 and the droplet-free to Ga-droplet transition occurring at 2.1. While the InAsBi morphology map (Fig. 2.5.4), in contrast, uses As/In BEP ratios between 0 and 3.2, all transitions can be found between As/In BEP ratios of 0.5 and 1.5 and the droplet-free to In-droplet transition occurs at 1.1. From the modeling done in Chapter 2.4, the droplet-free to Group III droplet transition is supposed to occur when the V/III flux ratio is equal to the inverse of the Group III

surface coverage (Eqn. 2.2.13). If we assume that the BFM sensitivity to Ga and In are similar, the values would indicate that the surface coverage of Ga associated with the growth of Ga droplets is about half of the In surface coverage required for the growth of In droplets (~0.5 vs ~1). This finding could suggest that at the growth temperatures used, the Ga-Ga bonding energy is higher in comparison to the Ga-As and Ga-Bi bonding energies than the equivalent In-In bonding energy is to In-As and In-Bi bonding energies.

The ranges of Bi/As BEP ratios seen in the morphology maps also differ. In the GaAsBi morphology map (Fig. 2.4.5), features of interest can be found between Bi/As BEP ratios of ~0.1-0.3, with the highest Bi/As BEP ratio used for a sample being around 0.38. In the InAsBi morphology map (Fig. 2.5.4), however, transitions are found between Bi/As BEP ratios of 0-0.05 and the highest Bi/As BEP ratio used for a sample was 0.14. The difference in Bi/As BEP ratios used explains some of the difference in Bi incorporation seen in the two systems, with much higher Bi-compositions achievable in GaAsBi where more Bi BEP was applied than in InAsBi, which had comparatively small Bi BEPs applied. The fact that the droplet-free-surface morphology was only seen to extend to a Bi/As BEP ratio of 0.045 in InAsBi, as opposed to 0.3 in GaAsBi, indicates that Bi droplets are able to form at much lower Bi BEPs in InAsBi. This finding is despite the facts that In and Bi are miscible in each other and that InAs has a larger lattice constant than GaAs, both of which facts would otherwise suggest that Bi could more-easily incorporate into the InAsBi film than into the GaAsBi film instead. While much higher Bi-content is possible in GaAsBi than in InAsBi, there are also more, and higher-magnitude, inhomogeneities. In our samples, GaAsBi has Bi compositions of up to ~18% Bi, but also has w_{OOM} values between ~0.2-2°. In contrast, our InAsBi samples have at most a Bi composition of ~4% Bi, but the w_{OOM} values for this material range from 0.05° to 0.4°, indicating that the film

quality is better in InAsBi. Likely, the lower Bi BEP in our InAsBi samples and Bi's miscibility with In allow it to more completely incorporate into the InAs film, leading to smaller-Bi-composition and more-homogeneous InAsBi films, with few localized fluctuations in Bi content or defects.

The placement of the transition also, from the modeling seen in Chapter 2.4 (Eqn. 2.4.1), would suggest that the kinetic parameter P^{rem}, the probability of removal of Bi from the surfactant layer by As, would be approximately 0.045 for InAsBi, as opposed to ~0.2 for GaAsBi, assuming the same kinetic processes occur on the surface of the film in both systems. Similarly, the R^{inc}/F_{III} parameter can be calculated from the location of the Bi-droplet to mixed-InBi-droplets transition (using Eqn. 2.4.4 as a basis) as being ~0.5. However, the behavior of the InAsBi system in terms of the lack of Bi incorporation in samples grown with a As/In BEP ratio above 1.1 indicates that the model of kinetic processes given in [31] may be incorrect for the InAsBi system, or it may otherwise be incomplete. For example, it could be that Bi in the InAsBi system is highly sensitive to As over-pressure, and is easily removed from the surface in either the surfactant layer or the growth layer. While this removal is partially described through the mechanisms of P^{rem} and P^{dis}, it is possible that there could also be another mechanism it occurs through, not found in GaAsBi, or that in this case each As atom is able to remove multiple Bi atoms from the surface. That being the case, while some comparisons between the GaAsBi and InAsBi systems can be made in terms of kinetic parameters, they cannot be assumed to have 1:1 correlations for all parameters.

Beyond just the exact values of the morphology transitions seen in the two morphology maps (Figs. 2.4.5 and 2.5.4), the shapes of the morphology transitions also differ at times. While the shapes of the droplet-free to Group-III-droplet, the Group-III-droplet to Group-III-Bi-droplet,

and the Bi-droplet to Group-III-Bi-droplet transitions are either similar or unknown, the droplet-free to Bi droplet transition is very different between the two material systems. In GaAsBi, the transition in question shifts significantly towards higher Bi/As BEP ratios as the As/Ga BEP ratio lowers, with the transition's lowest As/Ga BEP ratio of 1.8 associated with the transition's highest Bi/As BEP ratio of 0.29. In contrast, the transition as seen in InAsBi is constant at a Bi/As BEP ratio of 0.042 and independent of the As/In BEP ratio. This difference suggests that in InAsBi, the growth of Bi droplets is entirely controlled by the Bi BEP applied, whereas in GaAsBi, both Ga and Bi interact to control under what conditions Bi droplets grow.

A final set of differences between the two material systems is the possibility for non-epitaxial phases to arise in InAsBi. In GaAsBi, the immiscibility of Ga and Bi mean that the possible phases are GaAs, metastable GaAsBi, and the pure elements. In InAsBi, however, In and Bi can form several different compounds at similar BEP ranges, including $InBi$, In_2Bi, and In_5Bi_3, all of which form tetragonal crystal structures as opposed to the cubic structures found in InAs or InAsBi. There is an example in the literature of InBi precipitates in InAsBi films [21]. Likewise, pure In, As, or Bi phases could also form. In our samples, while there were some instances in the XRD scans suggesting the presence of small amounts of other phases, particularly pure Bi in films with Bi-droplet-covered surface, the dominant peaks were the InAs substrate peak and the InAsBi film peaks. When InAsBi film peaks were not present, our STEM micrographs suggest films were grown but no Bi was incorporated, and the XRD results for those samples (for example Fig. 2.5.5) likewise only show non-significant intensities for the anomalous peaks when they are present at all, confirming that significant amounts of other phases are not present.

Regardless, when TEM does show the presence of an InAsBi film when Bi droplets are present (Fig. 2.5.7.B), it behaves similarly to how the GaAsBi films behaved in the presence of Bi droplets (Fig. 2.4.6.B). In both materials, the area directly beneath a Bi droplet has low amounts of Bi, and sections of droplet trail can be seen in the micrographs. These trails have low amounts of Bi in the trail itself and are surrounded by regions of the film with lower intensity in BF micrographs or higher intensity in DF (dark field) micrographs, suggesting higher Bi-content. Both materials also have a tendency for high amounts of Bi in the initial film growth, but whereas the Bi incorporation in GaAsBi is mediated by the presence of droplets throughout the film, in InAsBi the incorporation of Bi drops off significantly as the film grows, leaving most Bi found near the buffer-to-film interface and not near the surface. This pattern of comparatively-enhanced Bi incorporation in the first parts of the film has been predicted in [32], where the Bi incorporation is highest in the first few monolayers of growth and drops off after droplets begin to form.

Conclusion

The campaign of InAsBi growths and characterization discussed here allows us to address our overarching research question of ***What surface morphologies, microstructures, and Bi-compositions arise in MBE-grown InAsBi films, and what can this tell us about their kinetics and thermodynamics*** by means of our specific research questions. For the first question, *What surface morphologies, microstructures, and Bi-compositions arise in In-As-Bi materials, and how does this change across a range of conditions*, we found that InAsBi films have three general surface morphologies (droplet-free, Bi-droplet-covered, and mixed-InBi-droplet-covered), with a fourth morphology, In-droplet-covered, possible but unconfirmed in conditions of extremely-low Bi BEP and low As_2 BEP. While the droplet-free and Bi-droplet-covered

morphologies have been seen in the literature before [19-20], it is unclear whether the mixed-InBi-droplet-covered morphology has been previously observed. All droplet-covered morphologies show evidence of droplet-induced VLS growth. The changes in morphology as the BEP ratios change at a constant temperature are seen in Fig. 2.5.4. The different morphologies have similar microstructures, with low amounts of inhomogeneous Bi content in the films (0-4% Bi). In the case of Bi droplets, low-Bi-content regions are left in the film as the droplet passes over it during growth.

For the question of *How do the kinetics and thermodynamics of the InAsBi system impact the observed morphologies, microstructures, and Bi-compositions,* we found that, in spite of the miscibility of In and Bi, the InAsBi system is capable of incorporating only a small amount of Bi (with a maximum of 3.9% Bi seen in our samples) even with kinetic freezing at a growth temperature of 200°C. There is a possibility of other phases being present in the growths, but such phases do not occur consistently and in these growths were only possibly present in small amounts. More-specific to kinetics, droplet-free surfaces can only be grown up to a Bi/As BEP ratio of 0.042, and film growth in the presence of droplets is highly impacted by the droplet-induced VLS growth, leaving rough surfaces and droplet-trails throughout the sample as the Bi preferentially bonds to other Bi in the droplets. When the kinetic surface model [31] is applied to the system, we can obtain estimates of the In-coverage as ~1, P^{rem} as ~0.042, and R^{inc}/F_{In} ~0.5. While we can estimate these parameters, there appears to be another mechanism through which Bi is lost from the surface under As overpressure, with said mechanism not accounted for in Tait et al's kinetic surface model.

Finally, for the question of *How do different group III elements compare, and what can this tell us about the kinetics and thermodynamics of the systems*, we determined that the two

materials systems, GaAsBi and InAsBi are superficially similar in terms of morphology and microstructure, but there are significant differences that relate to their kinetics and thermodynamics. The biphasic-GaBi-droplets and mixed-InBi-droplets are not equivalent, and act differently in terms of both surface presentation and microstructure, as in GaAsBi the biphasic droplets act as both individual types of droplet, while in InAsBi the droplets act uniquely in comparison to Bi droplets. Both materials systems exhibit VLS growth, but in GaAsBi said growth is evidenced by the microstructure and small areas void of droplets on the surface, while in InAsBi said growth is mainly evidenced by the large droplet trails roughening the surface. The surface morphology maps seen in Figs. 2.4.5 and 2.5.4 have major differences in terms of scale on the axes, the Bi content, and the film quality. Overall, the InAsBi map shows less, but relatively-homogeneous, Bi incorporation in our samples compared to the GaAsBi map. Based on the modeling and the map transitions, the estimated kinetic parameters for the two materials systems differ, with GaAsBi having parameter values of θ_{Ga} ~0.5, P^{rem} ~0.2, R^{inc}/F_{Ga} ~0.6 and InAsBi having parameters values of θ_{In} ~1, P^{rem} ~0.042, R^{inc}/F_{In} ~0.5. InAsBi has some kinetic process that prevents the incorporation of Bi when the As/In BEP ratio is greater than 1.1, whereas GaAsBi has no similar limitation.

Now that we have analyzed our second materials system, we can use the results for both systems to answer our overarching research question, ***What surface morphologies, microstructures, and Bi-compositions arise in MBE-grown III-AsBi films, and what can this tell us about their kinetics and thermodynamics***, as we conclude this section in the next chapter.

References

[1]   L. I. Berger, "Properties of Semiconductors," in *CRC Handbook of Chemistry and Physics*, 94th ed., W. M. Haynes, D. R. Lide, and T. J. Bruno, Eds. Boca Raton: CRC Press, 2013, pp. 80–93.

[2]   H. J. Welker, "Discovery and Development of III-V Compounds," *IEEE Trans Electron Devices*, vol. 23, no. 7, pp. 664–673, 1976, doi: 10.1109/T-ED.1976.18471.

[3]   C. Shih, E. A. Peretti Vol, B. C. Shih, and E. A. Peretti, "The System InAs-InSb," UTC, 2022. [Online]. Available: https://pubs.acs.org/sharingguidelines

[4]   M. A. C. S. Brown and P. Portequs, "The technology and properties of epitaxial indium arsenide lasers," *British Journal of Applied Physics*, vol. 18, pp. 1527–1535, 1967.

[5]   S. M. Currie *et al.*, "Proton tolerance of InAs based HEMT and DHBT devices," in *IEEE Radiation Effects Data Workshop*, 2006, pp. 66–71. doi: 10.1109/REDW.2006.295470.

[6]   J. Dobbert *et al.*, "Strained quantum well InAs micro-Hall sensors: Dependence of device performance on channel thickness," *IEEE Trans Electron Devices*, vol. 55, no. 2, pp. 695–700, Feb. 2008, doi: 10.1109/TED.2007.913000.

[7]   R. Rehm *et al.*, "InAs/GaSb superlattice infrared detectors," *Infrared Phys Technol*, vol. 70, pp. 87–92, Jul. 2015, doi: 10.1016/j.infrared.2014.09.034.

[8]   S. M. Hubbard, M. Bennett, A. Podell, and D. v. Forbes, "Optimization of growth and device performance for InAs quantum dot solar cells," in *Conference Record of the IEEE Photovoltaic Specialists Conference*, 2012, pp. 1788–1793. doi: 10.1109/PVSC.2012.6317940.

[9]   K. Y. Ma *et al.*, "Organometallic vapor phase epitaxial growth and characterization of InAsBi and InAsSbBi," *Appl Phys Lett*, vol. 55, no. 23, pp. 2420–2422, 1989, doi: 10.1063/1.102033.

[10]   H. Okamoto and K. Oe, "Structural and Energy-Gap Characterization of Metalorganic-Vapor-Phase-Epitaxy-Grown InAsBi," *Jpn J Appl Phys*, vol. 38, p. 1022, 1999.

[11]   A. J. Shalindar, P. T. Webster, B. J. Wilkens, T. L. Alford, and S. R. Johnson, "Measurement of InAsBi mole fraction and InBi lattice constant using Rutherford backscattering spectrometry and X-ray diffraction," *J Appl Phys*, vol. 120, no. 14, 2016, doi: 10.1063/1.4964799.

[12]   K. Y. Ma, Z. M. Fang, R. M. Cohen, and G. B. Stringfellow, "Ultra-Low Temperature OMVPE of InAs and InAsBi," 1992.

[13] R. Boussaha, H. Fitouri, and A. Rebey, "In situ monitoring of InAsBi alloy grown under alternated bismuth flows by metalorganic vapor phase epitaxy," *Mater Sci Eng B Solid State Mater Adv Technol*, vol. 241, pp. 22–26, Feb. 2019, doi: 10.1016/j.mseb.2019.02.006.

[14] I. Massoudi and A. Rebey, "Effect of InAs buffer layer thickness on physical properties of InAsBi heterostructures grown by MOCVD," *J Cryst Growth*, vol. 549, Nov. 2020, doi: 10.1016/j.jcrysgro.2020.125881.

[15] I. C. Sandall, F. Bastiman, B. White, R. D. Richards, J. David, and C. H. Tan, "Demonstration of an InAsBi photodiode operating in the MWIR," *Emerging Technologies in Security and Defence II; and Quantum-Physics-based Information Security III*, vol. 9254, no. October 2014, p. 92540Q, 2014, doi: 10.1117/12.2069697.

[16] P. Verma, M. Herms, G. Irmer, M. Yamada, H. Okamoto, and K. Oe, "Raman probe of new laser materials GaAs 1-x Bi x and InAs 1-x Bi x," in *Laser Diodes and LEDs in Industrial, Measurement, Imaging, and Sensors Applications II; Testing, Packaging, and Reliability of Semiconductor Lasers V*, Mar. 2000, vol. 3945, p. 168. doi: 10.1117/12.380534.

[17] J. Hader, S. C. Badescu, L. C. Bannow, J. v. Moloney, S. R. Johnson, and S. W. Koch, "Auger losses in dilute InAsBi," *Appl Phys Lett*, vol. 112, no. 19, 2018, doi: 10.1063/1.5022775.

[18] N. Elayech, H. Fitouri, R. Boussaha, A. Rebey, and B. el Jani, "Calculation of In-As-Bi ternary phase diagram," *Vacuum*, vol. 131, pp. 147–155, 2016, doi: 10.1016/j.vacuum.2016.06.009.

[19] P. T. Webster *et al.*, "Molecular beam epitaxy using bismuth as a constituent in InAs and a surfactant in InAs/InAsSb superlattices," *Journal of Vacuum Science & Technology B, Nanotechnology and Microelectronics: Materials, Processing, Measurement, and Phenomena*, vol. 32, no. 2, p. 02C120, 2014, doi: 10.1116/1.4868111.

[20] S. P. Svensson, H. Hier, W. L. Sarney, D. Donetsky, D. Wang, and G. Belenky, "Molecular beam epitaxy control and photoluminescence properties of InAsBi," *Journal of Vacuum Science & Technology B, Nanotechnology and Microelectronics: Materials, Processing, Measurement, and Phenomena*, vol. 30, no. 2, p. 02B109, 2012, doi: 10.1116/1.3672023.

[21] L. Dominguez *et al.*, "Formation of tetragonal InBi clusters in InAsBi/InAs(100) heterostructures grown by molecular beam epitaxy," *Applied Physics Express*, vol. 6, no. 11, Nov. 2013, doi: 10.7567/APEX.6.112601.

[22] J. Lu, P. T. Webster, S. Liu, Y. H. Zhang, S. R. Johnson, and D. J. Smith, "Investigation of MBE-grown InAs1-xBix alloys and Bi-mediated type-II superlattices by transmission electron microscopy," *J Cryst Growth*, vol. 425, pp. 250–254, 2015, doi: 10.1016/j.jcrysgro.2015.02.012.

[23] K. Y. Ma, Z. M. Fang, R. M. Cohen, and G. B. Stringfellow, "Investigation of organometallic vapor phase epitaxy of InAs and InAsBi at temperatures as low as 275°C," *J Appl Phys*, vol. 70, no. 7, pp. 3940–3942, 1991, doi: 10.1063/1.349204.

[24] H. Okamoto and K. Oe, "Growth of Metastable Alloy InAsBi by Low-Pressure MOVPE," *Japanese Journal of Applied Physics To*, vol. 37, p. 1608, 1998.

[25] R. Wang, B. C. Giessen, and N. J. Grant, "The crystal structure of In5Bi3," *Zeitschrift fur Kristallographie*, vol. 128, pp. 244–251, 1969.

[26] E. R. Jette and F. Foote, "Precision determination of lattice constants," *J Chem Phys*, vol. 3, no. 10, pp. 605–616, 1935, doi: 10.1063/1.1749562.

[27] A. J. Bradley, " LX. The crystal structure of metallic arsenic ," *The London, Edinburgh, and Dublin Philosophical Magazine and Journal of Science*, vol. 47, no. 280, pp. 657–671, May 1924, doi: 10.1080/14786442408634405.

[28] B. C. Giessen, M. Morris, and N. J. Grant, "METASTABLE INDIUM-BISMUTH PHASES PRODUCED BY RAPID QUENCHING," *TRANSACTIONS OF THE METALLURGICAL SOCIETY OF AIME*, vol. 239, no. 6, p. 883, 1967.

[29] National Bureau of Standards USA, 'Monograph 253', 1964.

[30] V. F. Degtyareva, "Structure solution in binary systems under high pressure: Phase decomposition and phase synthesis," in *Journal of Synchrotron Radiation*, Sep. 2005, vol. 12, no. 5, pp. 584–589. doi: 10.1107/S0909049505021321.

[31] C. R. Tait and J. M. Millunchick, "Kinetics of droplet formation and Bi incorporation in GaSbBi alloys," *J Appl Phys*, vol. 119, no. 21, p. 6, 2016, doi: 10.1063/1.4952988.

[32] G. V. Rodriguez and J. M. Millunchick, "Predictive modeling of low solubility semiconductor alloys," *J Appl Phys*, vol. 120, no. 12, 2016, doi: 10.1063/1.4962849.

CHAPTER 2.6

Conclusion

In the past few chapters focusing on the MBE-growth of III-As-Bi semiconductor films, we have characterized the microstructure and morphology of films of two different materials systems, GaAsBi and InAsBi. We were guided by the overall research question of ***What surface morphologies, microstructures, and Bi-compositions arise in MBE-grown III-As-Bi films, and what can this tell us about their kinetics and thermodynamics?*** We answered this question for each materials system by examining the surface morphology, the microstructure, and how they relate to each other in BEP-ratio-space, as well as through kinetic modeling and comparison between the materials systems.

In both the GaAsBi and InAsBi systems, there are four surface morphologies (droplet-free-surfaces, Bi-droplet-covered, III-droplet-covered, and III-Bi-droplet-covered) which when mapped onto BEP-ratio-space roughly occur in four quadrants. While the III-Bi-droplet-covered morphologies are similar between systems, they have differences stemming from the immiscibility of Ga and Bi [1] and the miscibility of In and Bi [2]. The different morphologies give rise to inhomogeneous films, with the amount and type of inhomogeneity varying based on the surface morphology. The general trend is for droplet-free-surface films to be the most homogeneous and the films with any sort of Bi droplets to be the least homogeneous, and for

GaAsBi to generally have higher Bi-content films (up to 18% Bi) and more inhomogeneities (w$_{OOM}$ up to 1.78) than InAsBi (Bi-content up to 4% and w$_{OOM}$ up to 0.35). Bi incorporates into GaAsBi across the observed As/Ga and Bi/As BEP ratios for our samples, while in InAsBi Bi does not incorporate above an As/In BEP ratio of ~1.1. In terms of kinetics, we are able to estimate the kinetic parameters given in the model [3], and find a plausible system for GaAsBi and significant differences between the estimated kinetic parameters for GaAsBi and InAsBi. The GaAsBi system has kinetic parameters of $R^{inc}/F_{Ga} = 0.60$ (from morphology map) or 1.58 ± 0.002 (from nonlinear modeling), $P^{dis} = 0.99$, and $P^{rem} = 0.20 \pm 0.001$, indicating a system where Bi incorporates into the film at relatively high rates compared to F_{Ga} but is likely to be removed from both the surfactant layer and growth layer by As, leading to the observed levels of incorporation. The InAsBi values for R^{inc}/F_{In} and P^{rem} are 0.49 (from morphology map) and 0.042, respectively, indicating that the rate of Bi incorporation in the film is lower in InAsBi and the probability of Bi removal from the surfactant layer by As is much lower than in GaAsBi.

These results lend themselves to a few implications. First, looking at those findings tied to our growth campaign more-or-less directly, we see that the best method to get films of uniform Bi composition and high film quality is to grow the film with BEP ratios that do not yield any kind of droplet. Droplets were associated with highly-inhomogeneous microstructures and film shoulders in XRD, though the effect is more pronounced in GaAsBi than in InAsBi. Likewise, the highest Bi-content droplet-free films were grown with high Bi/As BEP ratios and low As/III BEP ratios, but growth in this region of BEP-ratio-space must be carefully tuned to not yield droplets. However, if a layered, superlattice-like structure is desired, growth in the presence of biphasic GaBi droplets could be a valuable approach, as films grown with that morphology tended to spontaneously form semi-layered microstructure. In InAsBi films

93

specifically, care should be taken to keep the As/In BEP ratio below 1.1 in order to ensure that Bi incorporates into the film. While it is possible (based on the ternary phase diagram [2] and previous growths [4]) that other In-and-Bi-containing phases may form in InAsBi films, it is unclear what specific growth conditions lead to the formation of the inclusions and it appears to be unlikely in the course of non-equilibrium methods of growth such as MBE.

Second, we examine the implications that relate more towards the kinetic modeling that we completed. It is apparent that the KMC model reported in [5] is generally accurate but does not accurately predict the placement and Bi-incorporation behavior of the mixed or biphasic III-Bi-droplet-covered morphologies, based on the differences between the KMC morphology map and our work here for GaAsBi and InAsBi. As the authors of the KMC model assigned morphology to samples after ~15 monolayers of simulated growth, it could be that the morphology of a film may change part-way through growth or that Bi can accumulate in Ga droplets over the course of growth, resulting in apparently biphasic droplets when characterized afterwards. From the surface model proposed in [3], we were able to estimate kinetic parameters for the different processes in GaAsBi and a subset of the kinetic parameters in InAsBi. In GaAsBi, the estimated kinetic parameters describe a system in which Bi have a chance to be removed from the surfactant layer but will not spontaneously desorb, and in which Bi will incorporate into the film surface at high rates but also be displaced by incoming As atoms in nearly all cases. The interplay of R^{inc}/F_{Ga} and P^{dis} for GaAsBi, particularly the P^{dis} value of nearly unity, is different than that predicted for GaSbBi [3] and modeled for InAsSbBi [6], but is not necessarily wrong. In InAsBi, the estimated kinetic parameters suggest a system in which Bi is significantly less likely to be removed from the surfactant layer by As than in GaAsBi, but the rate of incorporation is also slightly smaller. The InAsBi system at high As/In BEP ratios is not

94

accurately modeled by [3], and there appears to be an additional kinetic process occurring on the surface in those growth conditions.

Future Work

There are several avenues that expansion upon the work described here could take. The most direct avenue is to build on and expand the work done here with the surface morphology maps. The maps could be built on in two ways. In the first way, similar surface morphology maps of the BEP-ratio-space could be completed for other III-V-Bi materials systems, particularly GaSbBi and InSbBi, with special attention paid to growing samples near the surface morphology boundaries. With such a baseline, more-comprehensive comparisons can be made between the various III-V-Bi compounds in terms of film quality, Bi incorporation, and the kinetic parameters, allowing us to better understand the effects of changing the group-III and group-V atoms on the materials systems. In the second way, similar morphology maps could be made from GaAsBi and InAsBi samples grown at different temperatures. It is expected that the placement of the boundaries between the morphologies would change with the growth temperature, and if enough data points were collected as the temperature was varied, it would be possible to model the kinetic properties estimated from the boundaries as Arrhenius equations [7] complete with activation energies for the different kinetic processes. With sufficient samples grown with the droplet-free-surface morphology, all the rate and probability kinetic parameters from [3] could be modeled. Similarly to our work here, the activation energies could then be compared between different materials systems.

A different avenue of future work could be to examine the InAsBi materials system in more detail and determine how the kinetic processes themselves differ from the GaAsBi

materials system and why the Bi-content of samples grown above a As/In BEP ratio of 1.1 was

nonexistent. Based on how the InAsBi materials system behaved, it is likely that there are kinetic

processes not accounted for in the model given in [3]. The model was originally derived for

GaSbBi, and it was applied effectively to GaAsBi in our work described in Chapter 2.4. The

main change when going to the InAsBi materials system then is the identity of the group-III

atom. With that in mind, it is likely that the unknown kinetic process is in some way related to

In, either in terms of its surface coverage during growth, or its bonding energy to Bi, or some

other factor. Studying the system and modeling it more accurately would fill in a gap in the

literature highlighted by our work reported here.

Finally, another avenue to expand our findings here relates more to increasing the

functionality of these materials for various applications. As noted above, it might be desirable to

grow films with superlattice-like morphology with high- and low-Bi-content regions, in which

case the use of samples with the biphasic Ga-Bi-droplet-covered morphologies could allow for

the growth of the structures without the need for fine timing on the Bi BEP. Films grown with

the biphasic Ga-Bi-droplet-covered morphology had thin regions of very high Bi-content and

thicker regions of low Bi-content, with the thickness of these films and their angle to the growth

direction likely controlled by the rates of growth and droplet movement across the surface. If the

droplet coverage were controlled and the growth rate lowered such that the rate of droplet

movement across the surface was much faster than it, it might be possible to grow films in such a

way that the high- and low-Bi-content layers were continuous across significant portions of the

film and consistent in thickness, making a pseudo-superlattice structure. It would also be

necessary to determine a way to more-finely control the Bi-content of the two layer types, such

that the Bi-compositions were both consistent within particular allowances and with sharp

delineations between the layers.

References

[1]   N. Elayech, H. Fitouri, Y. Essouda, A. Rebey, and B. el Jani, "Thermodynamic study of the ternary system gallium-arsenic-bismuth," *Physica Status Solidi (C) Current Topics in Solid State Physics*, vol. 12, no. 1–2, pp. 138–141, 2015, doi: 10.1002/pssc.201400147.

[2]   N. Elayech, H. Fitouri, R. Boussaha, A. Rebey, and B. el Jani, "Calculation of In-As-Bi ternary phase diagram," *Vacuum*, vol. 131, pp. 147–155, 2016, doi: 10.1016/j.vacuum.2016.06.009.

[3]   C. R. Tait and J. M. Millunchick, "Kinetics of droplet formation and Bi incorporation in GaSbBi alloys," *J Appl Phys*, vol. 119, no. 21, p. 6, 2016, doi: 10.1063/1.4952988.

[4]   L. Dominguez *et al.*, "Formation of tetragonal InBi clusters in InAsBi/InAs(100) heterostructures grown by molecular beam epitaxy," *Applied Physics Express*, vol. 6, no. 11, Nov. 2013, doi: 10.7567/APEX.6.112601.

[5]   G. V. Rodriguez and J. M. Millunchick, "Predictive modeling of low solubility semiconductor alloys," *J Appl Phys*, vol. 120, no. 12, 2016, doi: 10.1063/1.4962849.

[6]   S. T. Schaefer, M. S. Milosavljevic, R. R. Kosireddy, and S. R. Johnson, "Kinetic model for molecular beam epitaxy growth of InAsSbBi alloys," *J Appl Phys*, vol. 129, no. 3, Jan. 2021, doi: 10.1063/5.0035193.

[7]   X. Lu, D. A. Beaton, R. B. Lewis, T. Tiedje, and M. B. Whitwick, "Effect of molecular beam epitaxy growth conditions on the Bi content of GaAs1-x Bix," *Appl Phys Lett*, vol. 92, no. 19, pp. 1–4, 2008, doi: 10.1063/1.2918844

CHAPTER 3.1

Introduction

Introduction

Expanding the world's collective knowledge is a driving goal for science, but even the most stunning finding is useless unless it can be shared. Communication is the manner through which we can share our knowledge, and education the manner through which we can pass on our current knowledge and enable future minds to understand, create, and contribute to the sum of human knowledge. As such, education is a vital undertaking in our world, and understanding how to educate effectively can have a large impact on future generations.

Such a task is more easily said than done, however. Ways of teaching and learning are as varied as the people involved, and there are no simple, completely objective ways to determine the best methods to use. Instead, education itself must be studied, in all of its practices, participants, and outcomes, in order to determine how best to carry on the work. There are many ways to approach the study of education, and many theories of learning within each of those approaches. With the complexities of human actors and our current understandings of how our brains and societies influence each other, no one learning theory can be viewed as objectively correct or complete in any way. Instead, researchers and educators use theoretical frameworks to organize ways of understanding and approaching education and qualitative education research

[1]. These frameworks provide a lens through which different aspects of education can be viewed, directing lines of inquiry and identifying areas of interest to the user. In engineering education research, some example frameworks are situated learning (or the idea that learning is context-dependent and involves the process of moving towards the center of the community) [2], variation theory (or the idea that people must be taught to see or sensitized to variations in the critical aspects of things they learn in order to understand them) [3], and socio-cultural learning theory (or the idea that all learning comes through some sort of social interaction and is mediated by tools) [4]. In this work, we will be focusing on the theoretical framework of disciplinary literacy.

Disciplinary literacy as a theoretical framework for education has developed slowly over the past forty years by a variety of researchers and educators in various fields [5], including history [6], scientific literacy [7], English language arts [8], and mathematics [9]. From its roots in the development of pedagogical content knowledge (knowledge of how to best teach and convey particular content) [10], the framework shifted to be more-specifically centered on discipline-specific and contextualized literacy, both in terms of reading and understanding texts and in terms of understanding and taking on the discipline-specific ways of approaching, creating, and evaluating texts [5].

In the conception of disciplinary literacy we employ here [11], disciplinary literacy is concerned with disciplines, which it defines as fields of study united around particular practices and ways of thinking and communicating. A discipline does not exist independently of its practitioners but rather its practitioners, in practicing and carrying forward the discipline, create the discipline as a type of culture. This discipline-as-a-culture, like any other culture, is something that people learn about and join over time, learning what the discipline studies, how it

studies that thing, how to conduct disciplinary work, and how to communicate both within the discipline and to outsiders about the discipline. More-specifically, the theoretical framework of disciplinary literacy says that to join and learn about a discipline, a newcomer must learn and become literate in the disciplinary culture. Becoming part of a discipline means to become familiar with and take on the disciplinary culture. As such, the role of educators in a particular discipline is to facilitate students to enter the disciplinary culture. In terms of how education occurs, the framework of disciplinary literacy leads researchers and instructors to ask, "What are the disciplinary practices students must learn and how do we support their ongoing inclusion into the disciplinary culture?" Researchers who approach learning using a disciplinary literacy lens have identified a variety of tactics meant to support students' enculturation into the discipline, including epistemological processes [12], linguistics-related tactics [13], and interdisciplinary and inter-contextual strategies [14]. For example, the Expanded Four Resources model is a tactic that has students take on different roles throughout the learning process, being not just recipients of knowledge but active participants [15].

In all cases, the goal of this theoretical framework is that students are supported in becoming literate in a disciplinary culture, with all its various practices, ways of framing and approaching problems, and ways of communicating within and without the discipline. The challenge in higher education then lies in identifying appropriate ways to support students in various contexts and when learning various contents, and ensuring that the educational methods in use actually serve the larger, and often implicit, goals of disciplinary education: to expand and advance the disciplinary community. We choose to use the theoretical framework of disciplinary literacy to anchor our work because it helps us to consider how well current instruction does in

training students to think, act, and communicate like materials scientists, as well as consider what steps can be taken to help students more freely enter the discipline.

In the work described in the following chapters, we want to address the overarching research question of ***How are instructors using concepts of disciplinary literacy in MSE education?*** We will address this in two different aspects, each guided by a particular set of research questions. The first aspect we address is studying how prevalent are concepts of disciplinary literacy, to see how instructors use said concepts in literature on the teaching of crystal structures and crystallography (Chapter 3.2). This literature review is guided by the following overall and more-specific research questions:

- *In the case study of crystallography and crystal structures, how is disciplinary literacy supported in students?*
    - *What are the stated goals of the learning activities used in the publications describing teaching concepts of crystals structure and crystallography?*
    - *How are two tactics that are known to enhance disciplinary literacy explicitly used in the learning activities described in these publications?*

The second aspect we address is the use of representational fluency, a disciplinary literacy strategy, in MSE classrooms in order to compare the effectiveness of various types of representation for the teaching of crystal structures (Chapter 3.3). These classroom studies are guided by the following overall and more-specific research questions:

- *How can using different types of representation help students learn?*
    - *How do students use different types of representations to solve problems and learn concepts?*

o *How well can students learn particular crystal structure concepts when using different types of representations in active learning contexts?*

We then conclude with a summary and address our overarching research question (Chapter 3.4).

References

[1]   "Theoretical Frameworks," in *The SAGE Encyclopedia of Qualitative Research Methods*, 2455 Teller Road, Thousand Oaks California 91320 United States : SAGE Publications, Inc., 2008. doi: 10.4135/9781412963909.n453.

[2]   J. Lave, "Chapter 4: Situated Learning in Communities of Practice," *Perspectives on Socially Shared Cognition*, pp. 63–82, 1991.

[3]   F. Marton, U. Runesson, and A. B. M. Tsui, "The Space of Learning," in *Classroom Discourse and the Space of Learning*, 2004.

[4]   O. A. B. Hassan, "Learning theories and assessment methodologies - an engineering educational perspective," *European Journal of Engineering Education*, vol. 36, no. 4. pp. 327–339, Aug. 2011. doi: 10.1080/03043797.2011.591486.

[5]   E. B. Moje, "Developing socially just subject-matter instruction: A review of the literature on disciplinary literacy teaching," *Review of Research in Education*, vol. 31, pp. 1–44, 2007, doi: 10.3102/0091732X07300046.

[6]   S. S. Wineberg, "Teaching the mind good habits," *Chron High Educ*, p. B20, 2003.

[7]   P. C. Blumenfeld, R. W. Marx, H. Patrick, and J. S. Krajcik, "Teaching for Understanding," in *International handbook of teachers and teaching*, B. J. Biddle, T. L. Good, and I. F. Goodson, Eds. Dordrecht, the Netherlands: Kluwer Academic, 1997, pp. 819–878.

[8]   C. D. Lee and A. Spratley, *Reading in the disciplines and the challenges of adolescent literacy*. New York: Carnegie Corporation, 2006.

[9]   H. Bass, *What is the role of oral and written language in knowledge generation in mathematics? Toward the improvement of secondary school teaching and learning. Integrating language, literacy, and subject matter*. Ann Arbor: University of Michigan Press, 2006.

[10]   L. S. Shulman, "Those who understand: Knowledge growth in teaching," *Educational Researcher*, vol. 15, no. 2, pp. 4–14, 1986.

[11]   E. B. Moje, "Doing and Teaching Disciplinary Literacy with Adolescent Learners: A Social and Cultural Enterprise," *Harv Educ Rev*, vol. 85, no. 2, 2015, [Online]. Available: http://meridian.allenpress.com/her/article-pdf/85/2/254/2110423/0017-8055_85_2_254.pdf

[12]   R. Akkus, M. Gunel, and B. Hand, "Comparing an Inquiry-based approach known as the Science Writing Heuristic to traditional science teaching practices: Are there differences?," *Int J Sci Educ*, vol. 29, no. 14, pp. 1745–1765, Nov. 2007, doi: 10.1080/09500690601075629.

[13]   Z. Fang and M. J. Schleppegrell, "Disciplinary Literacies Across Content Areas: Supporting Secondary Reading Through Functional Language Analysis," *Journal of Adolescent & Adult Literacy*, vol. 53, no. 7, pp. 587–597, 2010.

[14]   E. Morrell, "Toward a critical pedagogy of popular culture: Literacy development among urban youth," *Journal of Adolescent & Adult Literacy*, vol. 46, no. 1, pp. 72–77, 2002.

[15]   F. Serafini, "Expanding the four resources model: reading visual and multi-modal texts," *Pedagogies: An International Journal*, vol. 7, no. 2, pp. 150–164, Apr. 2012, doi: 10.1080/1554480X.2012.656347.

CHAPTER 3.2

Disciplinary Literacy Prevalence in MSE

Background

Having seen a discussion of disciplinary literacy and its principles and tactics in the previous chapter of Chapter 3, it would be remiss to not discuss disciplinary literacy in the context of an actual discipline, namely materials science and engineering (MSE). In this chapter we examine the question, *How are instructors using concepts of disciplinary literacy in MSE education?* In the context of MSE, becoming literate in the discipline and the disciplinary culture would entail understanding and being able to perform the different disciplinary practices [1] as they exist in the discipline. A student would need to implicitly or explicitly understand how materials scientists frame problems and be able to frame problems in that way. The student would need to know how to collect data for topics related to MSE, what constitutes valid data in the discipline, and how to represent, use, and analyze that collected data. They would need to understand how to examine a claim for validity in the context of the discipline and be able to evaluate claims they encounter and create. The student would need to be familiar with the vocabulary and rhetoric used in MSE and be able to use the discipline-specific ways of communicating in order to convey their findings. Since MSE would not be the only culture of which the student is part, they would also need to understand how the disciplinary culture relates

to other cultures to which they belong, and learn to translate and communicate between them. Together, these types of sets of practices can be referred to as the disciplinary cycle [1].

Achieving literacy in a discipline is not a simple task, and helping students to achieve it likewise requires much work on the part of instructors and practitioners. Airey and Linder [2] discuss that disciplinary knowledge is not inherently known by novice learners when they enter into a discipline, but that they develop their disciplinary literacy as they interact with tools, activities, and representations of the discipline. Because instructors who teach at the undergraduate level are often working scientists themself, they are likely to forget that knowledge is formed over time through immersion within the discipline, and focus instead on imparting direct knowledge without the deeper context at a level accessible to the students [2]. For example, in the case of MSE (though these trends are found in many other STEM fields), there is often an emphasis on learning foundational knowledge in lower-level classes, with disciplinary context imparted through separate lab or design courses. At the University of Michigan, MSE course objectives for 200-level classes focus on being able to answer particular scientific and engineering questions with knowledge learned in the course, whereas objectives relating to communication, experimental procedures and design, and engineering design are found in specific 300- and 400-level classes [3]-[6]. Additionally, truly supporting learners' disciplinary literacy means including the affective, social, and cultural dimensions of learning [1]. Doing so creates opportunities for learners to regard their backgrounds, cultures, abilities, and developing knowledge as essential elements of their knowledge creation and disciplinary learning. Overall, applying a disciplinary literacy perspective to how teaching and learning happens within the discipline of MSE aids in our understanding of how we are developing learners' ability to effectively engage in our specific disciplinary practices.

Instructors commonly design learning activities to introduce students to the ways of knowing, thinking, believing, acting, and communicating within a specific discipline [7]-[8]. The experiences they choose are intended to acquaint students with discipline-specific resources— that is, vocabulary, concepts, tools, and practices (E.g. "crystal lattice", the concept of electronic structure, microscopes, and the design process, respectively)— that are deemed relevant and important by disciplinary practitioners. More specific to undergraduate science education, how instructors use these resources creates a shared way of knowing [2] and culture that supports students' ability to reason and behave as a scientist in that discipline [9]. These abilities include the disciplinary cycle as described above, which more succinctly includes working with information and data, being able to represent information in a number of ways (for example visually, symbolically, or as text), analyzing, summarizing, and synthesizing findings, examining and evaluating claims, and communicating those claims [1].

More generally, socio-cultural pedagogy, including that guided by disciplinary literacy, is united by three broad tenets: learning is socially-based, or reliant on cooperative interactions and social tools such as language to help students develop personal understandings; teaching consists of assisting the learner to learn and master societally-valued concepts and topics the student could not master unassisted; and performance is situative, or can be affected by the context in which it takes place [10]. Such a socio-cultural approach tends to be more meaningful and equitable, allowing students to become literate in the social and cognitive practices of experts within the discipline. For example, Finkenstaedt-Quinn et al. [11] take a socio-cultural approach to materials science education. In that work, students complete writing assignments that engage the disciplinary cycle as they communicate STEM topics to a hypothetical non-STEM audience and critique their peers' drafts. This method deliberately focuses on student-generated

106

communication to enhance learning, and has been applied to chemistry and across STEM [12-13] and discussed in Rivard [14]. Other socio-cultural strategies for disciplinary literacy education include the use of multiple representation types [15] and designing learning activities that engage various learner roles [16]. Observing how the literature implicitly employs these strategies helps us to see how the disciplinary practitioners intend to make students literate in the overall discipline, as well as what sorts of strategies are valued.

In order to study the prevalence and usage of disciplinary literacy principles in MSE education, we chose to do a systematic literature review on articles looking at the teaching and learning of one specific topic vital to MSE, crystal structures and crystallography. This topic was chosen as our lens for the review for two reasons. Firstly, it was chosen because it is critical to many disciplines in the sciences, with aspects of crystallography contributing to around 40 Nobel prizes in Physics over the years, and so represents a topic that is necessary to impart to students. Secondly, it was chosen because the topic is relatively well-defined, and so articles on the topic can both be found and be separated from similar but irrelevant-topic-focus articles relatively easily, yielding a manageable dataset for this review. Our review broadly addresses the following research question: *In the case study of crystallography and crystal structures, how is disciplinary literacy supported in students?* More specifically, it focuses on using the literature to answer these two main research questions, related to our overall research questions above and in the previous chapter:

RQ1. What are the goals of the learning activities used in the publications describing teaching concepts of crystals structure and crystallography?

A. What are the thematic categories for the explicitly stated purpose of the publications?

B. What are the types of learning activities that the students were asked to do?

C. What are the observed relationships between the themes and learning activities?

and

RQ2. Which tactics that are known to enhance disciplinary literacy are explicitly used in the learning activities described in these publications?

A. What are the observed relationships between the utilized forms of representation and learning activities?

B. What are the observed relationships between the supported learner roles when transacting with a learning activity?

Answering these research questions allows us to understand what is valued in the teaching of crystal structures and crystallography, to determine whether instructors are already using the principles of disciplinary literacy in their teaching of these topics, and to begin to shed light on where any gaps exist in current teaching practices about promoting the socio-cultural development of learners within this discipline.

Methodology

To conduct this literature review, we followed the method originally described by Extremera [17]. A flowchart summary of the process can be seen in Fig. 3.2.1, and descriptions of our inclusion/exclusion criteria are given in Table 3.2.1.
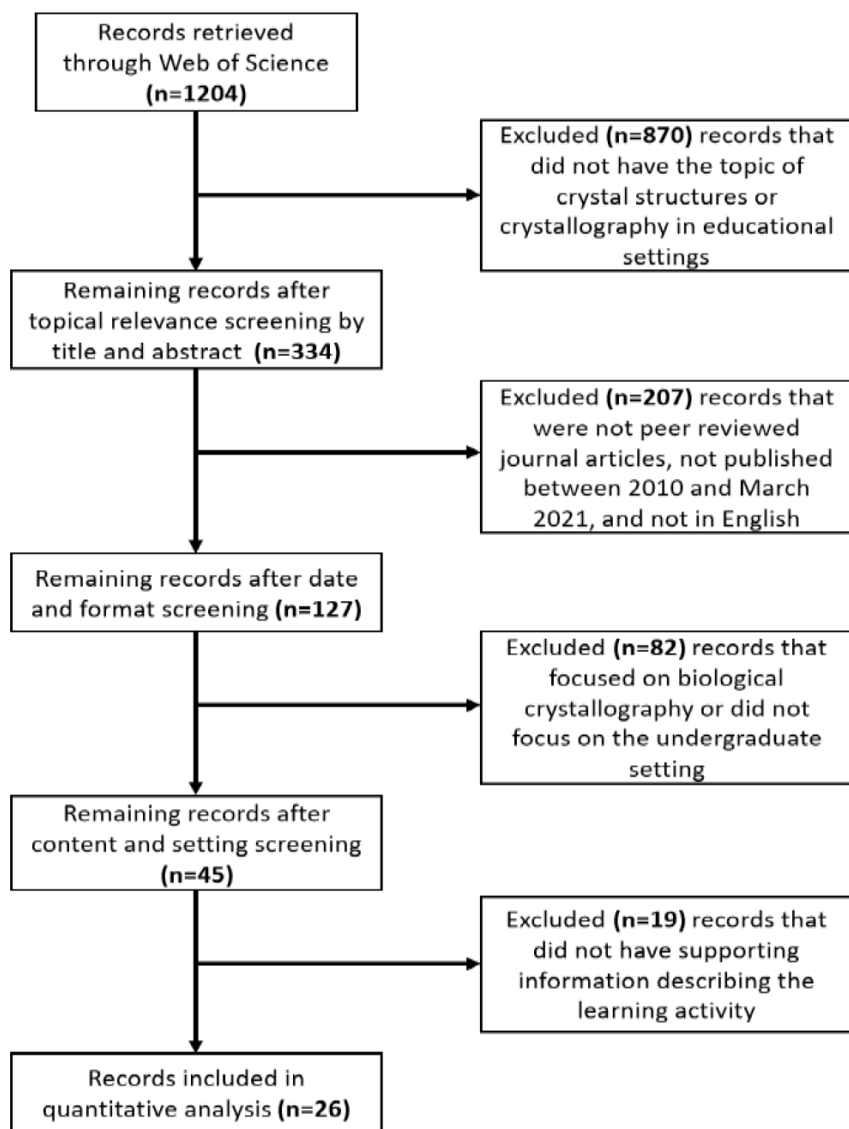
Figure 3.2.1: Summary of the process used in this review to select relevant works on the subject of crystal structures and crystallography

Table 3.2.1: Inclusion and exclusion criteria

Criteria	Inclusion	Exclusion
Time Period	Published from 2010 to March 2021	Studies outside this time period
Literature Type	Peer-reviewed journal articles	Literature that are not peer-reviewed journal articles (conference proceedings, popular press, book chapters)
Language	English	Non-English
Accessibility	Accessible online through the University of Michigan library	Not accessible
Topic	Concerned with teaching and learning of concepts related to crystal structure and crystallography in physical sciences (physics, chemistry, materials science, etc.)	Not concerned with teaching and learning of concepts related to crystal structure and crystallography, dealing with crystallography in the life sciences, descriptions of historical crystal- and crystallography-based courses not containing description of specific learning activities
Target Educational Level	Undergraduate	K-12, graduate-only, or professional-only
Supporting Information	Has supporting information including detailed descriptions of the learning activity	Does not have supporting information that includes detailed descriptions of the learning activity

Our review team consisted of two content experts, one pedagogical content/content expert, and one education researcher. On March 24th, 2021, we used the following string in the topic search of the Web of Science database: ((*crystal* OR nanostructure$) AND (teach* OR learn* OR train* OR educati*)). The query resulted in 10928 entries, and so the string was changed to refine the results: ((*crystallogra*) AND (teach* OR learn* OR train* OR educati*)). The revised query yielded 1204 entries. From that list, 870 entries were removed that did not have titles, abstracts, or keywords pertaining to the teaching of crystal structures and crystallography. From the remaining 334 entries, 207 entries were removed that were not in English, were not published during the time period of 01/01/2010-03/24/2021, or were not peer-reviewed journal articles. The non-English records were removed in order to ensure all articles in the final review were able to be read and understood by all four members of the review team. The records outside of the 2010-2021 time period were excluded for two reasons. The records from before that time

period were excluded because they were less likely to reflect current, as opposed to historical, thought on the subject. The records from after that time period were excluded in order to ensure that a defined set of entries could be included in the later analysis; without a defined end of record collection, the literature review would never progress past that stage. The non-peer-reviewed records were removed due to the standards of the field and due to our analysis needs. Such records tend to be conference papers, which in the fields of education and disciplinary education tend to not report on finished works. Additionally, such conference papers were unlikely to include enough detail on the activities reported for our team to accurately categorize them in our subsequent coding.

The abstracts of the remaining 127 entries were read and coded along three parameters: 1. The broad topic of the article, such as whether it was concerned with crystal structures, crystallography, a particular subfield, or a larger course that may contain those topics. 2. The target educational level of the described intervention or activity, such as the general public, high school, or undergraduate. 3. The general purpose of the article, such as reporting a novel visualization method or explaining an application of a teaching method. Our coding led us to remove 82 entries that focused on biological crystallography or did not target undergraduate education. The records on biological crystallography were removed because they tended to be focused highly on the crystallization process as opposed to crystal structure or crystallography. The records that did not target undergraduate education were removed because our aim was to study disciplinary literacy in the undergraduate context. Finally, in order to fully code the disciplinary practices employed in the reported activities or interventions, 19 entries were removed from the remaining 45 because they did not give a detailed description of the learning activities in supporting information. A final selection of 26 articles were included in this review.

The articles in this review describe a variety of contexts and have varied countries of origin. While all articles describe at least one learning activity aimed at undergraduate students, most of them (20 articles) were explicitly implemented in a chemistry course, while others were implemented in physics or interdisciplinary crystallography courses (for example, [18]). Similarly, most of the courses tended to be upper level or specialized undergraduate courses (17 articles), though there were some that were aimed at introductory courses such as general chemistry (for example [19]). The classrooms in which the activities were implemented were in a variety of countries, including in China [20], Germany [21], Japan [22], Poland [23], Russia [24], the UK [25], and the USA [19]. The 26 articles are included in this review regardless of academic or national context because they are united by an overarching common factor, that being that each of the articles was seen as valuable by their respective authors and editors to publish to an international audience of similar disciplinary practitioners.

The articles were coded in-line with the process described in [26] and [27]. All members of the review team read through a selected article and coded it for its general purpose and representation types used. The members then met to discuss the coding and settle on definitions and the types of codes used. A second article was then read by all the members to ensure that each member's use of the codes aligned. After the completion of the second article, members split into pairs (each consisting of one content expert and one pedagogical content or education expert) to review a further four articles and ensure coding consistency. After the total of six trial articles were completed and the codes were deemed usable, each member went on to code a further 8-9 articles individually. (The final number of articles was not settled until after the first round of coding, when we determined we would limit ourselves to articles with full activity descriptions, hence the seemingly too-large number for the four members' individual coding.)

Coding for the final two parameters, the activity type and the learner role, followed a similar process but was conducted by only two members of the review team.

In all and as mentioned above, there were four types of parameter that were coded for, the general purpose of the article, the type of activity described by the article, the types of representation used in the activity, and the learner roles supported by the activity. Full descriptions of the codes used and justification for each parameter are given in the following paragraphs.

The first parameter was the general purpose of each article. This parameter was chosen as it gave an indication of the intent of the authors of each article. Coding for this parameter was done by reading through the article and finding specific statements by the authors, so as to use their own words and not have our research team assume their intent. The collected purpose statements were then analyzed and grouped according to recurring themes, and each article was then classified as having a single overall theme for the purposes of our coding. In all, a total of six such themes were identified: General-Principle Experiment, Specific-Concept Activity, Implementation Guidelines, Technique/Equipment, Research Practice, and Virtual/Physical Models. The General-Principle Experiment theme applied to articles where the purpose of the author(s) was to describe an experiment activity that was chosen to convey a broader concept. The Specific-Concept Activity theme was used to indicate articles in which the purpose was to use a purposefully-designed activity to convey a specific concept to students. The Implementation Guidelines theme applied when the aim of the author(s) was to provide guidance for how to adapt or implement a certain type of learning activity or teaching tool across a variety of different contents and contexts. The Technique/Equipment theme indicated articles where the goal of the author(s) was to have students learn to perform a certain technique or familiarize

themselves with and learn to use a type of equipment. The Research Practice theme pertained to articles in which the primary intention was for students to be involved in some sort of authentic or semi-authentic research experience. Finally, the Virtual/Physical Model theme described articles that had the general purpose of introducing a new virtual tool or physical model of a crystal structure or crystallography concept and giving some demonstration of its classroom use.

Because we were basing the theme classification off of the authors' stated purpose, there were some cases where articles that describe similar activities were classified as having different themes merely because the authors of the articles spoke about the purposes differently. For example, both [28] and [29] described a learning experience in which students learned to synthesize and characterize a target material, but where [28] was classified as Research Practice after giving the purpose as "to prepare students for a research-focused independent term project," [29] presented the purpose as to "teach students basic research tools and procedures" and was classified as Technique/Experiment. In some cases, an article might, based on the activity described, be implied to have a secondary theme, but in such cases we attempted to classify the articles based only on what was explicitly stated as the purpose by the author(s). For example, many of the articles with the Specific-Concept Activity theme [19], [20], [30], introduced new ways of visualizing or modeling crystal structures, but because the authors noted that the purpose of the article was the activity that uses their novel visualizations, and not the visualizations themselves, they were not classified as having the Virtual/Physical Model theme.

The second parameter was the type of activity described. This parameter was chosen so that we would be able to describe, examine, and analyze the different components or learning activities that made up the larger activity described in the article. Coding for this parameter was done by reading through the article and the detailed activity description given in the article's

114

supplementary information in order to determine what sorts of things the students were asked to do. These activity types were then grouped into categories and the articles were coded according to which categories its described activity fell into. Overall, there were four identified categories of activity type: Experiment, Computer Visualization, Physical Visualization, and Writing/Speaking. The Experiment activity type included students conducting any type of experiment such as chemical synthesis or x-ray diffraction. The Computer Visualization activity type was identified in articles where students had to use computers to visualize and possibly interact with crystalline models. The Physical Visualization activity type was used for those articles where students interacted with a physical model of any sort, most often of crystals. Finally, the Writing/Speaking activity type included activities where students had to write or orally give a response to a prompt of some kind, be it participating in a class discussion, completing a lab report, or describing a phenomenon.

The third parameter was the types of representation used in the articles' described activities. The types of representation were chosen as a parameter in order to study the articles' use of disciplinary literacy tactics, specifically the use of varied media to promote representation fluency. To code for the different representation types, the Lesh model [15] was used. The Lesh model [15] described five categories of representations: Pictorial (e.g.: charts, figures, and schematics), Symbolic (e.g.: mathematical equations), Language (e.g.: verbal descriptions), Concrete (physical or tangible models), and Realistic. Lesh defines Realistic representations as those with "Real-World or Experienced Contexts" (Moore et al., [15]). For this review, we categorized representations as Realistic when students either performed experiments or worked with real experimental data.

The fourth and final parameter was the learner roles supported by the described articles. This parameter was included in order for us to examine the ways in which the described activities prompted and supported students to act. The role of the learner was coded according to the Expanded Four Resource Model [16]. According to Firkins [31], the four resource model is a schema and tool that instructors can use to plan and design learning activities. While a student could ostensibly take on any role while interacting with a learning activity, bringing their own experiences and skills to bear, learning activities can be intentionally designed to support and activate certain learning roles. The expanded four resource model consists of four categories– Navigator, Interpreter, Designer, and Interrogator– identifying what role learners take on when interacting with things like text, images, or audio resources. In the context of our study, we identified what learner roles were supported in the activities and coded for the four learner roles as follows. The Navigator role was said to be supported whenever students were expected to know or carry out a procedure. For example, one of the articles in the review supported the Navigator role by having students follow and conduct a detailed procedure to synthesize and then characterize a covalent organic framework [32]. Students were supported to take on the Interpreter role whenever they were tasked with analyzing data, interpreting results, or drawing conclusions. Illustrated in [33], students were supported to take on the Interpreter role when they analyzed crystal structure data taken from databases to find specific parameters and judge the quality of the proposed structure. The Designer role was emphasized and supported when students were called to actively engage with the activity and to make choices that affect the activity's trajectory. This role was supported in [28] by having students propose and carry out individual term projects. Finally, the Interrogator role was seen as supported whenever students were asked to put their current actions and activity in context of the topic at hand, the wider

116

scientific field, or their education. Seen in [25], this role was supported when students collaborated with researchers on authentic crystallography experiments, with a heavy emphasis given to the larger context. Each learning activity could be designed to support more than one role. For example, in [18], students previously familiar with powder diffraction were tasked with doing a diffraction experiment on a large single crystal, where they had to explore ways to mount the crystal (Designer), carry out the diffraction procedure (Navigator), and analyze data that included both expected and unexpected results (Interpreter).

Each article was classified as having one purpose theme and as many of the other parameter types as were applicable, with a minimum of one of each parameter type assigned to each article.

Results

General Purpose of the Articles

The first research question concerns itself with the goals and content of the learning activities described in the articles of our review. One aspect of this line of inquiry is to understand the articles' explicitly-stated purpose (RQ1A). The purpose of each article is categorized into only one of six overall themes: General-Principle Experiments, Specific-Concept Activities, Implementation Guidelines, Virtual/Physical Models, Technique/Equipment, and Research Practice (Table 3.2.2). The articles are roughly evenly distributed among the six themes, as seen in Table 3.2.2.

Table 3.2.2: List of the themes of the research articles, the frequency counts, and the articles that fall under each analysis category. All counts are out of the total of 26 articles.

Classification	Count	References
General-Principle Experiments	5	[18], [34]-[37]
Specific-Concept Activities	5	[19], [20], [23], [30], [38]
Implementation Guidelines	3	[33], [39], [40]
Technique/ Equipment	4	[25], [29], [41], [42]
Research Practice	4	[28], [32], [43], [44]
Virtual/ Physical Model	5	[21], [22], [24], [45], [46]

The first theme, General-Principle Experiment, encompasses articles where the purpose is to describe a particular experiment or set of experiments used to teach a broader principle such as structure-property relationships. In General-Principle Experiment-themed articles, the specific experiment is chosen by the authors because it illustrates a general principle that could not be conveyed directly. An example of this theme can be seen in [34], where the authors describe how different diffraction experiments are used to determine the structural characteristics of various intermetallic compounds including the type of lattice and unit cell dimensions. While being concerned with the intermetallic compounds, the emphasis of the activity, however, is on how to convey the general principle of structural characterization with X-ray diffraction, with the intermetallic compounds merely chosen to aid that goal. Similarly, in [37], the choice of chemical synthesis is made in order to introduce students to the general principle of mechanochemistry and green chemical synthesis. A third example of this theme is also seen in [35], where the general principle of the characterization of chemicals present in historical pigments through x-ray powder diffraction and scanning electron microscopy is taught through experiments around the synthesis and characterization of certain cobalt-based pigments.

The second theme was Specific-Concept Activities. Articles with the Specific-Concept Activity theme had the general purpose to carefully design activities to complement and encapsulate a particular concept. As an example, in [23] students are taught how to identify symmetry operations through the analysis of friezes, or decorative architectural flourishes, at a local historical building. The majority of the articles classified as having the Specific-Concept Activity theme [19], [20], [30] describe activities that involve building crystal models and learning their atomic arrangements and spatial properties. For example in [19], students learn to build specific crystal structures and stacking arrangements of atoms using spherical magnets and marbles, and are guided through calculations of unit cell volumes and packing efficiency.

The third theme was used for articles that revolve around providing general Implementation Guidelines for various teaching methods in chemical or crystallographic education contexts. In [39], for example, the authors discuss how extended field trips to experimental facilities can be designed, organized, and implemented in order to add richness to the topic at hand, (in this case specialized applications of x-ray diffraction,) and thus more deeply engage students. In this article, the emphasis is not on the particular activities and experiments done on the field trip per se, but rather on the advice it provides on how to best plan these types of field trips. This theme is also seen in [33], which aims to explain how to best implement case studies in crystallography courses, and in [40], which focuses on how to implement a crystallography module into a chemistry course at an institution where X-ray diffraction equipment is unavailable.

The fourth theme categorizing the authors' purpose was Technique/Equipment. For these articles, the general aim is to help students learn a particular experimental [29] or analytical [42] method. While there are similarities between this theme and the General-Principle Experiment

theme, this theme is distinct in that the authors explicitly state that the purpose is to learn the technique itself rather than the principle it embodies. For example, in [41], the author's stated purpose was that students learn how to use common synthesis and characterization techniques for crystalline solid state materials, while in [42], the students are intended to learn how to do a Rietveld refinement, a data analysis technique. The activity or experiments described in these articles are meant to impart specific, transferrable procedural knowledge to students.

A fifth theme that emerges from the authors' intended purpose is giving students opportunities for authentic Research Practice. In this theme, exemplified in [28], [32], [43], [44], the purpose is to help students learn about and gain appreciation for the process of research, including experimental design, data collection and analysis, and the communication of findings, rather than teaching principles or concepts, or training students in the use of particular techniques. For example, [28] aims to give students research practice through a semester-long course focused on independent research-like projects concerning inorganic chemical synthesis and characterization of metal-oxide zeolites, while [32] does the same through an experimental series that focuses on metal-organic and covalent-organic frameworks and which has students go through a mock research article submission process.

The sixth and final theme that emerges from the articles' purpose is Virtual/Physical Models. Articles with this theme, such as [22] and [46], focus less on any particular educational activity and more on the model being introduced for use in educational settings. For instance, [46] describes a new web application that enables the visualization of crystal structures and reports on the application's features, also including examples of using the application in a classroom setting and a sample learning activity. Though there are activity descriptions present, the stated purpose of the article is still to describe the application itself. Likewise, [22] discusses

a new method of modeling crystal structures using latex balls cut to fit into unit cell shapes, detailing how to properly construct the models. While the article also describes a learning activity that has been implemented in classrooms using the model, the stated purpose and the bulk of the article focuses on discussing the principles behind the design of the model, leaving the design of the learning activity using the model largely free for the reader to determine.

Types of Learning Activity

Our inquiry also led us to examine the types of learning activities, or what the students were asked to do (RQ1b). These categories consist of Experiments, Computer Visualization, Physical Visualization, and Writing/Speaking (Table 3.2.3). While each article is categorized under one theme based on the author(s) stated purpose, several learning activities could be described in each article.

Table 3.2.3: List of the Teaching Activities of the research articles, the frequency counts, and the articles that fall under each analysis category. All counts are out of the total of 26 articles.

Classification	Count	References
Experiment	14	[18], [28], [29], [32], [34]-[37], [39]-[44]
Computer Viz.	6	[25], [29], [32], [33], [40], [46]
Physical Viz.	6	[19]-[22], [24], [30]
Writing/Speaking	23	[18]-[23], [28]-[30], [32]-[38], [40]-[46]

Approximately half of the reviewed articles implement Experiments as a learning activity, where students engage in research techniques and laboratory procedures to learn the concepts of crystal structure and its relation to material properties. This activity type encompasses a wide variety of activities, including diffraction experiments on various materials (for example [36]) or material and chemical synthesis with particular methods (for example [28]

121

and [37], which use hydrothermal synthesis and mechanochemical synthesis, respectively). Non-structural characterization experiments (for example [43] which examines optical properties, or [29] which has students examine gas adsorption in covalent organic frameworks) are also included in this activity type. Often, more than one of these individual activities is done in the experiment series, though the activity type is only counted once. In one example, students synthesize various intermetallic alloys, then analyze their alloys as well as the elemental constituents using X-ray diffraction to determine the details of their crystal structures [34]. In a different article, students are given large crystal specimens of pyrite for X-ray diffraction analysis, and asked to compare the obtained results with those found in the literature for powdered samples [18].

A smaller subset of articles use learning activities centered around Computer Visualization, in which students interact with content using a computer interface to visualize models or data. This type of learning activities is sometimes implemented using structural databases such as the Cambridge Structural Database, and integrated into longer courses focused on teaching crystallography [25], [33]. In the database-assisted activities, students are provided with visualizations of chemical and crystal structures and are asked to interact with them and identify things like bond lengths and bond angles. Another approach to learning activities utilizing computer visualization is to provide students with and train students in the usage of software in which they can view and manipulate 3D models of crystals. For example, in [46], a web-based interactive tool with representations of crystals in unit-cell and extended configurations is developed and implemented to supplement instruction.

The next type of learning activity, Physical Visualization, requires students to build, manipulate, and interpret physical models of crystal structures in order to learn crystallography

concepts such as packing efficiency, coordination, and atom counting. This type of learning activity gives students tactile and visual feedback as they use physical models to understand the visuo-spatial relationships of atoms in crystal structures. In many of these articles, students assemble spheres into different packing/crystal structures unit cells, differentiated mainly by the type of materials used for the atoms (silicone [20], magnets, marbles [19], and latex [22]) and for the unit cells (acrylic boxes [22], and metal rods [30]). Also falling under the Physical Visualization activity type is the use of 3D printed model sets of crystals and molecules [24].

The final and most common type of learning activity is called Writing/Speaking. This type of activity includes anything where students are instructed to write or orally relay ideas in their own words. This type of learning activity could include students writing short responses to an assigned reading, describing their understanding of details of what they have learned regarding crystallography and material properties, or reporting findings of an experiment [33], [38]. For instance in [33], students participate in a guided discussion centered around research-based case studies. Other examples include learning activities wherein the student answers a series of open-ended questions designed to guide their thoughts and learning [18], [36]. For example, in [18] students perform a diffraction experiment that leads to a deliberately puzzling result, and then have to answer a series of leading questions until they are able to explain the unexpected result. This type of learning activity is most commonly seen in the completion of a lab report [20], [32], [37].

Comparison of Article Purposes and Learning Activity Types

Our inquiry finally leads us to observe the relationship between the article purpose themes and types of learning activities (RQ1C). Figure 3.2.2 shows the normalized frequencies of the four types of learning activities based on their occurrence in articles within each of the six

123

themes. Each type of learning activity has a unique frequency distribution. Writing/Speaking is the most common learning activity type, occurring in the majority of articles, and it is broadly distributed across each of the six article themes. The Experiment learning type is as common as Writing/Speaking in the General-Principle Experiment, Research Practice, Technique/Equipment, and Implementation Guidelines themes, but is not found at all in the Virtual/Physical Model and Specific-Concept Activity themes. The Physical Visualization learning activity type only occurs in articles with the Virtual/Physical Model or Specific-Concept Activity themes. The final activity type, Computer Visualization, occurs in Implementation Guideline-themed articles, and sometimes Research Practice, Technique/Equipment, and Virtual/Physical Model-themed articles, but is not found in articles of the General-Principle Experiment and Specific-Concept Activity themes.
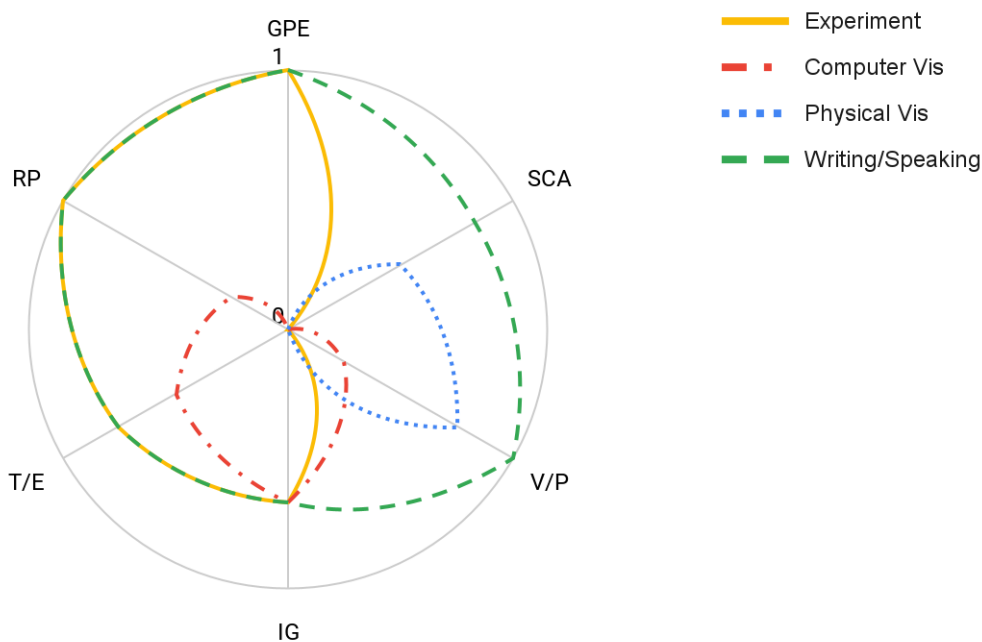
Figure 3.2.2: Radial plot of the frequency of the four learning activity types in articles with the six article themes- General-Principle Experiment (GPE), Specific-Concept Activity (SCA), Virtual/Physical Model (V/P), Implementation Guidelines (IG), Technique/Equipment (T/E), and Research Practice (RP). The frequencies are normalized, representing the fraction of articles with an article theme that reported a particular activity type. A frequency of one means that all articles within a specific article theme include that activity type. The normalized frequencies do not sum to one, because some articles reported as many as four activity types, though each article can have only one article theme.

Implementation of Disciplinary Literacy Tactics

For research question 2, we examined both what the articles described having the students do (the learning activities) and how those activities employed various types of representations and supported different learner roles.

Disciplinary Literacy Tactics: Representational Types

Our inquiry first leads us to examine the relationship between the types of learning activity and the types of representation used (RQ2A). Figure 3.2.3 displays the proportion of the articles with a particular learning activity that also have a particular Lesh model representation type. The summary of what papers employed which representation types is seen in Table 3.2.4.
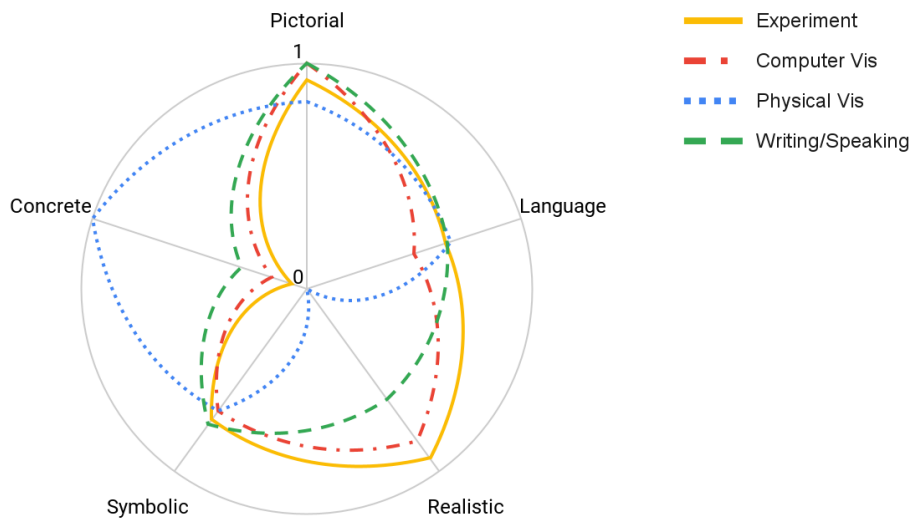
Figure 3.2.3: Radial plot of the proportion of the number of papers having a particular Lesh model representation type co-occur with one of the four learning activities divided by the number of papers having that learning activity. A frequency value of one means that the type of representation occurred in all articles within that activity type. Values do not sum to one, because articles may have as many as five representation types.

Table 3.2.4: List of the Lesh Model representations in the research articles, the frequency counts, and the articles that fall under each analysis category. All counts are out of the total of 26 articles.

Classification	Count	References
Pictorial	24	[18]-[23], [25], [28]-[30], [32]-[38], [40]-[46]
Language	15	[20]-[22], [28]-[30], [32]-[35], [37], [38], [42]-[44]
Realistic	16	[18], [25], [28], [29], [32]-[34], [36]-[44]
Symbolic	18	[18], [19], [22], [24], [29], [30], [32]-[34], [36]-[38], [41]-[46]
Concrete	8	[19]-[22], [24], [30], [35], [46]

For instance, Fig. 3.2.3 shows that of the articles that have Experiment learning activities, almost all of them have Pictorial representations. Each type of learning activity uses four out of the five types of representation frequently, but the identity of the four types varies. Indeed, two relationships between the types of activity and representations used are apparent. In all cases, the high frequency of Pictorial, Language, and Symbolic representations is nominally the same across all learning activity types, but the frequency of Realistic versus Concrete representations varies. The Experiment, Computer Visualization, and Writing/Speaking learning activities all have Realistic representations as their final high frequency representational type, and likewise have a low frequency of Concrete representations. In contrast, every article with Physical Visualization learning activities uses some form of Concrete representations (e.g. crystal structure models made from latex balls and acrylic plates in [22]), and has no usage of Realistic representations.

There are also notable differences in the frequency of representation type occurrences between the Experiment, Computer Visualization, and Writing/Speaking learning activities. Articles with the Experiment activity type have the highest occurrences of Realistic representations and a slightly lower frequency of Pictorial representations compared to Computer Visualization and Writing/Speaking learning activities. Computer Visualization learning

126

activities meanwhile have the lowest frequency of Language representations of all four activity types, with Language representations only being seen in half of the articles. Articles with Writing/Speaking learning activities have the lowest occurrence of Realistic representations for learning activities not classified as Physical Visualization, with Realistic representations being only moderately frequent.

To clarify a point, the fact that Language representations are not universal in articles with Writing/Speaking learning activities could seem like a discrepancy, but the two terms are not synonymous. In the Lesh model, Language representations refer to descriptions using words, while the Writing/Speaking learning activity type refers to any case where students are asked to write down or talk about something during the student activity, which includes producing descriptions that describe concepts but can also mean performing calculations or answering questions. Thus, not every production of words by a student includes descriptions of concepts, and not every verbal description observed of a concept is produced by students.

Disciplinary Literacy Tactics: Learner Role

Our inquiry finally leads us to examine the relationship between the types of learning activity and the learner roles supported (RQ2B). Figure 3.2.4 shows the proportion of the articles with a particular learning activity that also have a particular Extended Four Resources model learner role. The summary of what papers included which learner roles is seen in Table 3.2.5.
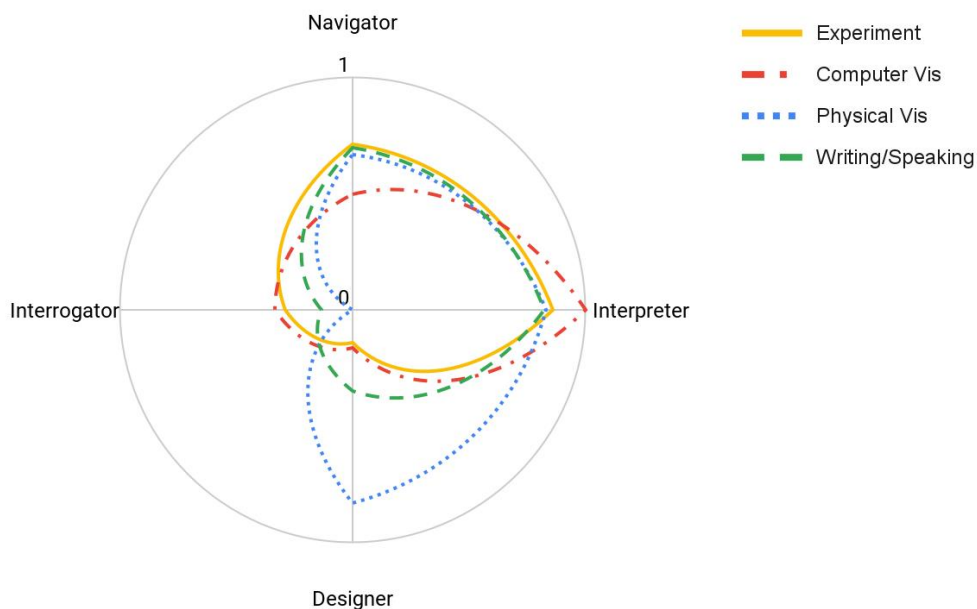
Figure 3.2.4: Radial plot of the proportion of the number of papers having a particular Extended Four Resources model learner role co-occur with one of the four learning activities divided by the number of papers having that learning activity. A value of one means that the learner role occurred in all articles with that learning activity type. Values do not sum to one, as any one article may have as few as one or as many as four learner roles.

Table 3.2.5: List of the Extended Four Resources Model learner roles in the research articles, the frequency counts, and the articles that fall under each analysis category. All counts are out of the total of 26 articles.

Classification	Count	References
Navigator	17	[18], [21], [22], [24], [28]-[30], [32], [34], [35], [37], [38], [42]-[46]
Interpreter	21	[18]-[23], [25], [28]-[30], [32]-[36], [39]-[41], [43], [44], [46]
Designer	9	[18]-[22], [25], [28], [30], [38]
Interrogator	5	[25], [29], [37], [39], [43]

As seen in Fig. 3.2.4 and Table 3.2.5, the Interpreter and Navigator roles occur frequently

across learning activity type, and Interrogator and Designer occur much less frequently. Only

one activity type, Physical Visualization, has frequent occurrences of the Designer role, but it has

no occurrences of Interrogator. In general, the frequent occurrence of the Navigator and

Interpreter roles relates to students performing a procedure (Navigator) and collecting and using

data (Interpreter). For example, in [32], the students are tasked with performing a computational

activity and a lengthy synthesis procedure to create covalent organic frameworks, then collecting

structural and functional data from the resulting covalent organic frameworks and comparing it to calculated data. The Designer role is most frequent in articles with the Physical Visualization learning activity, as those activities often give students more freedom to make choices that materially affect the system being modeled. For example, [20] has students construct models of various compounds, both small molecules and crystalline unit cells, but it also asks students to construct models of chemicals that interest them and use the models to help explain relationships between bonding, structure, and chemical properties. Least common of all the learner roles is the Interrogator role, as the learning activities reviewed do not often discuss how students are supported to put their current learning and doings in the context of the topic, field, or wider education. However, the role is not absent, and does occur in some articles, such as [39], which describes how a multi-day field trip to a synchrotron site could be arranged, and includes both an actual experiment and multiple seminars on crystallography topics that students cite as being illuminating on the breadth of crystallography and its place in scientific research.

Implications

In this work, we examine what is valued among disciplinary practitioners on the topic of crystal structure and crystallography instruction and the extent to which these practitioners use concepts and tactics from disciplinary literacy in describing learning activities on this topic. After examining the 26 articles found that describe learning activities on crystal structures and crystallography, we see that the articles tend to fall into six themes in terms of authorial purpose, split generally evenly between General-Principle Experiment, Specific-Concept Activity, Virtual/Physical Model, Implementation Guidelines, Technique/Equipment, and Research Practice. We also see that the activities themselves tend to be composed of several individual component activity types, of which the most common overall and universal across themes is

Writing/Speaking. In terms of disciplinary literacy tactics in use, the activities described in the articles tend to most frequently support the learner roles focused on procedural knowledge and analytical experience, and a variety of representational types are employed in conjunction with each other. These trends demonstrate the value that instructor-practitioners of the discipline place on hands-on experience with laboratory settings, discipline-related communication, and fluency in different types of representation in the teaching of students. The emphasis on experimentation and visualization tools does more than to familiarize students with the equipment and tools or train students to carry out specific procedures, it also serves to enculturate students into the disciplinary practices, attitudes, and historical context that the discipline values as important. For example, students' interactions with a physical tool (such as a microscope or a crystal model) can lead to both a situated understanding of how to conduct a piece of science and also access to some of the disciplinary context implicit in the tool's development and application [2].

Beyond just the trends in purposes, activity types, and disciplinary tactics used, the identity of the purpose themes themselves also tie into their use in the training of disciplinary literacy in crystal structures and crystallography. For example, using Moje's [1] "four E's" heuristic of Engage, Engineer, Examine, and Evaluate for teaching using the socio-cultural perspective of disciplinary literacy, most of the articles in this literature review, especially those that involve experiments as learning activities, are consistent with the first of the four E's in that they seek to "engage students in the everyday practices of the discipline" [1]. The General-Principle Experiment, Technique/Equipment, and Research Practice themes are clearly related to scientific practice overall, and even the Implementation Guidelines theme attempts to link learning activities to specific scientific practice. For example, [28] (classified as Research Practice) describes a seven-week project intended to give students the background and

experience necessary in synthesis, characterization, and the research process to conduct their own independent project later in the course. Likewise, [39] (classified as Implementation Guidelines) describes a substantive field trip to a national lab intended both to give students experience with a high-level research project and allow them to put their crystallography work in the context of the broader advancement of science.

Similarly to the identity of the themes alone, the relationship between the themes and the learning activities reveal the disciplinary attitudes and practices that are valued in the teaching of crystal structures and crystallography. For example, Moje [1] defines the "disciplinary cycle" within the Engage dimension that is common across disciplines, consisting of problem framing, working with data, using varied media, analyzing and synthesizing findings, examining and evaluating claims, and communicating claims. Many of the themes and learning activities identified in this review are either concerned with the entire disciplinary cycle (Research Practice and Experiments, for example) or portions of the cycle (Virtual/Physical Model and Writing/Speaking, for example, which are concerned with using varied media and communicating claims, respectively). The Experiment learning activity appears across a majority of the themes; having students do experiments places them in the role of scientists, and teaches them how to reason and behave as one. Writing/Speaking is also seen as extremely important, as it appears frequently across all of the themes. This prevalence of the Writing/Speaking activity type suggests that learning how to communicate technical information and engage in disciplinary discourse is a critical goal in science education [47]. Such a priority is understandable given that instructors of undergraduate-level STEM courses are usually scientists in addition to instructors. The other two activities, Computer Visualization and Physical Visualization, are highly localized and confined to a limited subset of themes. Perhaps this localization is partly because said subset

of themes (and the Virtual/Physical Model and Specific-Concept Activity themes especially) are focused on specific aspects of the disciplinary cycle, namely using varied media and analyzing and synthesizing findings. The specificity of the relationship between Physical (or Computer) Visualization learning activities and the Virtual/Physical Model (or Implementation Guidelines) theme begs the question of whether these activity types and themes are important specifically to teaching crystal structures and crystallography. An analysis of another subtopic within science could perhaps reveal additional or different themes and learning activities.

Addressing Moje's [1] Engineer level of the heuristic (developing activities such that they are developmentally appropriate facsimiles of disciplinary work) in the context of our review, we find that the articles do not provide us with enough information to draw full equivalencies. The articles in this review do not discuss how the instructors decided that the learning activities are developmentally appropriate outside of mentioning the students'/courses' level (e.g.: senior undergraduates, introductory course). While articles with the Implementation Guidelines theme attempt to offer some advice on how to design specific types of learning activities, there is not a strong description of how instructors recognize what is developmentally appropriate, nor what constitutes an appropriate facsimile. Indeed, recognizing students' prior knowledge, understanding, or skills, or how to teach across their inevitable variability is not discussed.

While some of the themes, as mentioned above, seem confined to the discipline of crystal structures and crystallography, they are not devoid of value in terms of imparting disciplinary literacy. The Engineering level is where content literacy, the disciplinary concepts and vocabulary, resides within the heuristic. The Specific-Concept Activity theme is purely didactic in that it is concerned with imparting content knowledge. For example, [30] describes an activity where students build 3D models of crystal structures in order to learn the atomic placements and

132

observe other features of the structure. Similarly, the Virtual/Physical Model theme is also didactic in nature, focusing on the introduction and discussion of concepts' representations. In [46] for example, a new crystal structure visualization application is introduced and described, focusing on the different representations possible in the application and their use for illustrating particular concepts. Both of these themes deal primarily with introducing students to novel concepts and helping them create and reinforce mental models, an important aspect of content literacy [1].

Finally, we address the last two E's of Moje's heuristic, Examine and Evaluate, which are both related to the use of language and discourse within the discipline. The Examine level exhorts instructors to help their students understand how and why specific technical language is used, and to use technical language appropriately. The predominance of Writing/Speaking learning activities across all themes demonstrates the importance placed by the instructors on learning to use technical language correctly. The Evaluate level guides instructors to provide students with opportunities to determine the appropriateness of technical language in various contexts. In science education, examples of Evaluation may include understanding in what circumstances to use the appropriate number of significant figures, or explaining scientific findings to various audiences. While we do not explicitly analyze the learning activities with respect to the Evaluate heuristic, authors rarely ask students to discuss scientific concepts in more than one context.

Examining in more detail the articles' use of disciplinary literacy tactics, we find that many authors of the reviewed articles appear to recognize that an important aspect of disciplinary literacy is being able to use multiple representations of any given concept. Our findings demonstrate that instructors teaching crystal structures and crystallography routinely use four out

of five types of representations over the course of the learning activities, consistent with best practices in the STEM fields [48], [49]. It appears that instructors seem to know, either through intuition, experience, or reading the literature, that presenting scientific concepts using varied representational forms— via illustrations, equations, or written explanation— deepens student learning and enables representational fluency.

When we analyze which learner roles are explicitly supported as part of the learning activities, we find that the articles emphasize the Interpreter and Navigator roles, but not the Interrogator or Designer roles. Taken in tandem with the fact that Writing/Speaking learning activities are present in the vast majority of the learning activities, this finding suggests that the learning activities in question are predominately about having students extract and restate knowledge correctly, rather than about critically assessing the knowledge. The scientific disciplines clearly value both Interrogating (as seen in the scientific method) and Designing (as seen in the engineering design cycle) in their practice, but this review illustrates that these ideals are not conveyed in the way crystals and crystallography topics are taught, at least not in the articles reviewed. It could be that this selection of learner roles is appropriate for introductory courses, but many of these articles describe activities aimed at upper-level students, suggesting that these aspects of disciplinary literacy are not integrated throughout degree programs.

From our results, this review strongly suggests that learning activities, courses, and programs must be explicitly designed to support the roles of Interrogator and Designer in learning experiences. In the case of crystal structures and crystallography education we see here, support of the Designer role most often takes the form of having students freely build and then analyze different crystal structures [21], [28], but could also extend to having students propose experimental procedures to use in a project. Similarly, from the articles reviewed the Interrogator

role can be supported through explicitly having students consider the relationship between crystallography and the wider discipline of chemistry [39], but it could also be supported by having students consider what materials in their daily lives could be characterized through crystallography.

More broadly, a final aspect of doing studies like this and re-examining the way scientific topics are taught is that how scientific topics are taught partially determines who studies science. Students pick what to study based on how well their own self-image matches the "prototype" of the field [50], and students are more likely to pick fields where they feel comfortable within the culture of that field. The process of becoming literate in a discipline involves the induction of students into the discipline's culture. However, there is a large cultural gap between science and other aspects of students' lives, as science is often perceived as disconnected and irrelevant to day-to-day reality. Using more critical socio-cultural approaches when designing learning activities (such as using familiar aspects of students' cultural environment to convey a point [23]) may be more inclusive. Changing pedagogy to bridge the gap between disciplinary culture and students' outside experiences could assist in making the sciences accessible to diverse learners, especially those who do not match the prototype of the field.

Limitations

There are multiple limitations and caveats associated with this literature review. First, the search process was limited by our choice of search engines and by our ability to identify and use search terms that were consistent with how we the research team understand crystal structure and crystallography. As such, it is conceivable that the search process did not capture all of the published studies on the teaching of crystal structure and crystallography during the specified duration of time. Second, our choice of scope for the literature review, namely to focus on peer-

reviewed articles, limits the conclusions that can be drawn from it. A more in-depth survey of learning activities could perhaps be achieved using discourse or curriculum analysis on course teaching materials. Comparing such results to those in this review would provide a glimpse into the differences between what instructors consider necessary to convey to students and what they consider worthy of publication. Third, the specific topic of crystal structures and crystallography may not be a representative subset for STEM or MSE in general, and our methodology specifically excluded articles concerning the topic's applications in biology, biochemistry, and medicine due to their slightly different focus and application. To mitigate this, we tried to keep our research questions specific enough to address variation within this topic and illuminate larger trends while keeping the scope of the review to a manageable level. Fourth, some of the themes and learning activities may be specific to this specific topic, such as the prevalence of Specific-Concept Activity-themed articles or physical visualization learning activities, both of which were found to mainly include crystal model building activities. The ubiquity of the Writing/Speaking learning activities and focus on experimentation in themes and activity choice, however, suggests that some themes and learning activities may be more generalizable across MSE. Thus even with this understanding of the review's limitations in mind, we believe this review is still a plausible representative sample of the published activities about teaching crystal structures and crystallography.

Conclusion

Addressing our overall research question of *How are instructors using concepts of disciplinary literacy in MSE education*, and more specifically in crystal structures and crystallography education, this literature review shows that published articles on the topic address a wide range of disciplinary practices, such as conducting experiments and

136

communicating findings, and implicitly employ literacy strategies such as representational fluency and learner roles with some success. Some disciplinary practices, such as communication, were nearly ubiquitous, and the different learning activity types routinely used multiple representational types. While students were only infrequently supported to take on learner roles related to contextualizing and designing their learning experiences, they were often supported to take on multiple learner roles in the activities, particularly those related to carrying out procedures and analyzing data. The learner role of Interrogator with its focus on contextualization, however, is particularly important for disciplinary literacy. To explain, we must consider related aspects to disciplinary literacy education, namely how these teaching methods and pedagogical frameworks set up who studies science. The "prototype" image of a field, and how well a student's self-image matches it, influences what students pick to study [50]. Since the process of becoming literate in a discipline involves the induction of students into the discipline's culture, teaching for disciplinary literacy may be vital in allowing a wide range of students to feel comfortable in the disciplinary culture. However, there is still a large cultural gap between science and other aspects of students' lives. The sciences often resist the introduction of social or human factors into its work and discourse, and conversely, science is often perceived as disconnected from and irrelevant to day-to-day reality. Having students put their learning into context, through Interrogating the knowledge they acquire and understanding how it relates to other knowledge they possess and contexts they belong to, can help to bridge this cultural gap. From a theoretical perspective, focusing on critical socio-cultural approaches when studying disciplinary learning may make the framework be more inclusive, enabling the current state of disciplinary literacy to be examined while keeping a focus on where current teaching practices may exclude or dissuade students from underrepresented groups from the field.

References

[1]   E. B. Moje, "Doing and Teaching Disciplinary Literacy with Adolescent Learners: A Social and Cultural Enterprise," 2015. [Online]. Available: http://meridian.allenpress.com/her/article-pdf/85/2/254/2110423/0017-8055_85_2_254.pdf

[2]   J. Airey and C. Linder, "A disciplinary discourse perspective on university science learning: Achieving fluency in a critical constellation of modes," *Journal of Research in Science Teaching*, vol. 46, no. 1, pp. 27–49, Jan. 2009, doi: 10.1002/tea.20265.

[3]   "MSE242 : Physics of Materials," *University of Michigan*, 2022. https://mse.engin.umich.edu/undergraduate/courses/mse242 (accessed Aug. 01, 2022).

[4]   "MSE250 : Principles of Engineering Materials," *University of Michigan*, Aug. 02, 2022. https://mse.engin.umich.edu/undergraduate/courses/mse250 (accessed Aug. 01, 2022).

[5]   "MSE360 : Materials Lab I," *University of Michigan*, 2022. https://mse.engin.umich.edu/undergraduate/courses/mse360 (accessed Aug. 01, 2022).

[6]   "MSE481 : Designing Sustainable Products and Processes," *University of Michigan*, 2022. https://mse.engin.umich.edu/undergraduate/courses/mse481 (accessed Aug. 01, 2022).

[7]   E. B. Moje and C. Lewis, "Examining Opportunities to Learn Literacy: The Role of Critical Sociocultural Literacy Research," in *Reframing Sociocultural Research on Literacy*, Routledge, 2020, pp. 15–48. doi: 10.4324/9781003064428-3.

[8]   J. Ahn, "Drawing Inspiration for Learning Experience Design (LX) from Diverse Perspectives Diverse Perspectives," *The Emerging Learning Design Journal*, vol. 6, no. 1, pp. 1–6, 2019.

[9]   J. L. Lemke, "Teaching All the Languages of Science: Words, Symbols, Images, and Actions," 1998. doi: 10.13140/2.1.4022.5608.

[10]   Teemant A., Smith M. E., Pinnegar S., and Winston Egan M., (2005), Modeling Sociocultural Pedagogy in Distance Education. Teachers College Record, 107(8), 1675–1698.

[11]   Finkenstaedt-Quinn S. A., Halim A. S., Chambers T. G., Moon A., Goldman R. S., Gere A. R., and Shultz G. V. ,(2017), Investigation of the Influence of a Writing-To-Learn Assignment on Student Understanding of Polymer Properties, J. Chem. Ed., 94(11), 1610–1617.

[12]   Reynolds J. A., Thaiss C., Katkin W., and Thompson R. J., (2012), Writing-to-learn in undergraduate science education: A community-based, conceptually driven approach, CBE Life Sciences Education, 11(1), 17–25. https://doi.org/10.1187/cbe.11-08-0064.

[13] Ortiz Cáceres L. M., and Candela Rodriguez B. F., (2022), La Estrategia De Escribir Para Aprender: El Caso Del Equilibrio Químico. Góndola, Enseñanza y Aprendizaje de Las Ciencias, 17(1), 168–183. https://doi.org/10.14483/23464712.16531

[14] Rivard, L. P., (1994), A Review of Writing to Learn in Science: Implications for Practice and Research, JOURNAL OF RESEARCH IN SCIENCE TEACHING, 31(9).

[15] T. J. Moore, S. Selcen Guzey, G. H. Roehrig, and R. A. Lesh, "Representational Fluency: A Means for Students to Develop STEM Literacy," in *Towards a Framework for Representational Competence in Science Education*, K. L. Daniel, Ed. Springer International Publishing AG, 2018, pp. 13–30. doi: 10.1007/978-3-319-89945-9_2.

[16] F. Serafini, "Expanding the four resources model: reading visual and multi-modal texts," *Pedagogies: An International Journal*, vol. 7, no. 2, pp. 150–164, Apr. 2012, doi: 10.1080/1554480X.2012.656347.

[17] J. Extremera, D. Vergara, L. P. Dávila, and M. P. Rubio, "Virtual and augmented reality environments to learn the fundamentals of crystallography," *Crystals (Basel)*, vol. 10, no. 6, 2020, doi: 10.3390/cryst10060456.

[18] N. Stojilovic and D. E. Isaacs, "Inquiry-Based Experiment with Powder XRD and FeS2 Crystal: 'discovering' the (400) Peak," *Journal of Chemical Education*, no. 400, 2019, doi: 10.1021/acs.jchemed.9b00099.

[19] D. C. Collins, "A unit cell laboratory experiment: Marbles, magnets, and stacking arrangements," *Journal of Chemical Education*, vol. 88, no. 9, pp. 1318–1322, 2011, doi: 10.1021/ed200019r.

[20] Y. Z. Ma, Z. L. Yang, Y. Wang, H. H. Wang, and S. J. Tian, "Using Magnet-Embedded Silicone Balls to Construct Stable Models for Close-Packed Crystal Structures," *Journal of Chemical Education*, vol. 97, no. 11, pp. 4063–4068, 2020, doi: 10.1021/acs.jchemed.0c00515.

[21] S. Lenzer, B. Smarsly, and N. Graulich, "Making It Clear: Exploring Crystal Structures by Constructing and Comparing See-Through Models," *Journal of Chemical Education*, vol. 96, no. 8, pp. 1630–1639, 2019, doi: 10.1021/acs.jchemed.9b00119.

[22] A. Ohashi, "Using latex balls and acrylic resin plates to investigate the stacking arrangement and packing efficiency of metal crystals," *Journal of Chemical Education*, vol. 92, no. 3, pp. 512–516, 2015, doi: 10.1021/ed5006954.

[23] M. Duda, A. Rafalska-ŁAsocha, and W. łasocha, "Plane and Frieze Symmetry Group Determination for Educational Purposes," *Journal of Chemical Education*, vol. 97, no. 8, pp. 2169–2174, 2020, doi: 10.1021/acs.jchemed.0c00093.

[24] A. V. Savchenkov, "Designing Three-Dimensional Models That Can Be Printed on Demand and Used with Students to Facilitate Teaching Molecular Structure, Symmetry,

and Related Topics," *Journal of Chemical Education*, vol. 97, no. 6, pp. 1682–1687, 2020, doi: 10.1021/acs.jchemed.0c00192.

[25] C. C. Wilson, A. Parkin, and L. H. Thomas, "Frontiers of crystallography: A project-based research-led learning exercise," *Journal of Chemical Education*, vol. 89, no. 1, pp. 34–37, 2012, doi: 10.1021/ed100953n.

[26] K. H. Krippendorff, *Content Analysis: An Introduction to Its Methodology*, 2nd ed. Sage, 2003.

[27] Y. S. Lincoln and E. G. Guba, *Naturalistic inquiry*. Los Angeles: Sage, 1985.

[28] M. N. Ismail, "Hydrothermal Synthesis and Characterization of Titanosilicate ETS-10: Preparation for Research Integrated Inorganic Chemistry Laboratory Course," *Journal of Chemical Education*, vol. 97, no. 6, pp. 1588–1594, 2020, doi: 10.1021/acs.jchemed.0c00165.

[29] M. Wriedt, J. P. Sculley, D. Aulakh, and H. C. Zhou, "Using Modern Solid-State Analytical Tools for Investigations of an Advanced Carbon Capture Material: Experiments for the Inorganic Chemistry Laboratory," *Journal of Chemical Education*, vol. 93, no. 12, pp. 2068–2073, 2016, doi: 10.1021/acs.jchemed.6b00258.

[30] D. P. Sunderland, "Studying crystal structures through the use of solid-state model kits," *Journal of Chemical Education*, vol. 91, no. 3, pp. 432–436, 2014, doi: 10.1021/ed400367x.

[31] A. S. Firkins, "The four resource model: A useful framework for planning programs both inside and outside the classroom in development education," May 03, 2021. https://palms.org.au/2021/05/03/the-four-resource-model-a-useful-framework-for-planning-programs-both-inside-and-outside-the-classroom-in-development-education/. (accessed May 16, 2022).

[32] S. J. Lyle, R. W. Flaig, K. E. Cordova, and O. M. Yaghi, "Facilitating Laboratory Research Experience Using Reticular Chemistry," *Journal of Chemical Education*, vol. 95, no. 9, pp. 1512–1519, 2018, doi: 10.1021/acs.jchemed.8b00265.

[33] M. G. Campbell, T. M. Powers, and S. L. Zheng, "Teaching with the Case Study Method to Promote Active Learning in a Small Molecule Crystallography Course for Chemistry Students," *Journal of Chemical Education*, vol. 93, no. 2, pp. 270–274, 2016, doi: 10.1021/acs.jchemed.5b00629.

[34] T. D. Varberg and K. Skakuj, "X-ray Diffraction of Intermetallic Compounds: A Physical Chemistry Laboratory Experiment," *Journal of Chemical Education*, vol. 92, no. 6, pp. 1095–1097, 2015, doi: 10.1021/ed500804b.

[35] P. Martín-Ramos, M. Susano, F. P. S. C. Gil, P. S. Pereira Da Silva, J. Martín-Gil, and M. R. Silva, "Facile Synthesis of Three Kobolds: Introducing Students to the Structure of

Pigments and Their Characterization," *Journal of Chemical Education*, vol. 95, no. 8, pp. 1340–1344, 2018, doi: 10.1021/acs.jchemed.7b00402.

[36]   N. Stojilovic, "Using Cu K α1/ K α2 Splitting and a Powder XRD System to Discuss X-ray Generation," *Journal of Chemical Education*, vol. 95, no. 4, pp. 598–600, 2018, doi: 10.1021/acs.jchemed.7b00546.

[37]   E. Colacino, G. Dayaker, A. Morère, and T. Friščić, "Introducing Students to Mechanochemistry via Environmentally Friendly Organic Synthesis Using a Solvent-Free Mechanochemical Preparation of the Antidiabetic Drug Tolbutamide," *Journal of Chemical Education*, vol. 96, no. 4, pp. 766–771, 2019, doi: 10.1021/acs.jchemed.8b00459.

[38]   B. A. Reisner *et al.*, "Virtual inorganic pedagogical electronic resource learning objects in organometallic chemistry," *Journal of Chemical Education*, vol. 89, no. 2, pp. 185–187, 2012, doi: 10.1021/ed200200.

[39]   B. J. Malbrecht, M. G. Campbell, Y. S. Chen, and S. L. Zheng, "Teaching Outside the Classroom: Field Trips in Crystallography Education for Chemistry Students," *Journal of Chemical Education*, vol. 93, no. 9, pp. 1671–1675, 2016, doi: 10.1021/acs.jchemed.6b00073.

[40]   S. L. Zheng and M. G. Campbell, "Connecting Key Concepts with Student Experience: Introducing Small-Molecule Crystallography to Chemistry Undergraduates Using a Flexible Laboratory Module," *Journal of Chemical Education*, vol. 95, no. 12, pp. 2279–2283, 2018, doi: 10.1021/acs.jchemed.7b00985.

[41]   T. Thananatthanachon, "Synthesis and Characterization of a Perovskite Barium Zirconate (BaZrO3): An Experiment for an Advanced Inorganic Chemistry Laboratory," *Journal of Chemical Education*, vol. 93, no. 6, pp. 1120–1123, 2016, doi: 10.1021/acs.jchemed.5b00924.

[42]   J. S. O. Evans and I. R. Evans, "Structure Analysis from Powder Diffraction Data: Rietveld Refinement in Excel," *Journal of Chemical Education*, vol. 98, no. 2, pp. 495–505, 2021, doi: 10.1021/acs.jchemed.0c01016.

[43]   L. J. Small, S. Wolf, and E. D. Spoerke, "Exploring electrochromics: A series of eye-catching experiments to introduce students to multidisciplinary research," *Journal of Chemical Education*, vol. 91, no. 12, pp. 2099–2104, 2014, doi: 10.1021/ed500238j.

[44]   I. J. Bazley *et al.*, "X-ray Crystallography Analysis of Complexes Synthesized with Tris(2-pyridylmethyl)amine: A Laboratory Experiment for Undergraduate Students Integrating Interdisciplinary Concepts and Techniques," *Journal of Chemical Education*, vol. 95, no. 5, pp. 876–881, 2018, doi: 10.1021/acs.jchemed.7b00685.

[45]   C. V. Cushman and M. R. Linford, "Using the Plan View To Teach Basic Crystallography in General Chemistry," *Journal of Chemical Education*, vol. 92, no. 8, pp. 1415–1418, 2015, doi: 10.1021/acs.jchemed.5b00011.

[46]   C. Gruber, A. James, J. T. Berchtold, Z. J. Wood, G. E. Scott, and Z. Alghoul, "Interactive Unit Cell Visualization Tool for Crystal Lattice Structures," *Journal of Chemical Education*, vol. 97, no. 7, pp. 2020–2024, 2020, doi: 10.1021/acs.jchemed.9b01207.

[47]   M. Mouton and I. R. le Grange, "Scientific discourse: Can our first-year students express themselves in science?," in *International Conference on Higher Education Advances*, 2020, vol. 2020-June, pp. 579–586. doi: 10.4995/HEAd20.2020.11110.

[48]   S. Ainsworth, "The functions of multiple representations," *Computers & Education*, vol. 33, no. 2–3, pp. 131–152, Sep. 1999, doi: 10.1016/S0360-1315(99)00029-9.

[49]   A. W. Glancy and T. J. Moore, "Theoretical Foundations for Effective STEM Learning Environments," 2013. [Online]. Available: http://docs.lib.purdue.edu/enewphttp://docs.lib.purdue.edu/enewp/1

[50]   T. Perez, J. G. Cromley, and A. Kaplan, "The role of identity development, values, and costs in college STEM retention.," *Journal of Educational Psychology*, vol. 106, no. 1, pp. 315–329, Feb. 2014, doi: 10.1037/a0034027.

CHAPTER 3.3

Representational Fluency in MSE

Background

While the previous chapter focused broadly on disciplinary literacy in MSE as a whole, the current chapter will examine a vital aspect of disciplinary literacy more closely, that aspect being representational fluency. Representational fluency, as an aspect of disciplinary literacy, means "the ability to fluently translate among and between representations" [1]. Representational fluency is generally implemented as having experience with different types of representations and being able to translate between the different types, creating a mental model of the concept being represented that mediates between the different representations that students are shown. Representational fluency is especially important in STEM fields, where students learn about concepts and phenomena that often cannot be seen or are too complex to represent exactly. In these cases, many different representations may be used for the same concept, each emphasizing particular properties and simplifying others away.

The case of crystal structures can illustrate the issue. In crystal structures, the atomic arrangements themselves are far too small to see and understand with the naked eye. Looking at a TEM micrograph with well-defined lattice fringes may help a student to visualize a lattice, but the micrograph itself is only a 2D projection of a 3D lattice, thus emphasizing the arrangement of

atomic columns while making it impossible to see the structure of the crystal along the beam direction. To represent the 3D structure of the lattice, a student might instead be given a physical model made of balls and sticks, but such models are always limited in size and often misrepresent the relative size of the atoms and the details of the bonding. When doing a homework problem, a student might be given only lattice vectors and atomic radii, or be told just "a simple cubic crystal has lattice points at all eight corners of a cube and holds exactly one atom", both of which are representations that the student must understand and add to their mental model of what a crystal is and how it works. The challenge of instilling representational fluency, then, is to ensure the student could be given any or all of these representations and understand them both in relation to each other and in isolation, recognizing the salient points of each one. While there are five types of representation given by the Lesh Translation Model [2] discussed in Ch. 3.2, the remainder of this discussion will focus on the more-visual types of representation, that is, Pictorial, Concrete, and Realistic representations.

Instructors must not only provide students with a variety of representations of a concept that help the student to construct their mental model, but must also make sure that the representations chosen are appropriate and accurate. Instructional time and students' attention are limited, particularly in introductory classes, and so, out of the many ways that exist to represent a concept, particular representations must be selected to help students build an accurate mental model in the time available. Given this limitation, then, many practitioners seek to either identify the more useful representations for a particular concept [3-5] or to propose new representations to correct flaws found in the commonly-used representations for that concept [6, 7].

In STEM, and particularly in materials science and engineering, there are many concepts that are inherently multidimensional (E.g., crystalline structures of materials, the circulatory system as it exists in a body, the interplay of forces on a satellite in near-earth orbit, the shape of an enzyme as it catalyzes biochemical reactions). Two-dimensional (2D) representations are often used due to their familiarity to the instructor and their ubiquity, being easily presented on a variety of 2D media like paper or computer screens, but often involve a deliberate simplification of the concept by collapsing extra dimensions or eliminating some detail, which can lead to difficulty in its interpretation [8] or even to inadvertent inaccuracies [9]. A closer approximation of the concept can in many cases be made through the use of a three-dimensional (3D) physical model, such as a small model of a human skeleton showing the different bones of the body. The use of such models have their own drawbacks and come with their own considerations, however. Physical models take up space, can be unwieldy or expensive, it may not be feasible for students to have full access to the model [10], and models often sacrifice motion and flexibility in favor of stability [11]. For the skeleton example, the joints may be fused to ensure the skeleton does not fall apart. Similarly, computer models are at the mercy of the visualization software used; while the models may have many of the features physical models lack, such as dynamics, ease of creation, and ease of distribution, the models are still usually displayed on a 2D screen and require more expertise to generate and interact with than a similar 2D representation drawn on paper [12]. The drawbacks of computer 3D models can be lessened by using a form of virtual reality to view them. Virtual reality (VR) allows users to see and interact with representations in 3D in a virtual 3D space, and can allow users to see spatial relationships of arbitrary 3D models in a manner similar to having a physical model. The drawbacks of virtual reality are that the creation of 3D models requires more work than a similar 2D representation and the training

needed for users to learn how to use the virtual reality visualization program, as well as the cost of VR systems [13].

Independent of which individual representation (and representational medium) is most efficient to convey a particular topic, representational fluency is concerned with students' ability to transition between representations and form a mental model of the concept [1]. Acquiring representational fluency in a topic means being able to recognize what is conveyed in a representation and to translate that information into another representation, such as a drawing or a verbal explanation, through the intermediary of the mental model. Our goal in applying the framework of representational fluency to MSE education is to answer the question, *How can using different types of representation help students learn?* We approach this question by describing two studies that we conducted on the use of VR representations in the teaching of crystal structure concepts. The first study we will describe looked to understand how students use different types of representation (either paper or VR), while the second study we will describe looked to compare how well students in an MSE class could learn particular crystal structure concepts when using different types of representations in active learning contexts.

Arthea

In the studies described here, we employed the virtual reality visualization tool Arthea. Arthea is a 3D model VR visualization and manipulation tool (https://arthea.io) for the Oculus Rift, Oculus Go, and HTC Vive headsets. Oculus Rift headsets were used for this work. The Arthea tool allows a user to upload a 3D model to a web interface and then access that model in the virtual reality environment. Arthea supports multiple popular 3D formats, including FBX, OBJ, STL, WRL, PDB, DAE, and DICOM, which enables its usage across multiple domains and needs. The Arthea web interface allows for easy upload and management of a user's models, and

users can share 3D models with one another in addition to being able to share files with large

groups of other users. Once 3D models have been uploaded to the web interface, users load the

model into their VR headsets by clicking on the model name in the VR user interface (UI). This

action loads the model into the virtual environment and allows for manipulation, measurement,

and annotation of the model. Examples of the web interface and the Arthea VR environment can

be seen in Fig. 3.3.1.
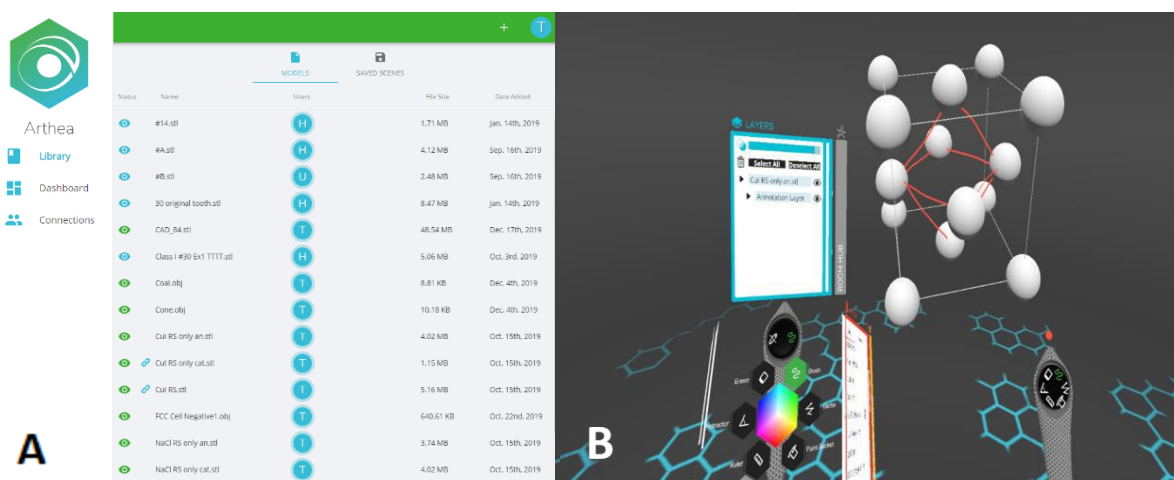
Figure 3.3.1: Screenshots of the Fall 2019 Arthea web interface (A) and the VR environment's user interface (B). The virtual user file interface and manipulation/annotation menus are linked to the hand control for the user's non-dominant hand (here the left hand), while the other hand control is used to select options from the menu, interact with models, and annotate. A model of a face-centered-cubic crystal structure and annotations on the model outlining an octahedral interstitial site are also shown in 3.3.1.B.

Arthea functionalities include image manipulation controls (rotate/translate/resize), measurement

tools (length and angles), the ability to view and interact with multiple images simultaneously,

and the ability to draw or make annotations or color changes on images. In addition to the

manipulation controls, users can take advantage of the virtual environment and just walk around

the images to see different perspectives of them. While only the person wearing the VR headset

can experience the Arthea environment in 3D, a 2D version of the field of view is shown on the

computer running the Arthea program, allowing the VR view to be shared with observers. Arthea

went through many iterations through the time when this work was being done, and so not all studies were done with the version shown in Fig. 3.3.1 above, though all versions used here had the same general functionalities.

Representational Use by Students

In order to determine how students employ different representations to solve problems and learn concepts, we conducted a pilot case study to see what sorts of questions about crystal structures students could answer when using either paper or VR representations and to see how students approached and employed the different types of representation [14]. The questions used are shown in Table 3.3.1.

Table 3.3.1: Questions used in the VR pilot case study

#	Question
1	Given in figures 1-4 are four crystal structures, please identify them.
2	For each structure identify and shade in the densest packed plane of atoms
3	Explain why FCC (2) and HCP (4) have the same packing factor, i.e. density of atoms
4	Compare and contrast FCC (2) and DC (3)

Said questions were loosely constructed to escalate along Bloom's Taxonomy [15], which orders different cognitive domains for learning (Knowledge, Comprehension, Application, Analysis, Synthesis, and Evaluation, in order) and provides action verbs for each cognitive domain that give examples sorts of actions would promote the use of the different cognitive domains (the Knowledge domain, for example, has action words such as Define, Identify, and List) [16]. Six undergraduate students and one graduate student in STEM were recruited to complete an activity on crystal structures, with equivalent representations given either on paper or in VR through

148

Arthea. The participants had varying levels of prior knowledge on the topic, with one having no familiarity, four classified as "beginners," and two classified as "intermediate." There were two beginner- and one intermediate-experience participants who used each type of representation, while the no-prior-experience participant used VR representations. All representations were of different types of crystal structure, presented as 2x2x2 unit cells of reduced sphere models. Participants were asked a set of four questions of increasing complexity aloud, and were recorded as they talked through their reasoning to answer the questions. Participants were scored on correctness, with partial credit given according to a rubric. The first question was the only one which required prior knowledge, while the others could be answered correctly with just observation. Student answers are listed in Table 3.3.2.

Table 3.3.2: The representational type, familiarity, and normalized scores for each individual in the study

#	Type	Familiarity	Q1	Q2	Q3	Q4
1	VR	None	0.00	0.88	0.33	0.33
2	VR	Beginner	0.50	0.38	0.67	0.33
3	VR	Beginner	0.75	0.62	0.33	0.67
4	VR	Intermediate	0.33	1.00	0.33	1.00
5	Paper	Beginner	0.67	0.75	0.33	0.33
6	Paper	Beginner	0.92	0.75	0.00	0.67
7	Paper	Intermediate	0.58	0.12	0.33	1.00

The first question, intended to access the Knowledge domain of Bloom's Taxonomy, focused on identification, and asked students to correctly name a body-centered cubic structure (BCC), a face-centered cubic structure (FCC), a diamond cubic structure (DC), and a hexagonal close-packed structure (HCP). The one participant without prior knowledge got a score of 0,

which is expected for the Knowledge domain of Bloom's taxonomy, which focuses on accessing

and relaying previous knowledge. All six other participants got at least 0.33 on this question,

while the highest score was obtained by a participant using paper representations. The average

score for the experienced VR participants was 0.53, while the average score for the paper

participants was 0.72. In terms of the intrinsic features of the two representation types, the

respective scores for VR and paper participants is understandable, as the paper representations

are similar to those used when teaching crystal structures, and would thus be more immediately

familiar and without the novel context of the Arthea environment.

The second question also focused on identification, but as opposed to identification of the

crystal structure as a whole, this question required identification of features of the different

crystal structures and required interaction with the different representations, either through

examination to determine the answer or through relation of the representations to mental models

in order to properly convey a previously-known answer. As such, it could be answered by

accessing either the Knowledge of Comprehension domains of Bloom's Taxonomy. Participants

were asked to identify and shade in the closest-packed plane of atoms in each crystal structure.

On this question, the four VR participants got on average 0.72, while the paper participants got

an average of 0.54. Similarly for the first question, the respective scores for VR and paper

participants make sense, as the second question requires some understanding of the spatial

relationships of atoms in the structures. In VR, the participants can freely rotate the structures

and examine many different possible answers before making their choice, while when given

paper representations, participants have only two views given to them to connect to their mental

model which can make it difficult to identify which atoms are coplanar.

The third and fourth questions were open-ended in nature. The third question focused on explanation, accessing the Evaluation domain of Bloom's Taxonomy. The question asks participants to explain why the FCC and HCP crystal structures have the same density of atoms. Participants tended to have a more difficult time with this question, with the VR participant average being 0.42 and the paper participant average being 0.22. Finally, the fourth question focused on comparison and accessed the Analysis domain of Bloom's Taxonomy. The question asked participants to compare and contrast the FC and DC crystal structures. For this final question, the VR participant average score was 0.58, while the paper participant average was 0.67. Participants' comments as they went through the two open-ended questions help to illustrate the two different general approaches they used to build an explanation or comparison. Participants given paper representations tended to try to rely on prior knowledge to answer the question, saying things such as "*I don't think I remember enough of this to answer these questions adequately*" or recalling a formula for packing density. Participants using VR representations, on the other hand, were more likely to rely on the representations, saying things such as "*The planes with closest packing are the same, [...], it's just FCC rotated*" or overlaying the representations on each other to highlight the differences.

While still a small-scale case study, the student's answers were helpful in illuminating the different benefits and costs of using different types of representations. The paper representations were familiar to participants, and helpful for them to try to recall previous knowledge. However, the participants were seemingly less-likely to attempt to pull information from the paper representations if they did not already have the relevant knowledge. In contrast, the VR representations were unfamiliar to participants, but were still useful in providing defined spatial relationships for the participants to use when answering the second through fourth questions.

Participants seemed likely to use and rely on the VR representations when comparing different crystal structures. This pattern is especially visible in the scores for the VR representations participant with no prior experience with crystal structures. While said participant scored 0 on the first question on nomenclature, the participant's score for the second question, identifying close-packed planes, was above average at 0.88. Similarly for the third and fourth questions, the participant was able to use the VR representations to give partial explanations and comparisons, receiving a score of 0.33 for each question. This participant's success suggests that even in the absence of prior knowledge, VR representations can assist in helping people to understand and answer higher-level problems.

The successes of the student without prior knowledge on crystal structures raises a salient question on representational fluency, namely the following. "If a representation is accurate and intuitive enough to understand without explanation or prior knowledge that someone without a mental model of a concept can essentially adopt the representation wholesale as their model and still understand higher-level aspects of the concept, are other representations and representational fluency truly needed?" We would answer that, yes, representational fluency is still vital. No one representation of a concept, no matter how cleverly constructed, can convey all the necessary information about the concept, nor is every representation universally-accessible and -available. If someone is only familiar with one representation of a concept to the exclusion of all other representations, they will be limited in their ability to transfer their knowledge to new contexts or to communicate their knowledge [17]. To use a highly simplified example, if a child were given a red rubber ball (a concrete representation), but was never taught the words that describe the ball (language representations, E.g. "red," "rubber," "ball," "round," "bouncy"), the child would not be able to describe the ball if it went missing. Multiple representations, and understanding of

how they are connected to each other, are important to understand both what a particular concept is and what the concept is not, and fluency in representations is important for communicating with others [1].

Comparison of Representational Efficacy in MSE Classrooms

To study and compare how well students could learn particular crystal structure concepts when using different types of representations in active learning contexts, we also implemented and evaluated VR active learning activities in an MSE classroom. While the case study above is useful for seeing how students approach and employ different types of representation, there is still the question of how well the different types of representation allow students to learn 3D concepts in actual instructional scenarios. To study the use and efficacy of VR to increase representational fluency and involve students in active learning scenarios, we designed crystal structure learning activities using either paper or VR representations and implemented them over two years in MATSCIE 220 classes at the University of Michigan. Active learning, or actively engaging students in tasks that promote analysis, synthesis, and evaluation [18], was chosen as central to the design of the activity because it has been shown to lead to better academic performance [19], and also because it appears to improve student performance related to the recall of 3D objects [20]. MATSCIE 220, Introduction to Materials and Manufacturing, introduces how the macroscopic properties of materials — metals, polymers, semiconductors, ceramics, and composites — are determined by their atomic structures. The course consists of three one-hour lectures per week (~140 students), in addition to smaller (~30 students) once-a-week discussion sections led by graduate student instructors (GSIs). This course was chosen as the test case due to a number of factors. The course is a technical elective taken by a variety of

majors in the College of Engineering, including Aerospace, Industrial and Operations Engineering, and Chemical Engineering, and has a high proportion of female students, at over 40% female in both iterations. While some Materials Science and Engineering students take the course (~10% in the two semesters studied), it is primarily taken by students from other majors and skews towards third- and fourth-year students, with no first-year students in the sample population of this study.

The crystal structure learning activities were designed based on previous work done by Gentry [21] and adapted for use with paper and VR representations in the MATSCIE 220 class context. For the first iteration, completed in Fall 2018, the learning activity was designed to take a discussion period, starting with a pretest on students' crystal structure knowledge and continuing with an active learning activity where students first individually completed a worksheet on crystal structures and then in pairs completed one of the same questions as in the individual worksheet. The activity was timed to coincide with the course's instruction of crystal structures, so students had been first introduced to the concept in the week previous. For the pretest, Gentry's [21] crystal structure concept inventory was used. The concept inventory consisted of six questions where students were given a crystal structure and a miller index and asked to identify which of five possibilities was the correct atomic plane. The individual learning activity consisted of six questions. The first two questions asked students to identify the miller indices of three planes and the names of three crystal structures, respectively. The second pair of questions asked students to draw atomic planes and compare planar densities, either for a single plane and various crystal structures (question 3), or for various planes and a single crystal structure (question 4). To demonstrate what a proper answer would look like, a space-filling drawing of the (100) plane of the simple cubic crystal structure was given to students. The final

two questions asked students to explain how they determined atomic planar density and to compare all the atomic planes they had drawn and determine the most dense plane. The paired activity had students work together to answer question 4 of the individual activity, where they had to draw the space-filling (100), (110) and (111) atomic planes of the FCC crystal structure. Students were also asked to reflect on whether working in pairs helped the students catch errors. All students completed the individual and paired activities in the class discussion using paper representations of the miller planes and crystal structures, as seen in Fig. 3.3.2, and a subset of the students volunteered to complete the paired activity again with VR representations for extra credit in the course. VR representations were only used in paired contexts in order to facilitate the completion of the activity without frequent instances of putting on or taking off the VR headset. Student pairs completing the activity with VR representations were encouraged to switch roles between monitor and VR-user before reaching agreement of answers. Other considerations included having the student not wearing the headset act as a safety monitor for the student in VR, as well as limitations on the availability of VR stations.
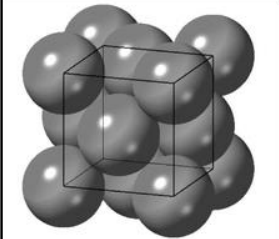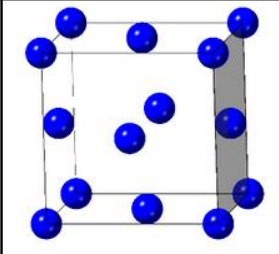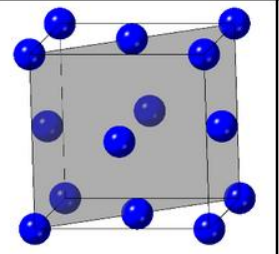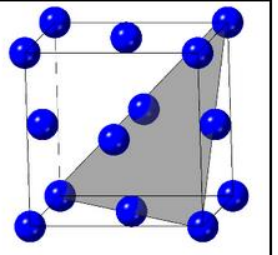
Space-Filling FCC:			
Planes of FCC: (Pictures shown in reduced sphere representation)			
Space-filling drawing of atoms lying on the plane shown:			
Planar Density Rank (1 = Highest)			

Figure 3.3.2: Example of the paired activity used in the Fall 2018 iteration of the crystal structure learning activity. One example of a single unit-cell of the space-filling FCC crystal structure is given, while each miller plane ((100), (110), and (111) from left to right) is shown superimposed on single unit-cells of a reduced-sphere FCC crystal structure.

The VR representations consisted of models of the three miller planes and the space-filling FCC model. Students were given tutorials on the features of Arthea but were not told how to best use the representations to complete the activity.

In the second iteration, completed in Fall 2019, the activities were revised to streamline them for time and give more focus to the paired activities. The activities were held over two weekly discussion sessions, again timed to coincide with the course's coverage of crystal structure concepts. In the first discussion session, all students were given a new tutorial on how to use Arthea that walked them through how to use the file system, manipulation tools, and annotation tools to construct a snowman in VR. In the second discussion session, students

156

completed as a pre-test the same crystal structures concept inventory from Gentry [21], before being paired up and completing the crystal structure activity using VR representations. The paired activity consisted of questions 3 and 4 from the first iteration's individual activity, with the wording changed slightly to ensure clarity. Students were given VR models of the BCC and FCC crystal structures (space-filling and extending over one unit cell) and of the (100), (110), and (111) miller planes. After completion of the activity, students were asked to complete the crystal structure concept inventory again as a post-test online through their course website during the following two weeks.

Grading for all the activities was based on correctness. For the crystal structure concept inventory, all questions were multiple choice, and so all answers were either correct or incorrect. For the individual and paired activities, given the open-ended nature of the questions and the need for students to produce drawings, the answers given by the students were oftentimes ambiguous. While the answers were still scored on correctness, we also made notes of what types of drawing errors, if any, were made by the students. The list of drawing errors compiled from this dataset was similar to the list determined by Gentry [21], and consisted of missing atoms, additional atoms, atoms touching when they should not, and atoms not touching when they should. An answer was marked correct only if none of these errors was present. While other types of errors could exist, such as drawing the face-centered atom in the (100) FCC plane too small compared to the corner atoms, consistently defining and identifying such errors on hand-drawn representations was determined to be beyond the scope of our analysis. For the Fall 2018 iteration results, we limit our discussion to the trends for question 4 of the individual activity (seen in Fig. 3.3.2, and which was the question done in the paired activities) from the students who completed the individual activity and both the paper and VR paired activities to ensure

consistency and similar sample sizes. For the Fall 2019 iteration results, we discuss trends from all the students who completed the VR paired activity, though not all of them completed the post-test during the sampling period.

For the Fall 2018 iteration, the correct response rates for question 4 can be seen in Table 3.3.3. To compare answers across the different versions of the activity, one-way between subjects ANOVA tests were performed.

Table 3.3.3: Correct response rates for activities completed in Fall 2018, and one-way ANOVA significance testing between the paired paper activity and the paired VR activity

Crystal Plane	(100) FCC	(110) FCC	(111) FCC
Individual activity score (%)	0.58	0.68	0.00
Paired paper activity score (%)	0.63	0.74	0.11
Paired VR activity score (%)	0.58	0.86	0.68
F(2,54)	0.09524	0.10588	26.460***

*** indicates p<0.001

For the (100) FCC crystal plane, there was no significant difference between the correct response rates for the different activities, though there was a slight improvement on the paired activity with paper representations compared to the other two versions of the activity. For the (110) FCC crystal plane, while there were increases in the correct response rate from the individual activity to the paired activity with paper representations to the paired activity with VR representations, the increases were not significant with the population size (N = 9 pairs). For the (111) FCC crystal plane, however, there were no correct answers reported during the individual activity, and in the paired activity, students achieved a significant (p<0.001) improvement in their correct response rates going from the paper representations to the VR representations.

For the Fall 2019 iteration, the correct response rates for questions 3 and 4 on the paired activity with VR representations can be seen in Table 3.3.4, while Table 3.3.5 gives the correct response rates for the crystal structures concept inventory pre- and post-tests.

Table 3.3.4: Correct response rates for the Fall 2019 paired VR activity for N = 36 pairs of students

Crystal Plane	Correct Response Rate
(100) BCC	0.78
(100) FCC	0.86
(110) FCC	0.81
(111) FCC	0.31

Table 3.3.5: Correct response rates for the Fall 2019 concept inventory pre- and post-tests, for N = 63 students. The difference in results between pre- and post-test are provided with t-test significance levels with ** indication $p<0.01$ and *** indicating $p<0.001$

	BCC			FCC		
Worksheet	100	110	111	100	110	111
Pre-test	0.476	0.746	0.079	0.905	0.508	0.317
Post-test	0.683	0.825	0.095	0.889	0.683	0.190
Δ	**0.206***	**0.079**	**0.016**	**-0.016**	**0.175**	**-0.127**

Table 3.3.4 shows that while correct response rates in this iteration were generally high, students struggled to correctly draw the atomic arrangement of the (111) FCC crystal plane, which was an issue in the previous iteration as well. As seen in Table 3.3.5, there was statistically-significant improvement on the correct response rate between the pre- and post-tests for the (100) BCC and (110) FCC crystal planes and no statistically-significant differences for the (110) BCC, (111)

BCC, and (100) FCC crystal planes. However, there was a statistically-significant decrease in the correct response rate between the pre- and post-tests for the (111) FCC crystal plane.

Taken together, the trends seen in the two iterations lend themselves to a few conclusions. First, as seen in the Fall 2018 iteration, the VR representations are effective in the paired activity, with comparable correct response rates for the (100) FCC crystal plane with the individual activity and the paired activity with paper representations, and improved or much improved correct response rates compared to the other versions of the activity for the (110) FCC crystal plane and the (111) FCC crystal plane, respectively. While some of the improvement seen on the (111) FCC crystal plane could be attributed to the study design, as the VR paired activity would be the third time students would encounter the question, the difference in improvement between the (110) FCC and (111) FCC crystal planes from the paired paper to paired VR representations implies that familiarity was not the only factor. The paper representation for the determination of the (110) and (111) FCC crystal planes can be seen in Fig. 3.3.2. The (110) plane is a diagonal rectangle cutting through the center of the FCC unit cell, and the representation requires only a slight mental rotation around the vertical axis to have the rectangle be facing the viewer directly, where the head-on view is essentially the answer required of the students. In contrast, to reach a similar head-on view of the (111) plane as it intersects the FCC unit cell, students must mentally rotate the triangular cross-section on two axes by a significant amount, which increases the difficulty of the problem. In VR, however, the students can bypass their spatial reasoning and rotate the models freely on the different axes, seeing the plane directly. Similarly, in a previous study, the researchers found that students who directly manipulated models on a computer screen did better on tasks than students who did not [22]. With this in mind, the large change in correct response rates from the paper representations to the

VR representations could also be due to the difficulty of the problem and the varying amounts of mental work and understanding required of the students.

Second, as seen in the Fall 2019 iteration, while the VR representations allow students to produce the correct answer during the activities, it does not necessarily lead to improvements on the pre/post-test. Based on the changes in correct response rate and the make-up of the activities as compared to the concept inventory, we can split the questions into 4 categories. In the first category, consisting of the (110) and (111) BCC crystal planes, the questions were about planes that were not addressed in the learning activity, and the students had no significant differences in the correct response rate. This category in some ways acts as a control (there was no instruction so we expect no results) but also shows that the activities did not help students learn to generalize their model of how to determine what different crystal planes look like in different crystal structures. In the second category, consisting only of the (100) FCC crystal plane, the question was on a plane that was covered by the activity, but the change in correct response rate was not significant, and was nearly static. This trend can be explained by noting that the correct response rate for this question on the pre-test was already high at 0.905, and that it could have already been saturated, essentially. In the third category, consisting of the (100) BCC and (110) FCC crystal planes, the questions were on planes covered by the activity, and there was significant improvement in the correct response rates. This pattern is essentially what was expected from the study, that students improve on answering questions on a topic after they have been given instruction on it, but it was only seen for these two questions.

Finally, in the fourth category, consisting of the (111) FCC crystal plane, the question was on a plane covered by the activity, but there was a significant decrease in the correct response rates between the pre- and post-test. This result is unexpected, and suggests that there is

some factor at play for that particular question in the study that affects students' understanding of the crystal plane. While the VR representations did help students to answer the question correctly in the Fall 2018 iteration, as seen in Table 3.3.3, and students answered the question more correctly in VR on their first exposure to the question in the Fall 2019 iteration than they did in their first or second exposures in the Fall 2018 iteration, as seen in Table 3.3.4, the students had difficulty choosing the correct answer for what the plane looked like. There are a number of possibilities for why this difficulty may exist. In the VR activity, determining the answer for what a crystal plane looks like is usually done by overlaying the plane model on the crystal structure model. As such, while students may do so correctly and draw the correct resulting crystal plane, there are many possibilities for misalignment or intermediate steps that might be remembered instead of the end product. It could also be that being given VR representations lessened students' reliance on and building up of their mental models of the concept, and so the mental models were less-developed when they needed to complete the concept inventory as the post-test. The process where information processing requirements are lowered by taking physical actions (i.e., rotating or handling a physical or virtual model to reduce the cognitive demands of mentally transforming it) is called cognitive offloading [23]. A previous study on problem solving in VR found that students did worse recalling things involved with activities that allowed for cognitive offloading than recalling things involved with activities without the cognitive offloading aspect [24]. Another possibility is that the activity trained students how to use VR representations, but did not adequately train students on representational fluency between the paper representations and VR representations, allowing them to succeed in some instances and fail in this instance.

The results seen here raise many questions on how 3D concepts are taught. Static 2D representations, like those printed on paper, are near-universal and the standard for teaching, being easily displayed and communicated in textbooks, printouts, and digital resources. It is hard to imagine that a graduate in any STEM field has achieved their expertise without relying heavily on visual representations of this type, leaving many proven success cases advocating for their use in different fields. These success cases, however, leave out anyone for whom such representations were not enough, or any people who were unable to grasp required concepts using the standard representations. Does the presence of success cases mean that the students who were not able to succeed were acceptable losses? Does being labeled a success case mean the methods that allowed the student to be successful were the only methods or the best methods to do so? Looking more to the study design itself, the concept inventory post-test used static 2D representations, which are different from the VR representations used in the activity. If the concept inventory had been adapted to a VR context somehow, would students have still had the same issue with the (111) FCC crystal plane? More generally, does the reliance on 2D static images in testing and evaluation limit the usefulness of other types of representation for the teaching of 3D concepts, or can training for representational fluency allow students to benefit fully from all types of representation? Is it obligatory or just traditional to use the static images in evaluation, and what could evaluation look like with different types of representation? These questions cannot be answered by the current study, and would require input from education researchers, STEM practitioners, course designers and instructors, administrators, and more to answer fully.

Conclusions

In all, answering our research question of *How can using different types of representation help students learn particular 3D topics,* the results suggest that while VR as a representation type is a useful tool in teaching 3D topics and can be effective in certain cases, it cannot be a simple replacement for more-traditional, paper-based representations. The type of representation used to help students learn concepts must be carefully chosen, and VR is but one type of representation. VR representations can be useful for situations where there are complex visual representations, and can be a visualization aid for students who have less trained or innate spatial reasoning, allowing them to recognize aspects of a concept that are considered higher-level without the traditional incremental approach. However, that same ability to make visualization less demanding of the student is associated with worse memory of the concept later. The solution, then, would be to not rely exclusively on any one type or method of representation. As seen in our first study, paper representations may not prompt students to interact with a concept in the same way that VR representations may, and the opposite is also true. If both types of interaction are seen as valuable, both should be encouraged through the choices of representation and representational media. Beyond using multiple types of representation, however, students must be taught how to transition between the types, to recognize commonalities and understand how the different types represent the same concept in different ways [1]. Giving students different types of representation of the same thing and assuming students will instinctively understand them both and be able to use them together in complex ways is an error born of expertise. Though we as practitioners may understand how to integrate a new representation of a concept into our mental model, such models must be built up over time and students, particularly lower-level students, may not have a full mental model yet when the representation is introduced.

Through these studies on representational fluency, we can see a small example of the breadth of

disciplinary literacy in MSE, and the ongoing research into its improvement and dissemination.

References

[1]   T. J. Moore, S. Selcen Guzey, G. H. Roehrig, and R. A. Lesh, "Representational Fluency: A Means for Students to Develop STEM Literacy," in *Towards a Framework for Representational Competence in Science Education*, K. L. Daniel, Ed. Springer International Publishing AG, 2018, pp. 13–30. doi: 10.1007/978-3-319-89945-9_2.

[2]   R. Lesh, T. Post, and M. Behr, "Representations and translation among representations in mathematics learning and problem solving," in *Problems of representations in the teaching and learning of mathematics*, C. Janvier, Ed. Hillsdale, NJ: Lawrence Erlbaum, 1987, pp. 33–40.

[3]   D. Nicholson, C. Chalk, W. Funnel, and S. Daniel, "Can virtual reality improve anatomy education? A randomized controlled study of a computer-generated three-dimensional anatomical ear model," *Medical Education*, vol. 40, no. 11, pp. 1081–1087, 2006.

[4]   C. Loukas, N. Nikiteas, M. Kanakis, and E. Georgiou, "Evaluating the effectiveness of virtual reality simulation training in intravenous cannulation," *Simulation in Healthcare*, vol. 6, no. 4, pp. 213–217, 2011.

[5]   R. Edsall and E. Wentz, "Comparing strategies for presenting concepts in introductory undergraduate geography: Physical models vs. computer visualization," *Journal of Geography in Higher Education*, vol. 31, no. 3, pp. 427–444, Sep. 2007, doi: 10.1080/03098260701513993.

[6]   C. V. Cushman and M. R. Linford, "Using the Plan View To Teach Basic Crystallography in General Chemistry," *Journal of Chemical Education*, vol. 92, no. 8, pp. 1415–1418, 2015, doi: 10.1021/acs.jchemed.5b00011.

[7]   S. Lenzer, B. Smarsly, and N. Graulich, "Making It Clear: Exploring Crystal Structures by Constructing and Comparing See-Through Models," *Journal of Chemical Education*, vol. 96, no. 8, pp. 1630–1639, 2019, doi: 10.1021/acs.jchemed.9b00119.

[8]   A. Z. Sampaio, M. M. Ferreira, D. P. Rosário, and O. P. Martins, "3D and VR models in Civil Engineering education: Construction, rehabilitation and maintenance," *Automation in Construction*, vol. 19, no. 7. Elsevier B.V., pp. 819–828, 2010. doi: 10.1016/j.autcon.2010.05.006.

[9]   W. French, "Two-Dimensional and Three-Dimensional Migration of Model-Experiment Reflection Profiles," *Geophysics*, vol. 39, no. 3, pp. 265–277, 1974.

[10] B. Wainman, A. Aggarwal, S. K. Birk, J. S. Gill, K. S. Hass, and B. Fenesi, "Virtual Dissection: An Interactive Anatomy Learning Tool," *Anat Sci Educ*, vol. 14, no. 6, pp. 788–798, Nov. 2021, doi: 10.1002/ase.2035.

[11] D. P. Sunderland, "Studying crystal structures through the use of solid-state model kits," *J Chem Educ*, vol. 91, no. 3, pp. 432–436, 2014, doi: 10.1021/ed400367x.

[12] T. Jaakkola, S. Nurmi, and K. Veermans, "A comparison of students' conceptual understanding of electric circuits in simulation only and simulation-laboratory contexts," *J Res Sci Teach*, vol. 48, no. 1, pp. 71–93, Jan. 2011, doi: 10.1002/tea.20386.

[13] D. Richards and M. Taylor, "A Comparison of learning gains when using a 2D simulation tool versus a 3D virtual world: An experiment to find the right representation involving the Marginal Value Theorem," *Comput Educ*, vol. 86, pp. 157–171, Aug. 2015, doi: 10.1016/j.compedu.2015.03.009.

[14] Caro, V., Carter, B., Dagli, S., Schissler, M., & Millunchick, J. (2019). Can Virtual Reality Enhance Learning: A Case Study in Materials Science. Proceedings - Frontiers in Education Conference, FIE. https://doi.org/10.1109/FIE.2018.8659267

[15] B. Bloom, *Taxonomy of Educational Objectives*. New York: Longmans, Green, 1964.

[16] A. Sharunova *et al.*, "Looking at Transdisciplinary Engineering Design Education through Bloom's Taxonomy*," *International Journal of Engineering Education*, vol. 35, no. 2, 2019.

[17] F. Marton, U. Runesson, and A. B. M. Tsui, "The space of learning," *Classroom Discourse and the Space of Learning*, vol. 9781410609, pp. 3–42, 2004, doi: 10.4324/9781410609762.

[18] C. Bonwell and J. Eison, "Active Learning: Creating Excitement in the Classroom," 1991.

[19] S. Freeman *et al.*, "Active learning increases student performance in science, engineering, and mathematics," *Proc Natl Acad Sci U S A*, vol. 111, no. 23, pp. 8410–8415, 2014, doi: 10.1073/pnas.1319030111.

[20] M. Keehner, D. R. Montello, M. Hegarty, and C. A. Cohen, "Effects of interactivity and spatial ability on the comprehension of spatial relations in a 3D computer visualization," 2004.

[21] S. P. Gentry, T. Faltens, W. A. Wheeler, and A. Schleife, "Measuring student learning of crystal structures using computer-based visualizations," *ASEE Annual Conference and Exposition, Conference Proceedings*, vol. 2018-June, 2018.

[22] F. Meijer and E. L. van den Broek, "Representing 3D virtual objects: Interaction between visuo-spatial ability and type of exploration," *Vision Research*, vol. 50, no. 6, pp. 630–635, 2010, doi: 10.1016/j.visres.2010.01.016.

[23] E. Risko, "Cognitive Offloading," *Trends in Cognitive Sciences*, vol. 20, no. 9, pp. 676–688, 2016.

[24] T. Alothman and K. Johnsen, "The effect of egocentric interaction techniques and user-performed tasks on problem solving in virtual reality," Univ. of Georgia, 2017.

CHAPTER 3.4

Conclusion

In the past few chapters focused on MSE education, we have examined various topics related to disciplinary literacy. Our examination was organized around the overarching research question of ***How are instructors using concepts of disciplinary literacy in MSE education?*** We examined the question in two aspects, the first being the prevalence of disciplinary literacy concepts in crystal structures pedagogy, and the second being the application of the disciplinary literacy concept of representational fluency to MSE classrooms.

To address the first aspect, we conducted a systematic literature review of published articles describing crystal structures and crystallography learning activities, and identified authors' usage of various disciplinary literacy concepts and tactics. We found that the articles could be separated into six categories of goals that were generally aligned to different parts of the disciplinary cycle (from Moje [1]), though there were a few articles that were aligned to the cycle as a whole. Similarly, the articles' four learning activity types were seen to align to different parts of the cycle, while two of the activity types were most prevalent, Writing/Speaking and Experiment. The learning activities routinely provided students with multiple types of representation, with Concrete representations being the least common but all the other four commonly used [2]. The learning activities also routinely provided students with

opportunities to take on two of the four learner roles [3], Navigator and Interpreter, with the other two roles being less common.

To address the second aspect, we conducted two different studies on the efficacy and use of different types of representation to teach crystal structures, looking at how students employed paper-based and virtual reality (VR)-based representations in the first, and at how efficacious VR representations were in the second. In the first study we found that the students with paper-based representations tended to do better with questions requiring prior knowledge and recognition and may approach the questions as trying to recall knowledge. Meanwhile, students using VR-based representations tended to do better on questions requiring examining or interacting with the representations and may be more reliant on what they see, rather than remember. In the second study we found that students performed significantly better on the harder questions when they used VR-based representations, but they did not retain what they learned for the harder questions.

From the two aspects we studied and the results we obtained, there are a number of implications. In terms of the prevalence of disciplinary literacy concepts in crystal structure learning activities literature, we see that some aspects of disciplinary literacy seem to be implicitly understood among practitioners and educators by the prevalence of the different purposes, activity types, representational types, and learner roles. Particularly, certain disciplinary practices, such as writing and conducting experiments, are extremely common, and even in the absence of those things, the authors aim to target other aspects of the disciplinary cycle. Overall, instructors seem to understand that students should be familiarized with the disciplinary cycle as it applies to the discipline, and would target this through research projects, hands-on experiments, and communication. However, there are relatively few articles that target

169

the entire cycle, and it is unclear how deliberate the authors are in their activity design in that respect.

Practitioners and educators likewise seem to understand the value of multiple and varied representations, as the learning activity types generally are only lacking one or another type of representation. For three of the learning activity types, the Concrete representation type is the one lacking, which may be due to the difficulty in designing, building, and storing relevant models for different activities, especially those of the Experiment activity type. Concrete representations are well-represented in the Virtual/Physical Model activity type, but activities of that type are lacking Realistic representations, suggesting that the integration of tangible models (Concrete) in activities with real-world data (Realistic) is challenging and should be addressed.

Finally, the role of the learner does not seem to be as well-understood, with most of the articles implicitly supporting the Navigator and Interrogator learner roles by having students follow a procedure and work with data, but at the same time not supporting the Designer or Interrogator learner roles. While the lack of these learner roles makes some sense when considering the prevalence of experiment- and data-based learning activities and disciplinary practices, it does show that students are not being given agency or asked to make productive choices (Designer) or examine and contextualize their work (Interrogator) in disciplinary contexts. It is possible that students are supported in taking on these roles in other parts of their studies, but learning to conduct themselves in a disciplinary manner, and particularly to take agency as they do so, should not be confined to design courses or capstone projects.

In terms of the implications on our studies of the use of different types of representation for learning, we see that different types of representation have different strengths. Paper representations are more familiar to students, and are the medium by which many disciplinary

communications are conveyed, including most tests and textbooks. Conversely, VR representations are able to convey complex topics more easily, and can bypass the need for a previously-constructed mental model. While one could argue that in proper contexts and with appropriate support, either type of representation could be sufficient, the benefits of representational fluency are seen when the strengths of both types can be accessed. In the current state of affairs, VR representations alone may not be the best choice for a learning activity, but they can serve as a valuable learning tool if used with other representations and if the ability to go between representational types is emphasized.

Future Work

Future work on the promotion of disciplinary literacy in MSE could take multiple different directions. While we found evidence of disciplinary literacy concepts in use in the literature on crystal structure learning activities, it is an open question if the literature on that particular topic is representative of MSE's disciplinary education as a whole. The literature we studied consists of discrete activities on crystal structures and crystallography and not the day-to-day pedagogy being employed, and likewise the topic itself is one that may lend itself towards certain types of representation. A more comprehensive study might instead use the methodology of discourse analysis [4], wherein texts and communication used in MSE pedagogy, such as textbooks, class notes and slides, lectures, homeworks, and laboratory activities, are studied and analyzed in order to determine what is being discussed, both formally and in passing, explicitly and implicitly, and how those things are being discussed. With a large enough and multi-institutional pool of data, researchers could get a better sense of what the day-to-day state of disciplinary education is and how the disciplinary culture is related to and supported in students. Particularly, it would be of interest to see in what contexts are students supported in taking on the

Designer and Interrogator learner roles and whether those are spread throughout a curriculum or confined to certain course types or years in the program.

Alternatively, a similar study to our literature review could be conducted on a different topic that is less-inherently-3D, such as binary phase diagrams or reaction kinetics, in order to see what different author goals and learning activity types might emerge. For instance, it is quite likely that the Physical Visualization learning activity type, or the Virtual/Physical Models goal, would be less prominent for published learning activities about a topic that does not have a physical (if nanoscale) form. Similarly, it would be valuable to see if the prevalence of the Writing/Speaking learning activity type holds true across different topics, as that is an area that is well aligned with disciplinary literacy strategies and is an important aspect of students' entry into the disciplinary culture. On the other hand, other topics might employ learning activity types or have articles published with other author goals, and these new categories could be studied for how well they align with or diverge from disciplinary literacy concepts such as the disciplinary cycle.

Relating more to the study of representational fluency with VR representations, future work could examine a range of things. For example, it could expand on the type of work we were doing, for example seeing if the use of paper-based and VR-based representations concurrently and with a focus on representational fluency could lead to better performance and retention on difficult questions. However, future work could also look past the classroom study model and examine more directly how best to actually teach representational fluency, looking both at how disciplinary experts employ and understand various representations (mirroring studies related in [5]) and how pedagogy could be targeted to bring students from novice understanding closer to that expert level. Further research could also be useful to determine the relative strengths and

weaknesses for a variety of different representation types and mediums, such that instructors, particularly novice instructors with low amounts of pedagogical content knowledge [6], could have a guide to deliberately tailor their choices of representation to the goals they set for student learning.

The ultimate goal of all education research is that the knowledge gained through this course of research be able to enhance the state of teaching and learning in general. However, even cases where there are clear results with straightforward implications for pedagogy, enacting change to the status quo is not a simple proposition. Therefore, one more branch of future work we would propose would be to study how concepts of or related to disciplinary literacy are or could be disseminated into pedagogy. According to [7], prescribed-type methods of enacting change in pedagogy, such as developing and disseminating "best practice" curricular materials, are not effective in actually enacting their desired changes. Rather, more effective strategies are to work with instructors over a longer-term period of time and either align with or work to change the instructors' prior beliefs on the subject, with the instructors having the final control on what form the enacted change would take in their pedagogy. With this in mind, the form this research could take could be to examine where disciplinary practitioners' and instructors' current implicit understandings of the disciplinary literacy concepts seen here come from, and to study how further concepts related to disciplinary literacy could be adapted into and included in instructor development resources, such as those provided by teaching and learning centers.

References

[1]   E. B. Moje, "Doing and Teaching Disciplinary Literacy with Adolescent Learners: A Social and Cultural Enterprise," *Harv Educ Rev*, vol. 85, no. 2, 2015, [Online]. Available: http://meridian.allenpress.com/her/article-pdf/85/2/254/2110423/0017-8055_85_2_254.pdf

[2]   T. J. Moore, S. Selcen Guzey, G. H. Roehrig, and R. A. Lesh, "Representational Fluency: A Means for Students to Develop STEM Literacy," in *Towards a Framework for Representational Competence in Science Education*, K. L. Daniel, Ed. Springer International Publishing AG, 2018, pp. 13–30. doi: 10.1007/978-3-319-89945-9_2.

[3]   F. Serafini, "Expanding the four resources model: reading visual and multi-modal texts," *Pedagogies: An International Journal*, vol. 7, no. 2, pp. 150–164, Apr. 2012, doi: 10.1080/1554480X.2012.656347.

[4]   G. Light and J. M. Case, "Emerging Methodologies in Engineering Education Research," *Journal of Engineering Education*, vol. 100, no. 1, pp. 186–210, 2011.

[5]   Committee on Developments in the Science of Learning, "How Experts Differ from Novices," in *How People Learn: Brain, Mind, Experience, and School: Expanded Edition*, National Academies Press, 2000, pp. 31–50.

[6]   L. S. Shulman, "Those who understand: Knowledge growth in teaching," *Educational Researcher*, vol. 15, no. 2, pp. 4–14, 1986.

[7]   C. Henderson, A. Beach, and N. Finkelstein, "Facilitating change in undergraduate STEM instructional practices: An analytic review of the literature," *J Res Sci Teach*, vol. 48, no. 8, pp. 952–984, Oct. 2011, doi: 10.1002/tea.20439.